UNIVERSITY OF CALGARY

Effect of Rate and Oil Viscosity on Solution-Gas Drive in Heavy Oils

by

Olufemi Talabi

A THESIS

SUBMITTED TO THE FACULTY OF GRADUATE STUDIES IN PARTIAL

FUFILMENT OF THE REQUIREMENTS FOR THE DEGREE OF

MASTER OF SCIENCE IN CHEMICAL ENGINEERING

Department of Chemical and Petroleum Engineering

Calgary, Alberta

August 2003

UNIVERSITY OF CALGARY

FACULTY OF GRADUATE STUDIES

The undersigned certify that they have read, and recommended to the Faculty of Graduate studies for acceptance, a thesis entitled "Effect of Rate and Oil Viscosity on Solution-Gas Drive in Heavy Oils" submitted by Olufemi Talabi in partial fulfillment for the degree of Master of Science in Chemical Engineering.

M. Pooladi-Darvish

Dr. Mehran Pooladi-Darvish (Supervisor)
Department of Chemical and Petroleum Engineering

T. Okazawa

Dr. Tadahiro Okazawa
Imperial Oil Resources Limited

A. Kantzas

Dr. Apostolos Kantzas
Department of Chemical and Petroleum Engineering

Dennis Coombe

Dr. Dennis Coombe
Computer Modeling Group

August/20/2003
Date

Abstract

Some heavy oil reservoirs under primary production have shown higher recovery than expected. Many studies have shown that gas mobility in these reservoirs is low contributing to improved oil displacement and also that gas mobility may depend not only on gas saturation but also on depletion rate and oil viscosity. Despite the observed effect of oil viscosity and depletion rate on gas mobility, it is not yet clear to what extent these factors affect relative permeability and critical gas saturation. The major objective of this research is to investigate the effects of depletion rate and oil viscosity on solution gas drive process in heavy oil systems.

This research is divided into two parts. In the first part, a two-phase numerical model was developed to study solution gas drive in heavy oil. In the model, the relative permeability to gas is allowed to change with local parameters in addition to gas saturation. It is shown that a relative permeability function that depends on parameters other than gas saturation, can model many features of solution gas drive in heavy oils including the high recoveries obtained at high viscosities and high depletion rates. The local parameters (local velocity and oil viscosity) are combined using two terms; a well-known 'capillary number' term and a newly defined 'depletion index'. These terms, in the model represented the ratio of viscous forces to capillary forces.

In the second part, depletion experiments in a linear unconsolidated sand-pack were conducted. Three oils were used, with oil viscosities that varied by a factor of 30. The experiments were conducted at two different depletion rates for each of the oils. Experimental results show that as oil viscosity or depletion rate increases, critical gas saturation increases, gas mobility decreases. and oil displacement becomes more effective. Furthermore, it is found that relative permeability to gas decreases as withdrawal rate or oil viscosity increase. In the analysis of the experimental results, the effects of oil viscosity and withdrawal rate are combined in the form of a depletion index, such that oil recovery increased as the depletion index increased. The experimental results are simulated using a commercial simulator and a correlation between gas relative permeability endpoint and depletion index is obtained.

Acknowledgements

To,

my parents, friends and family

TABLE OF CONTENTS

CHAPTER FOUR: GAS MOBILITY MEASUREMENTS

CHAPTER FIVE: RESULTS

LIST OF TABLES

LIST OF FIGURES

NOMENCLATURE

a,b,c,d	=	Correlation constants
A	=	area, m^2
B	=	Formation volume factor, m^3/m^3
D	=	diameter, m
f	=	Friction factor
g	=	Gravitational constant
h_i	=	Transfer coefficient
I'	=	Depletion index, $m^{1+2\alpha} sec^{-(1+\alpha)}$.
J	=	Nucleation rate, bubbles /s
k	=	Permeability, Darcy
k_r	=	Relative permeability
L	=	Core Length, m
N	=	Number of bubbles
N_{ca}	=	Capillary Number
P	=	Pressure, Pa
P_c	=	Capillary pressure, atm
P_{eq}	=	Equilibrium pressure, Pa
q	=	Flow rate, m^3/s
R	=	Rate constant
Re	=	Reynolds number
R_{so}	=	Solution gas oil ratio
S	=	Saturation
s	=	Supersaturation
S_{gic}	=	Constant in critical gas saturation correlation
t	=	time co-ordinate
T	=	Temperature, °K

v	=	Local velocity, m/s
V_{cg}	=	Volume of continuous gas flow, m^3
V_i	=	Constant
W	=	Free energy
x	=	Distance, m
Z	=	Constant
z	=	gas compressibility factor
ΔP	=	Pressure drop
ΔT	=	Transmissibility
μ_R	=	Viscosity ratio
β_m	=	Eigen Values
μ	=	Viscosity, cp
σ	=	Surface Tension, N/m
θ	=	Contact angle
ρ	=	Density, kg / m^3
α	=	Depletion exponent
η	=	Diffusivity constant
γ	=	Gas constant, Pa. m^3/Kmol.^{o}K
λ	=	Phase mobility
ϕ	=	Porosity
φ	=	Kinematic viscosity, m^2/s

subscripts

g, G	=	gas
l	=	phase
o	=	oil
w	=	water

org	=	value at residual saturation
r	=	relative value
sc	=	standard conditions
n,w	=	wetting and non-wetting phase
org	=	residual oil saturation
gc	=	*value at critical gas saturation*

superscript

0	=	endpoint value
n	=	time step number
n_g, n_o	=	Corey Exponent

INTRODUCTION

1.1 Background

Heavy oils are hydrocarbon liquids occurring naturally in porous media. Heavy oils are often classified as having API gravity between 10 and 20 degrees and viscosities ranging from 200 to 30,000cp. They contain only small percentage of volatiles and easily distillable hydrocarbons, a high percentage of asphaltenes, and significant quantities of oxygen, nitrogen, and sulphur-bearing compounds. Due to the high viscosity of these oils, there is a challenge in getting these oils out of the reservoir. There are different types of drive mechanisms used to recover hydrocarbons from reservoirs. As a rough estimate, the recovery factors of various recovery mechanisms are shown in the Table 1.1 below [Bora *et al* (2000)].

Table 1.1: Recovery factors for different mechanism

Recovery mechanism	Recovery factors
Solution-gas drive	5-25%
Gas Cap Drive	30-50%
Water Drive	40-80%
Gravity Drainage	<60%

'Solution-gas drive' which is the major recovery mechanism in cold production of heavy oil typically has the lowest recovery factor. However, some high recoveries have been observed in heavy oil reservoirs particularly reservoirs in Canada and Venezuela producing under solution-gas drive. Numerous research works into solution-gas drive in

heavy oils in recent times is as a result of these observed abnormal behaviors. A better understanding of solution-gas drive process is the major objective of this work.

1.2 Solution-gas drive mechanism

Solution-gas drive mechanism occurs when a reservoir, which is originally above its bubble point, is depleted. As the oil is produced, the pressure within the reservoir decreases. Initially, the oil is expelled from the reservoir by the expansion of the rock and the liquid phase. When the average reservoir pressure drops below the bubble point pressure of the hydrocarbon mixture, gas bubbles start to evolve from the oil. Since gas evolves internally, this mechanism is called "internal gas drive". With further reduction in pressure, more and more gas bubbles evolve out of solution. When gas saturation within the reservoir reaches a certain value, it coalesces and starts to flow as a continuous phase. After gas evolution, the oil is expelled from the reservoir by the expanding gas bubbles. The above-described mechanism is an overview of what happens during solution-gas drive.

1.3 Effect of viscous forces

Various research results have shown that during conventional oil solution-gas drive in light oils, capillary forces control the distribution and flow of gases but during solution-gas drive in heavy oil reservoirs, viscous forces become important on a microscopic scale. Peculiar to solution-gas drive in heavy oil reservoirs is the fact that the recovery observed during depletion is dependent on viscous forces [Kumar et al. (2002)]. Depletion rate and oil phase viscosity are major contributors to the viscous forces, and these parameter have been looked at extensively in literature. Although the individual effect of either viscosity or depletion rate has been extensively reported in literature, we

are unaware of any investigation of the combined effects of depletion rate and oil viscosity.

1.4 Research objectives

The overall objective of this research is to improve our understanding of how viscous forces affect the flow of gas during solution-gas drive in heavy oil reservoirs. In this work, the role played by oil viscosity and depletion rate on gas mobility during solution-gas drive is investigated.

With better understanding and proper modeling of solution-gas drive in heavy oil reservoirs, higher recoveries can be achieved at a lower cost. Furthermore, the reservoir can be optimally produced in such a way that subsequent application of thermal processes is more effective.

Kumar *et al* (2002) observed that gas mobility under solution-gas drive is low and that gas relative permeability is dependent on viscous forces. Part of this research work is to further investigate these conclusions and in addition develop a correlation between gas mobility, depletion rate and oil viscosity.

1.5 Research methodology

In this work, we conducted depletion experiments in a sand-pack. These experiments were conducted at different rates and with oils of three different viscosities. The properties of the oils were very similar except for viscosity. From these experiments, we estimated recoveries and hence determine the effect that viscous forces have on the gas mobility. Critical gas saturation was also estimated. The results of the depletion experiments were then correlated with a parameter that combines both rate and viscosity.

The application and technical contribution of this study include:

1) An overall understanding of the role of viscous forces (combined effect of rate and oil viscosity) on solution-gas drives in heavy oil reservoirs.

2) Understanding the quantitative variation of critical gas saturation and gas mobility with viscous forces. A new mobility correlation is proposed.

3) Establishment of an equilibrium technique to model solution-gas drive in heavy oil reservoirs while accounting for viscous forces.

1.6 Layout

This study starts with a literature review in Chapter 2. Chapter 3 describes the development and validation of the equilibrium model. In Chapter 4, the detailed experimental work on gas mobility dependence on viscous forces is described. Chapter 5 discusses the experimental and simulation results. This study is concluded in Chapter6 with summary, recommendation and future work.

LITERATURE REVIEW

2.1 Introduction

At the fast rate at which conventional oil reservoirs are been depleted, heavy oil in recent times has been looked at as a viable alternative. A number of these heavy oil reservoirs have been produced in the recent past and there are a lot more production coming up. There are several ways by which oil can be displaced and produced from the reservoir; these are referred to as reservoir mechanisms or drives. When one mechanism is dominant, the reservoir is considered as operating under that particular drive. However, most reservoirs operate under a combination of drive mechanisms.

Solution-gas drive is one of the numerous drive mechanisms and it typically results in low recoveries. However, some reservoirs in Canada and Venezuela have shown good recoveries from primary production sometimes called 'cold production'. This has triggered a lot of research into solution-gas drive, which is the basic mechanism in these reservoirs. In this chapter, the literature on solution-gas drive is reviewed.

2.2 What is solution-gas drive?

2.2.1 Traditional solution-gas drive mechanism

Solution-gas drive mechanism is a kind of recovery mechanism in which the reservoir energy is obtained from gas coming out of solution. As the pressure of an undersaturated reservoir is reduced below the thermodynamic bubble point pressure, the gas phase is generated.

During classical solution-gas drive mechanism, displacement occurs by expansion of the gas. When the pressure in a solution-gas drive reservoir falls below the reservoir bubble point pressure, gas bubbles start to form within the pore space. The gas

phase, which is the non-wetting phase, occupies the large pore spaces, which contributes to fluid flow through the reservoir. The presence of small gas saturation drastically reduces the permeability of the oil phase. As the gas saturation builds up and increases above a certain critical value, known as the 'critical gas saturation', the gas begins to flow as a continuous phase and the producing GOR rises exponentially. This leads to the rapid decline in the reservoir pressure and results in low ultimate recovery.

2.2.2 Unconventional solution-gas drive

Heavy oil solution-gas drive that is encountered in many Canadian and Venezuelan heavy-oil reservoirs during production is a slightly different form of two-phase flow. Unlike normal two-phase flow, which requires a fluid phase to become continuous before it can flow, it involves flow of dispersed gas bubbles.

It is expected that the ultimate recovery of oil during solution-gas drive in heavy oils be lower than that for light oils because of the higher oil viscosity. However, experience from the field has shown high recoveries from these reservoirs. Some other anomalous behavior during the primary production of heavy oil reservoirs has also been observed. Some of the characteristics of solution-gas drive in heavy oil reservoirs are listed below.

1) Slower decline in pressure.

2) Lower than expected GOR.

3) High flow-rates.

4) High ultimate recovery (10-15%).

From the above, it is evident that solution gas process in heavy oil reservoirs maybe different from the solution-gas drive process in conventional reservoirs.

There are different explanations for the abnormal characteristics observed during solution-gas drive in these heavy oil reservoirs. These explanations can be divided into

two categories: one deals with sand production as a plausible explanation for the above-mentioned anomalous behavior while the other category attributes these observations to abnormal fluid properties.

Sand production has been reported for many Canadian fields. It is believed that the sand production increases the fluid mobility in the near-well zone by increasing the permeability in the affected zone [Dusseault and El-Sayed (2000)]. The enhancement of fluid mobility resulting from sand production can explain the improved flow-rates of cold-production wells, but it does not explain the improvement in the primary recovery factors.

Some authors have suggested that in addition to sand production, the high primary recoveries during solution-gas drive in heavy oil reservoirs can be attributed to fluid properties. In the next section, the various explanations for these abnormal behaviors are discussed.

2.2.3 Low viscosity model

Smith (1988) was probably the first to propose a reduced oil viscosity model in order to explain the enhanced oil rates during solution-gas drive. He concluded that the apparent insitu viscosity of the oil was below the oil viscosity and above that of the gas viscosity. Islam and Chackma (1990) from their mathematical model also concluded that the viscosity of a gas oil mixture is lowered during solution-gas drive. They conducted flow experiments in a core and capillary tubes and externally generated microbubbles, which was injected into the core. This external drive approach has raised some concerns about the applicability of the results to solution-gas drive mechanism, which is an internal drive. Claridge and Prats (1995) supported the theory of Smith. They suggested that gas bubbles are stabilized by asphaltenes accumulation on the bubble interface. The separation of asphaltenes from the oil leads to the lowering of insitu viscosities.

However, Sheng *et al.* (1999) and Maini *et al.* (1999) did not observe any effect of asphaltenes in their experiments. Shen and Batycky (1999) also proposed a correlation for effective viscosity with lubrication effects. They suggested that the favorable behavior for heavy oil reservoirs is due to increased oil mobility due to nucleation of gas bubbles at the pore walls.

2.2.4 Pseudo-bubble point model

Kraus *et al.* (1993) described a "pseudo-bubble point" model for primary depletion in heavy oil reservoirs. In this model, the pseudo-bubble-point pressure was an adjustable parameter in the fluid property description. It is assumed that all of the released solution gas remains entrained in the oil phase until the reservoir pressure drops to the pseudo-bubble-point pressure. Below this pseudo-bubble-point pressure, only a fraction of the released gas remains entrained with the rest forming free gas phase. They suggested that the entrained gas fraction decreases linearly to zero with declining pressures. The entrained gas is considered a part of the oleic phase, but its molar volume and compressibility are evaluated with those of the free gas. This model (used in a reservoir simulator), was used to explain three anomalous production characteristics observed during solution-gas drive in heavy oil reservoirs, namely high oil recovery, low producing GOR, and natural pressure maintenance.

2.2.5 Modified fractional flow model

In order to explain the high recoveries during solution-gas drive, Lebel (1994) described a model that assumes that all released solution gas remains entrained in the oil phase up to a certain system-dependent limiting-volume fraction. Consequently, as the gas saturation increases from zero, the fractional flow of gas increases linearly with saturation until the limiting entrained gas saturation is reached. Beyond this limiting volume fraction of dispersed gas, further increase in gas saturation results in free gas flow. The effective viscosity of the oil was assumed to decrease marginally as the volume fraction of gas increases. The density of the oil was taken as a volume-weighted average of the densities of the oil and gas components. The equilibrium gas-in-oil PVT relationship was assumed to be applicable. This model is equivalent to a manipulation of the gas relative permeability curve, which, up to certain adjustable gas saturation, becomes a function of oil viscosity and oil relative permeability.

2.2.6 Reduced gas mobility model

Firoozabadi and Pooladi-Darvish (1999) advocated a relative permeability-based approach similar to Lebel (1994). Their main idea is that the improved recovery results primarily from reduced relative permeability of gas, which decreases as the oil viscosity increases. Assuming that the relative permeability concept can be applied to dispersed gas flow, the decrease in gas relative permeability with increasing oil viscosity is expected when it is the pressure gradient in the oil that is causing the dispersed bubbles to move.

Kumar and Pooladi-Darvish (2002) later incorporated very low values for gas relative permeability along with increased sand permeability to match the production data of a typical well in the Frog Lake and Lindbergh reservoirs. The increased permeability was related to sand production observed in the field.

In the next section, we examine the mechanism that constitutes the solution-gas drive process.

2.3 Gas generation and flow during solution-gas drive in heavy oil

During depletion of heavy reservoirs, below the bubble point pressure, gas comes out of solution. It initially forms small bubbles, then these bubbles grow in larger dispersed bubbles and finally these bubbles join together. Although most of the various stages involved during the gas formation and flow during solution-gas drive has been thoroughly investigated in the literature, there are still discrepancies as to what actually happens during flow in porous media. However, all these ideas share one thing in common; gas forms (nucleates), grows (bubble growth), coalesce and flows. In this work, the fundamental steps involve during solution-gas drive in heavy oil reservoirs is divided into early time and late time processes and the individual processes are described below:

> Early-time processes

a) Supersaturation

b) Bubble nucleation

c) Bubble growth

> Late-time processes

d) Bubble coalescence, breakup and flow

The limitation of using the above classification is that both the early time and late time processes may overlap. However, the importance of the early time processes reduces with time as the solution-gas-drive mechanism progresses. Due to the size of the reservoir, a part of the reservoir may be in the early time while the other part may be going through the late time processes.

2.4 Early-time processes

This term describes non-equilibrium processes like supersatuartion, nucleation and bubble growth that occur during the early stages of solution gas drive, and refers to the duration (hours, days or months) when gas comes out of solution and accumulates (before critical gas saturation).

2.4.1 Supersaturation

Lots of experimental data has shown that the oil under solution-gas drive could exist in a supersaturated state upon fluid depletion [Kumar et al. (2002)]. A liquid system is supersaturated with gas when the amount of gas in the liquid solution exceeds the equilibrium concentration at the existing pressure and temperature [Karmath and Boyer (1995)]; the oil contains more dissolved gas than that predicted from equilibrium relationships. Kennedy and Olson (1952) observed supersaturations up to 770psi. They observed that bubbles formed rapidly and with considerable violence. They observed that the rate of bubble formation decreased with decreasing supersaturation. Kumar et al. (2002) concluded from their analysis that oil may remain supersaturated even after gas nucleate for many reasons.

In terms of pressure, supersaturation is defined as the difference between the system pressure and the equilibrium bubble point pressure.

$$\Delta P = P_{eq} - P_{syt} \tag{2.1}$$

P_{eq} is the equilibrium pressure while P_{syt} is the system pressure.

Supersaturation is the driving force for the evolution of bubbles in a gas-oil solution. The manner in which the bubbles form and grow controls the displacement of oil during solution-gas drive. Therefore it is believed that displacement of oil depends on the degree of supersaturation. The greater the supersaturation, the higher the recovery efficiency, due to the larger amount of bubbles formed [Stewart *et al.*, (1954].

Various factors have been reported to affect supersaturation. The presence of asphaltenes has been reported to increase supersaturation [Bora *et al* (2000)]. Higher depletion rates resulting in higher supersaturation has been reported by several researchers [Wall and Khurana (1972)]. Recent experimental results [Guo-Quig and Firoozabadi (1999), Kumar *et al.*(2002)], have also confirmed similar results.

2.4.2 Bubble nucleation

A bubble is formed in the body of a liquid when the molecules of the liquid vaporize into a cavity in the liquid. This can occur due to the lowering of pressure below the bubble point pressure. Bubbles grow out of nuclei. A nucleus is a bubble at the threshold of growth. A nucleus can grow continuously leading to rupture of the liquid phase or it can re-dissolve in the liquid with equal probability (Bernath 1952). Nucleation can be into two types:

1) Primary nucleation

2) Secondary nucleation

2.4.2.1 Primary nucleation

Primary nucleation can be further classified into homogeneous nucleation and heterogeneous nucleation.

A) Homogeneous Nucleation: It involves formation of bubbles in the absence of any pre-existing bubbles or foreign matter like porous media. It is described as nucleation in a bulk liquid. Nucleation starts with the formation of an embryo. The spontaneous formation occurs in a liquid when the thermodynamic fluctuation of sufficient magnitude occurs to form a cluster of certain critical size bubbles [Bora (1998)]. This process requires a considerable amount of supersaturation [Hemmingsen (1975)] and a large number of small bubbles are formed. For homogeneous nucleation, the expression for rate of nucleation is given by the following equation (Wankat, 1990)

$$J = \frac{dN}{dt} = Ze^{(\frac{-W}{RT})} = Ze^{(\frac{16\pi\sigma^3}{3kT(P_g - P_o)^2})} \qquad (2.2)$$

where N is the number of nuclei per unit volume and W is the energy of nucleation. Equation (2.2) suggests that nucleation rate is enhanced by increasing supersaturation and retarded by increased interfacial tension.

B) Heterogeneous Nucleation: This process involves the formation of nuclei in the presence of pre-existing bubbles, impurities or a rough surface. Nucleation in porous media is believed to be heterogeneous [Firoozabadi and Aronson (1999)]. The presence of other particles lowers the supersaturation required for nucleation. Rate of bubble nucleation during heterogeneous nucleation may be described with an equation of the form of,

$$J = Ze^{-(\frac{A}{(s)^2})} \tag{2.3}$$

where s is the supersaturation and J is the rate of bubble nucleation per unit time. Moulu (1989) gave an example of nucleation rate expression for a given crude oil in porous media as

$$J = 9 \times 10^{-3} e^{-(\frac{-16.5}{(s)^2})} \tag{2.4}$$

2.4.2.2 Heterogeneous nucleation: Progressive and instantaneous nucleation

The formation of a new gas/liquid interface during gas bubble formation requires energy. Therefore, the liquid becomes supersaturated. Supersaturation is the driving force for gas formation. Depending on the nature of formation of gas bubbles, nucleation can be divided into two categories [Firoozabadi and Kashchiev (1993)]

1) Instantaneous nucleation

2) Progressive nucleation

1) Instantaneous nucleation

In this type of nucleation, all the bubble nuclei are formed at a single supersaturation, after which they grow. No further nucleation takes place afterwards. It is an idealization of the progressive nucleation in which the nucleation takes place over a short span of time. This is very likely when depletion rates are high. Kennedy and Olsen (1952) reported from their experiment that pressure decline rate affects supersaturation and moreover that bubbles in porous media occur instantaneously. Theoretical analysis by Firoozabadi and Kashchiev (1993) showed that pressure decline rate has a strong effect on instantaneous nucleation.

2) Progressive nucleation

In this type of nucleation, new bubble nuclei appear continuously. Bubbles nucleate at all values of supersaturation. The porous media offer active nucleation sites for the bubbles to be nucleated at any supersaturation.

The question about whether the nucleation in porous media is instantaneous or progressive is still a subject of active debate. Yortsos and Parlar (1989) defined nucleation as the appearance of macroscopic bubbles, which arise from various sites on the walls containing trapped gas. The sites become activated when the local saturation exceed the capillary pressure of the site. Kashchiev and Firoozabadi (1993) proposed progressive and instantaneous nucleation.

The effect of various depletion parameters on nucleation has been investigated in the literature. Several researchers [Danesh *et al.* (1987), Wall and Khurana (1972), Kumar *et al.* (2002)] have reported that faster depletion rate leads to nucleation of more bubbles and hence higher oil recovery. The micromodel study of Bora *et al* (2000) showed that fast drawdown lead to very high bubble density and a slow depletion leads to conventional solution-gas drive. Wong *et al* (1999) reported that the number of bubbles formed is independent of fluid viscosity. However, Pooladi-Darvish and Firoozabadi (1999) and later Guo-Quig and Firoozabadi (1999) reported more number of bubbles when conducting experiments with heavier oils as compared to that observed with light oils. Bora *et al* (2000) also reported similar results.

2.4.2.3   Secondary nucleation

Secondary nucleation is the process of formation of nuclei induced by pre-existing nuclei or cavities. Yortsos *et al* (1989) describes this nucleation as nucleation that occurs in the presence of cavities at the pore walls containing pre-existing or trapped gas, which acts as nucleation sites. Yortsos and Parlar (1989) were probably the first to introduce this idea to solution gas drive. This method is utilized in crystallization techniques in which the seed crystals are added purposefully to a solution to induce nucleation.

2.4.3   Bubble growth

The process of solution-gas drive involves nucleation of bubbles in the oil as pressure falls below the thermodynamic bubble point pressure after which the nucleated bubble grows. Growth of an isolated bubble is controlled by mass, momentum and heat transfer across the bubble-liquid interface, and by compression and expansion. Bubble size growth typically obeys a form of growth model. A gas bubble can grow by diffusion of gas into the bubble and by expansion due to pressure reduction. Smaller bubbles have a lower growth rate than larger bubbles because of their higher amount of surface energy to unit volume [Kumar (2000)]. The forces that determine the growth of a bubble can be broadly classified into two. One is hydrodynamic (inertia, pressure and viscous) force and the other is diffusion force [Kumar (2000)]. Many of the authors have looked at the effect of one or more of these forces on the bubble growth rate.

2.4.3.1   Bubble growth in porous media

Scriven (1959), Patel (1980), Szekely and Martins (1971) reported that a number of factors: viscosity, initial bubble radius, surface tension, and diffusivity play a significant role in the determination of the rate of growth of a bubble. Various experimental and theoretical works have been done to investigate these factors.

Moulu (1989) developed a theoretical model for heterogeneous bubble nucleation, followed by bubble growth and nucleation. He obtained a good match with experimental data. He however neglected the moving boundary term in the diffusion growth equation.

Kashchiev and Firoozabadi (1993) in their work reviewed many limiting models when either hydrodynamic or mass transfer forces. It was shown that in some cases, the growth rate could be modeled by the bubble growth $R = at^b$. They used this model to match experimental data of gas phase growth during the solution-gas drive process. In a recent work, Kumar (2000) studied bubble growth rate in a system producing at a constant depletion rate. They incorporated both hydrodynamic and diffusion terms. They suggested that a simple power law model might not be adequate for simulating bubble growth in a closed domain. They noticed that the rate of bubble growth in light oils is larger than the rate of bubble growth in heavy oils due to the smaller diffusion coefficient in heavy oil systems. They observed that viscous forces and in general hydrodynamic forces have no influence on bubble growth and that only diffusion controls the rate of bubble growth in heavy oil systems. Li and Yortsos (1991), (1993) combined pore network visualization experiments with pore network models to investigate bubble growth. They identified four regimes during bubble growth: early-time, percolation, transition and viscous regime. They concluded that the rate of growth depend on mass transfer, growth pattern, and competition between capillary and viscous forces.

2.5   Late-time processes

Late time processes determine phase saturation distribution and flow during solution-gas drive and hence has a strong influence on phase mobility.

2.5.1   Bubble coalescence and breakup

This is defined as merging of gas bubbles and occurs when two bubbles come close to each other.   With continued pressure decline, gas bubbles grow to such an extent they coalesce through the pore throats and form gas channels. Pooladi-Darvish and Firoozabadi (1999) reported that the bubbles in porous media do not remain isolated in heavy oil reservoirs but coalesce to form bigger gas phase before flowing. An alternative hypothesis by Maini *et al.* (1999) concerning the nature of foamy-oil flow suggests that as the growing bubbles migrate with the oil, they breakup into smaller bubbles. This counteracts the effects of bubble coalescence hence maintaining dispersed flow.

Coalescence is affected by different factors including: bubble size, liquid property and porous media. Dusseault (1993) reported from experiments that coalescence happened more rapidly in light oils than heavy oil due to the high viscosity of the oil and capillary forces. Bora *et al* (2000) showed from experiments that the presence of asphaltenes stabilizes the bubble and hinders coalescence. Kovscek and Radke (1994) extensively discussed the effect of porous media on coalescence. They concluded that, in porous media, coalescence occurs when the lamella reach the pore throat.

The role of bubble coalescence cannot be overemphasized. As gas coalesce and flow towards the well bore, it flows rapidly due to its high mobility and becomes less effective in displacing the oil. When gas exists as discrete, dispersed bubbles, the

evolved gas improves the displacement efficiency. On the other hand, when bubbles join together, to form a continuous phase, the reservoir looses energy. The most favorable situation for solution-gas drive is that after coalescence of gas bubbles, large amount of gas is trapped in the reservoir.

2.6 Critical gas saturation

As pressure reduces during solution-gas drive below the bubble point pressure, gas is generated. Initially, the gas saturation is too low for gas flow to occur. As depletion progresses, the gas phase grows by diffusion, pressure reduction and coalescence. At a certain gas saturation known as 'critical gas saturation', gas starts to flow as a continuous or dispersed phase. Critical gas saturation has been defined in different ways by different researchers. Li and Yortsos (1995) defined critical saturation as a sample-spaning cluster at which gas flows. Kumar and Pooladi-Darvish (2002) defined critical gas saturation as the gas saturation at which gas flow is sustained, though intermittent. Sahni et al. (2001) describe critical gas saturation as gas saturation when the producing gas oil ratio becomes greater than the solution gas oil ratio. Bora (1998) defined critical gas saturation as the minimum saturation at which a continuous gas phase can exist in the porous medium under capillarity-controlled conditions.

There is a large difference in the values of critical gas saturation during solution-gas drive in heavy oils reported in literature. Firoozabadi et al. (1992) reported very low critical gas saturation values (0.5%-1.5%) in their experiments using heavy oils suggesting that high recovery during solution-gas drive in heavy oils may not be explained by high critical gas saturation. In recent experiments, Kumar and Pooladi-Darvish (2002) also reported low critical gas saturation (3-4%). However, Loughead and Saltuklaroglu (1992), Sarma and Maini (1992), Islam and Chackma (1990), have all

reported high critical gas saturation. Treinen *et al.* (1998) reported high critical gas saturation (about 9%). They used this to account for good oil recovery.

2.7 Factors affecting critical gas saturation

The (critical) gas saturation at which gas flows in the reservoir may depend on a multitude of factors, including bubble density, oil viscosity (diffusion coefficient) fluid characteristics and chemistry, geometric or topological features of porous media as well as interaction between capillary and viscous forces.

Numerous researchers including Firoozabadi *et al.* (1992), Karmath and Boyer (1995) have studied the effect of depletion rate on critical gas saturation. In a set of recent experiments, Kumar *et al.* (2002) concluded that high depletion rate results in high supersaturation and high critical gas saturation. Firoozabadi *et al.* (1992) related critical gas saturation to supersaturation and pore structure. They also concluded that critical gas saturation decreases with decrease in supersaturation.

The effect of other parameters on critical gas saturation has also been reported in literature. In some recent experiments, Tang and Firoozabadi (2001) suggested that an increase in solution GOR increases the critical gas saturation significantly. They concluded that high solution GOR resulted in a larger number of nucleation sites and this causes a higher gas saturation build up before other gas bubbles can coalesce to form a continuous phase.

Various authors have investigated the effect of oil viscosity on critical gas saturation. Higher viscosity has been observed to impede the growth of gas bubbles and gas bubble clusters because of low molecular diffusion. Firoozabadi and Aronson (1999) conducted constant rate depletion experiments in a special transparent vertical core

holder. They used three kinds of oils for their depletion experiments. They concluded that critical gas saturation for heavy oil systems is not very high: it is within the same range for lighter oils. Tang and Firoozabadi (2001) also observed minimal variation of critical gas saturation with oil viscosity in their experiments. Akin and Kovscek (2002) recently conducted a series of depletion experiments using a mineral oil (220cp at 20 °C) and heavy Hamaca crude oil in order to investigate the mechanisms of heavy oil solution-gas drive. They observed that the lower viscosity mineral oil showed conventional solution-gas drive while the heavy oil showed foamy flow. Observed critical gas saturation was about 3-4% for both oils.

To a lesser extent, initial water saturation has also been reported to affect critical gas saturation. Tang and Firoozabadi (2001) reported lower critical gas saturation for higher water saturation. High water saturation may impede the diffusion of gas phase from the oil, resulting in lower amount of gas evolution and hence smaller gas saturations. Gas gets connected at lower saturations and hence lowers critical gas saturation for higher water saturation.

Dumore (1970) investigated the effect of permeability on critical gas saturation. He concluded from solution-gas drive experiments using bead packs that gas connected earlier in the lower permeability medium. Gas remained dispersed for a longer time in the high permeability medium, which implied higher critical gas saturation.

The knowledge of critical gas saturation is important for estimating recovery in a solution-gas drive process. The value of critical gas saturation determines when gas flows in the reservoir. It is highly beneficial if critical gas saturation could be predicted taking into account most if not all the factors discussed above.

2.8 Gas flow in heavy oil solution-gas drive

At saturations above critical gas saturation, gas flows in the reservoir. The way gas flows after critical gas saturation has attracted a lot of attention in literature because this determines the amount of gas that stays in the reservoir and hence recoveries during solution-gas drive process.

Several microscopic and macroscopic studies have been conducted to understand and model gas flow in porous media. In general, two types of flows have been reported in literature: 'Capillary dominated' flow and 'Viscous dominated flow'. Bora *et al* (2000) observed that at slow depletion tests, the bubbles do not vacate the original pore and migrate towards the outlet before coalescence. Thus the slow depletion tests displayed classical solution-gas drive behavior. They observe a contrary behavior for the fast depletion tests. The bubbles were observed to nucleate, grow and then move towards the outlet end. In this process, the bubbles split and the split bubbles would then grow and split again as they move towards the outlet. This was referred to as 'Foamy flow'. Kumar and Pooladi-Darvish (2002) also observed two types of gas flow: Dispersed flow and continuous gas flow through gas channels. According to them, dispersed flow represents low gas mobility whereas gas mobility in continuous flow is higher. Wall and Khurana (1972) conducted pressure depletion experiments and reported an increase in flow rate leads to intermittent gas flow at higher equilibrium saturation.

High depletion rate is not the only condition for viscous dominated flow during solution-gas drive. High viscosity has also been reported to lead to viscous dominated flow. Pooladi-Darvish and Firoozabadi (1999) during their depletion experiment with oil of two different viscosities observed intermittent, dispersed flow in the more viscous oil.

In terms of reservoir characteristics, dispersed flow is more likely to occur when the permeability is high, the oil is viscous, and the interfacial tension between the oil and the released solution gas is low. To generate the required viscous force, a high drawdown

pressure is required. The viscous trapping force decreases when the pore-body/pore-throat aspect ratio becomes low. Therefore, dispersed flow is more likely to occur in well-sorted unconsolidated sands [Maini (1999)].

2.9 Foamy flow

A slightly different kind of flow behavior called 'Foamy oil' flow has been widely reported in literature. Maini *et al.* (1993) reported from their sand-pack experiments that oil continuous foam is present in the sand-pack. They suggested that this situation does not imply that the gas bubble and the oil would have the same average interstitial velocity. They suggested that promoting this type of flow requires conditions that generate high-pressure gradients in the reservoir. The required pressure-gradient magnitude depends on the oil characteristics and the interfacial tension between the oil and the released gas. They concluded that such foam delays the formation of a continuous gas phase and thereby acting as a natural pressure maintenance mechanism.

In some recent experiments, Maini (1999) also suggested that because the gas remains dispersed in the oil, the produced GOR remains low, and a higher recovery factor is obtained. They argued that the transition between the conventional flow and dispersed flow does not occur abruptly at a certain critical capillary number. It is a gradual transition that occurs above a threshold capillary number. Their foamy flow model is also consistent with visual observations of Bora *et al* (2000) in micromodels. The conditions required for this type of flow to occur is summarized as follows.

1) Viscous forces acting on growing bubbles should exceed the capillary trapping forces.

2) Gravitational forces should not be capable of inducing rapid gravity segregation of the two phases.

3) Interfacial chemistry effects that hinder bubble coalescence also may be needed

2.10 Gas mobility

Regardless of the type of flow in porous media: foamy, dispersed or intermittent flow, the more favorable flow type is one that causes the gas to stay in the reservoir (low gas mobility). Gas mobility typically refers to the late time processes of gas flow after critical gas saturation, which involves bubble coalescence and gas flow. By definition, the mobility of a particular phase is the ratio the effective permeability of that phase to the viscosity of that phase. In an oil-gas system, gas mobility is typically orders of magnitude higher than oil mobility due to the small value of gas viscosity. Because the gas viscosity varies insignificantly with pressure and temperature, gas relative permeability is often representative of gas mobility.

Reduced gas mobility, as a plausible explanation for high oil recovery during solution-gas drive has in recent times gained wide acceptance among many researchers. Many researchers have studied gas relative permeability during solution-gas drive in heavy oil reservoirs and have reported low values. Pooladi-Darvish and Firoozabadi (1999) attributed the improved heavy oil recovery under solution-gas drive to discontinuity of the gas phase and low gas mobility. They suggested that low gas mobility is due to dispersed flow and increased number of bubbles. This theory was later supported by Guo-Quig and Firoozabadi (1999). Kumar et $al.$ (2002) reported low gas relative permeability (1×10^{-6} to 1×10^{-4}), which decreased with increasing depletion rate. Otero et $al.$ (1998) and Kumar et $al.$ (2001) had to reduce gas relative permeability significantly to match field data. A major objective of this work is to investigate gas

relative permeability of solution gas drive in heavy oil reservoirs. The next section describes the relative permeability concept and how phase relative permeability is obtained.

2.10.1 Relative permeability concept

Flow in porous media is defined by a system of equations. These equations are material balance, momentum balance and energy balance across the porous media. One of the equations that define flow in porous media is Darcy's equation. This equation relates superficial velocities to individual pressure gradient and viscosity. Darcy's law for single-phase flow in a horizontal porous media in one-dimension can be described as

$$q = -\frac{kAdP}{\mu dx} \qquad (2.5)$$

where q is the volumetric flow-rates, k is the absolute permeability and μ is the phase viscosity.

In solution-gas drive, once the pressure goes below the bubble point pressure, gas forms. After the critical gas saturation, the gas starts to flow. This flow may be represented by a modified Darcy's equation for two-phase flow, which involves the use of relative permeability to define the flow of each phase.

Effective permeability is the permeability of a phase in the presence of another phase. Relative permeability is defined as the ratio of the effective permeability to a phase divided by the absolute permeability. This implies at single phase, the relative permeability equals one. The Darcy's two-phase flow equation is given by

$$q_l = -\frac{kk_{rl}AdP_l}{\mu_l dx} \qquad (2.6)$$

where k_r is the phase relative permeability.

Relative permeability functions are an important property of porous media and are essential for understanding multi-phase flow behavior. Accurate estimation of this property is important for reservoir production forecasting. Since the reservoir itself is inaccessible for determination of relative permeability, this property is often determined through laboratory experiments. Relative permeability functions are then inferred from the analysis of various experimental data.

Typically, relative permeability is a function of saturation only for a particular porous media and at typical interfacial tension [Honarpour et al. (1994)]. A number of measurements have been done in the lab to determine phase relative permeability entirely as a function of phase saturation. Osaba et al. (1951) and Richardson et al. (1952) determined two phase relative permeability by flowing two phases simultaneously until the flow become steady state. On the other hand, Efros (1956), Johnson et al. (1959), Watson et al. (1988), Helset et al. (1998), Sarma and Bensten (1990) have all determined relative permeability by displacing one phase with another. This is an unsteady state process. In steady state experiments, each experimental run gives only one point on the relative permeability curve (relative permeability vs. saturation). The experiments are made at different flow fractions in order to make a reasonable determination of the whole curve.

Either steady or unsteady state, relative permeability determined from these experiments involves external drive processes and these results have been applied directly to predict performance during solution-gas drive. However, the mechanism for external gas drive processes is different from that of an internal gas processes like solution-gas drive. Stewart et al. (1954) pointed out that there is a difference in the relative permeability under external drive and solution-gas drive. Tang and Firoozabadi (2003) recently suggested a simple mathematical model for the estimation of gas and oil

relative permeability from 1-D depletion experiments that are under two-phase pseudo-steady state conditions and exhibit a small capillary pressure gradient.

$$k_{rl} = (\frac{\mu_l q_l L}{2kA(\Delta P + \rho_l gL \sin\theta)})$$

(2.7)

where k_{rl} is the phase relative permeability and ρ is the phase density.

When the phase relative permeability is estimated, the phase saturation also needs to be determined. Several methods are used to determine phase saturation in the core. Earlier methods involve core weighing [Osaba et al. (1951), Richardson et al. (1952)] and material balance calculations [Fatt and Dykstra (1951), Rapport and Leas (1951)]. Others have determined "in situ saturation" by using non-intrusive techniques. Oak et al. (1990), Oak and Ehrlich (1998), Morgan et al. (1950)] used X-rays, Sarma and Bensten (1990), Parsons (1975)] used microwave, Hoyos et al. (1990), and Kalaydjian (1992) used ultrasound, Chardaire (1989) used gamma rays. In more recent experiments, Burns (1999) used digital image analysis to examine saturations in porous media. Sahni et al. (2001) used CT scanning to determine in-situ saturation after conducting depletion experiments on a core.

When it is impossible to determine the relative permeability through experiments, appropriate correlations may give a good estimate. These correlations are at most times expressed as a function of saturation only. Examples are Corey type equation.

$$k_{rg} = k_{rg}^0 S^{n_g}$$

(2.8.1)

$$k_{ro} = k_{ro}^0 (1-S)^{n_o}$$

(2.8.2)

where

$$S = \frac{S_g - S_{gc}}{1 - S_{gc} - S_{org}} \qquad (2.8.3)$$

Due to the different recoveries observed during solution-gas drive in heavy oil experiments, it is possible that gas relative permeability depends on other factors apart from saturation. In order to estimate values of relative permeability as a function of saturation and other parameters, history matching field or experimental data has been suggested. Andarcia *et al.* (2001) determined relative permeability end points by history matching production data from their depletion experiments. They later used these relative permeability endpoints for field simulations.

As mentioned above, a number of studies of solution-gas drive in heavy oils refer to the slugs of gas being produced and intermittent gas flow [Sheng *et al.* (1999), Pooladi-Darvish and Firoozabadi (1999), Kumar and Pooladi-Darvish (2002), Tang and Firoozabadi (2003)]. The concept of relative permeability may therefore be invalid for flow of a discontinuous gas phase. In the absence of mathematical models that account for the intermittent flow of gas, current simulation models use the relative permeability to characterize the two-phase flow of gas and oil. In the past, the concept of relative permeability has been successfully used for other forms of discontinuous flow of the phases [Vassenden and Holts (2000)]. In this work, relative permeability may be a function of other parameters in addition to phase saturation. Here, it is assumed that the concept of relative permeability applies to solution-gas drive in heavy oils, and the dependency of the relative permeability functions to gas saturation, withdrawal rate and oil viscosity is examined. Non-continuous phase flow (Dispersed, intermittent, or foamy flow) is approximated by low gas relative permeability flow.

2.10.2 Role of viscous forces on gas flow during solution-gas drive in heavy oils. ·

Hydrodynamic, diffusive and capillary forces are the major forces acting in porous media during fluid flow. Hydrodynamic forces represents the force causing flow. They are sometimes referred to as viscous forces. Pressure gradient and buoyancy are the major contributors to this force. Capillary forces on the other hand occur due to the interfacial tension between multiple fluids in minute pore spaces. Capillary forces depend on the surface tension between the two fluids and also on the pore sizes and local saturations. Capillary forces determine the distribution of different saturations in porous media. In porous media, capillary forces are typically larger than viscous forces. In viscous dominated flow, the difference between these two forces reduces.

Both capillary dominated flow as well as viscous dominated flow has been reported in literature for heavy oil reservoirs. It is likely that during solution-gas drive in heavy oil reservoirs, the flow goes from capillary to viscous dominated flow. As described earlier, during capillary dominated flow, the capillary forces determine phase distribution and relative permeability is strictly a function of saturation. One consequence of this assumption is that the fluid distribution is the same under static and flowing conditions, and it is not affected by the local pressure gradient. Another consequence is that the gas phase must become continuous before it can start flowing, with isolated gas bubbles remaining trapped by capillary forces. However, this assumption may not be valid in solution-gas drive in heavy-oil reservoirs. Because of the high oil viscosity and high drawdown pressure used in cold production, the local capillary number may be high enough to mobilize isolated bubbles [Maini (1999)]. This leads to dispersed flow. This research focuses on viscous dominated flow and how viscous forces affect solution-gas

drive in heavy oils. Two dimensionless groups are often used to differentiate capillary / viscous dominated flow: Capillary number and Viscosity ratio.

1) Viscosity ratio is the ratio of the viscosity of the different phases in porous media. Viscosity ratio is defined as

$$\mu_R = \frac{\mu_n}{\mu_w} \tag{2.9}$$

where n and w represents the non-wetting phase and the wetting phase respectively

Odeh (1959) conducted relative permeability experiments at various viscosity ratios for different oil –brine systems and observed that the relative permeability for the non-wetting phase decreases with decreasing viscosity ratio.

2) Capillary number is the ratio of viscous forces to capillary forces. Capillary number has been defined in many ways in literature. Chatzis and Morrow (1981) defined capillary number as $\frac{k\Delta P}{\sigma L}$. Du Prey (1970) and Erlich et al. (1974) defined capillary number as shown in equation 2.10. In this work we have adopted this nomenclature.

$$N_{Ca} = \frac{v\mu}{\sigma} \tag{2.10}$$

A large value for capillary number, suggests viscous flow. Capillary number has been used extensively in literature in gas condensate modeling and to a lesser degree in heavy oil research. Blom and Hagoort (1998) while modeling gas condensate reservoirs explicitly found a capillary number dependent correlation for relative permeability in order to model viscous dominated flow. Pope and Wu (1998) also used a similar approach. In heavy oil solution gas research, Javadpour and Pooladi-Darvish (2001) used capillary number to investigate the effect of viscous forces on gas mobility.

2.10.2.1 Depletion experiments

Core depletion experiments give a good representation of solution-gas drive. Pooladi-Darvish and Firoozabadi (1999), Kumar *et al.* (2002) and Maini *et al.* (1999) have all used core depletion experiments to simulate the solution-gas drive process. Firoozabadi and Aronson (1999) used a special core holder to visually observe formation of gas bubbles on the rock surface. The porous media used in these experiments are usually core or unconsolidated sand in a core holder with or without confining pressure. Flow is typically in one-dimension and usually two-phase.

Because bubble nucleation is driven by supersaturation, the degree of supersaturation required before nucleation occurs depends on the depletion rate. Therefore early time processes are likely to be more significant in laboratory depletion experiments, which are run on a much smaller time scale compared with the field case. Nucleation and growth of bubbles becomes less significant when the time scale moves from a few hours or a few days in the laboratory to years in the field.

Although core depletion experiments improve our understanding of solution-gas drive, these experiments may be highly system -specific and hence may not be applicable to other cores or fields. In the next section, the effect of various depletion parameters particularly depletion rates and viscosity is reviewed.

2.10.2.2 Effect of depletion rate on gas relative permeability

An important factor contributing to viscous forces is the depletion rate at which the reservoir is produced. The effect of this parameter on gas relative permeability has been extensively reported in literature. Kumar *et al.* (2002) reported results of depletion experiments in heavy oil. Their objective was to examine the effect of depletion rate on

the process. They investigated both the early-time non-equilibrium effects and the late-time mobility effects. They reported that recovery efficiency improved with increased depletion rate. The analyses of their data confirmed that gas relative permeability in these experiments was low (10^{-5}–10^{-4}). Turta *et al.* (2001) investigated the effect of pressure gradient on the gas-in–oil dispersions during solution-gas drive in heavy oil reservoirs. They used special sand-pack with three different sections to produce three different pressure gradients. They concluded that oil mobility in two-phase flow varies with pressure gradient. They also suggested that oil relative permeability could exceed one in two phase gas flow. Sahni *et al.* (2001) conducted depletion experiments on a sand-pack at two different rates using CT scanning to determine saturations. They concluded that higher depletion rates resulted in higher nucleated bubbles, higher gas saturation and higher recoveries.

2.10.2.3 Effect of viscosity on gas relative permeability

The oil viscosity can affect the early time processes of bubble nucleation and growth and may also affect the late time process of gas flow.

Handy *et al.* (1958) in their experiments observed higher recoveries with viscous oils during solution-gas drive experiments. They concluded that low diffusion coefficients produced the same effects as high depletion rate. Wall and Khurana (1972) showed that relative permeability to gas decreases with increase in oil viscosity.

Kumar and Pooladi-Darvish (2001) analyzed a set of recently published experimental data where effect of temperature on solution-gas drive was studied. They reported that changing temperature results in change in oil viscosity. Analyses of the data showed that gas mobility decreased as temperature decreased (oil viscosity increased). In a theoretical study, Javadpour and Pooladi-Darvish (2001) studied gas relative permeability using a 2-D network model. Effect of various parameters such as oil

viscosity, interfacial tension and capillary number were investigated. The results indicated that by increasing oil viscosity, the relative permeability to gas decreases. Tang and Firoozabadi (2001) studied the effect of temperature on gas and oil relative permeability during solution-gas drive in heavy oils. They used a visual core holder to perform depletion experiments with Hamaca crude oil (API = 8.75). They varied the oil phase temperature from 35 °C to 46 °C this changed the oil phase viscosity from 54,000cp to 22,000cp. They observed that an increase in temperature decreased the gas relative permeability by one order of magnitude (10^{-6} at 46°C to 10^{-7} at 35 °C). In a recent study, Lago et al. (2002) studied depletion in a series of heavy oils and light oils. They concluded that more bubble nucleate in heavy oils due to high supersaturation.

Despite the clear effect of oil viscosity and depletion rate on gas relative permeability from the above studies, it is not yet clear why these factors affect gas mobility. It is possible that higher oil viscosity affects the early-time phenomena of bubble nucleation and growth (because of change is diffusion coefficient for example). Alternatively, it is possible that it is the late-time phenomenon of flow that is affected by increasing the ratio of viscous forces to capillary forces, when oil viscosity increases. Similar to effect of oil viscosity, higher depletion rate my affect the time-dependent phenomena of bubble nucleation and growth or it may affect the late time flow by increasing the Capillary number. It seems as if the two possibilities exists during solution gas drive in heavy oils and both have been extensively investigated in literature.

2.11 Modeling solution-gas drive in heavy oils

The modeling of gas flow during solution-gas drive is a complex process at microscopic level. A proper comprehensive modeling should take into account the non-equilibrium phenomena: Supersaturation, nucleation, bubble growth, coalescence,

breakup, gas flow and the effect of porous media among other parameters. At macroscopic levels, Darcy's equation can be altered to represent the flow. Numerical simulation of primary depletion in foamy-oil reservoirs is still based primarily on empirical adjustments to the conventional solution-gas-drive models. The two-phase flow of oil and gas mixtures is described by relative permeability relationships, with some adjustment to the relative permeability curves and/or to other fluid properties to account for the effects of viscous flow. The rock/fluid properties that have been adjusted in such simulations include the critical gas saturation, oil/gas relative permeability, fluid and/or rock compressibility, pressure-dependent oil viscosity, absolute permeability, and the bubble-point pressure.

In general, three routes have been reported in literature for modeling solution-gas drive in heavy oils. The first route involves pore scale detailed, mechanistic modeling of all the non-equilibrium processes. One of the challenges in using mechanistic models is that multitude of processes included. Such modeling requires knowledge of a large number of parameters, often difficult to obtain. These models are discussed in the next section.

The second is an extension of the equilibrium models to include the dependence of the rate constants on flow conditions. The third route is to make flow parameters in equilibrium models functions of flow conditions.

All the models proposed in literature are still unique to the system they represent and extending the concept involved in one model to another is difficult. However, they all account for observed results during solution-gas drive in heavy oils.

2.12 Non-equilibrium model: "mechanistic model"

It is readily apparent that the initial processes involved during solution-gas drive in heavy oil reservoirs are time and reservoir condition-dependent. Therefore, the flow behavior of viscous dominated flow can be expected to be a function of time as well as of the imposed flow conditions. Mechanistic models attempt to capture the time-dependent changes in the early time processes of solution-gas drive in heavy oil reservoirs.

Sheng *et al.* (1999) developed a dynamic numerical model including the early-time processes of bubble nucleation and growth. Multi-phase flow was described with usual relative permeability curves. The authors used the model to match their depletion experiments and observed that recovery increased with increased depletion rate.

Egermann and Vizika (2000) developed a mechanistic model where an exponential function similar to that of homogenous nucleation was used to represent bubble nucleation. Bubbles were allowed to grow based on a diffusion-dominated growth equation in the bulk and then flow. The authors examined their model against two-phase flow data obtained from light-oil experiments and showed good matches. Arora and Kovscek (2002) developed a mechanistic population balance model for describing bubble nucleation and growth. This model gave a good match with experimental data for the initial period of solution-gas drive before the onset of gas flow. The model did not consider gas mobility and critical gas saturation.

2.13 Dynamic models

This is a blend between pore scale non-equilibrium mechanistic model and equilibrium macroscopic model. Coombe and Maini (1994) described a model that

accounts for the kinetics of physical changes occurring in the morphology of the gas-in-oil dispersion. It defines three nonvolatile components in the oil phase: dead oil, dissolved gas, and gas dispersed in the form of microbubbles. The dissolved gas changes to dispersed gas by means of a rate process that is driven by the existing local supersaturation. The dispersed gas changes into free gas by a second rate process. The model was implemented in a commercial simulator by use of existing chemical-reaction routines. Both rate processes were modeled as chemical reactions with specified stoichiometry and reaction-rate constants. The rate constant was determined by history matching.

A similar approach was used by Sheng *et al.*, (1996) who modeled the rate of release of solution gas by exponential decay of the local supersaturation and assumed that the gas evolved from solution remained initially dispersed in the oil. The dispersed gas disengages from the oil to become free gas at a rate that is proportional to the volume fraction of the dispersed gas in the dispersion. Thus, two sequential-rate processes with associated rate constants described the kinetics of the process involved in transfer of the solution gas to the free-gas phase. This model was used successfully for history matching laboratory solution-gas-drive experiments. However, it was found that the rate constants depended on the depletion rate used in the tests.

2.14 Equilibrium models

The motivation for developing such models comes from their ease of implementation by use of existing reservoir simulators that assume complete local equilibrium between different phases. Most simulators also assume that the mobility of fluids is independent of the viscous forces. Consequently, such models are inherently incapable of accounting for the non-equilibrium effects and, generally, cannot predict the

effect of operating conditions on solution-gas-drive performance. As suggested above, non-equilibrium concepts are incorporated into equilibrium models by altering flow parameters. However, such models have been successful in attracting considerable attention in the literature and continue to be used in reservoir simulation studies. Pooladi-Darvish and Firoozabadi (1999), Tang and Firoozabadi (1999) used a commercial simulator, with low relative permeability to gas to match their heavy oil experiments.

2.15 Network models

Network models are simplified mathematical representation of the real porous media. The porous network model provides an idealization of the complex geometry of real porous media, so that the related fluid can be treated mathematically at a manageable level of complexity. [Javadpour *et al* (2001)]

Constantinides and Payatakes (1996) used network simulation to investigate the effect of viscosity ratio on gas relative permeability. Javadpour and Pooladi-Darvish (2001) investigated effect of oil viscosity and other parameters on the mobility of dispersed bubbles using a converging–diverging network model. Their network model results were in qualitative agreement with most of the previous experimental works.

2.16 Modeling summary

Most of the equilibrium models described above have been used in a history-matching mode and the predictive ability of many remains questionable. The modeling approach suggested in this work differs from the detailed mechanistic modeling by trying to introduce a limited number of processes, thereby reducing the number of unknowns needed. Such modeling, although may not include all the microscopic phenomena, could

prove useful if it could provide a good representation of the key processes affecting recovery.

In order to model the effect of viscous forces in heavy oil reservoirs during solution-gas drive using a relative permeability concept, the relative permeability of the gas phase and/or the critical gas saturation must be correlated against viscous forces. Urgelli *et al.* (1999) concluded from their experiments that in order to mimic the behavior of gas phase during simulation of cold production process, it is necessary to use a critical gas saturation, which depends on depletion rate and consequently the distance to the producers. Foulser *et al.* (1992) modeled the oil release mechanism of surfactant flooding by making the relative permeabilities a function of capillary number. Egermann and Vizika (2000) have recently reported the experimental verification of the differences in relative permeability in the far field and the near-wellbore region. They concluded that a model based on capillary-number-dependent relative permeability would not account for the changes in dispersion properties with time, but may be a reasonable approximation for fully developed flow in the field.

Hence it is important to develop a correlation between simulation parameters (for example gas relative permeability and critical gas saturation) and viscous force parameters in order to account for viscous forces in equilibrium models. In the next section an equilibrium numerical model is presented.

NUMERICAL MODELING

3.1 Objective

As discussed in the previous chapter, both the early time and the late time processes during solution-gas drive in heavy oil reservoirs may be affected by viscous forces. Viscous forces may become important at high depletion rate as well as at high viscosity. Also in the previous chapter, the effect of viscosity and depletion rate on gas mobility was extensively discussed. The objective of this chapter is to develop a simulator that accounts for the effect of these factors on gas mobility on a local scale. Although the simulator developed in this chapter combines the effect of viscosity, interfacial tension and rate into a single group called capillary number (defined earlier), the experimental data simulated only shows the rate dependence of gas mobility during solution gas drive. Nevertheless, we use the capillary number as a correlating factor as this dimensionless group is one of the important dimensionless groups affecting two-phase flow. In Chapter 5, it will be shown that a more general term known as depletion index better explains the combined effect of depletion rate and oil viscosity on solution gas drive in heavy oil.

The effect of depletion rate and oil viscosity on bubble nucleation and growth in porous media is incorporated in the modeling work by making critical gas saturation vary with these factors. Both critical gas saturation and gas mobility are varied independently with capillary number in a way that is inline with recent experimental observations.

It is important to note that the objective of this modeling work is not to develop a universal numerical model but to show that a depletion rate and oil viscosity-dependent model can be developed to model different flow conditions and recoveries. Hence, an equilibrium model is developed using Darcy's law, which accounts internally for the

dependence of flow on viscous forces during solution-gas drive in heavy oil. In other words, the model will be able to adjust internal parameters (like relative permeability) depending on the local flow conditions. This will be very useful in modeling the different recoveries observed at different depletion rates during solution-gas drive in heavy oil systems. Although this equilibrium approach does not allow modeling of kinetics of the solution gas process, it involves fewer variables in comparison to the more detailed 'mechanistic models'.

In the following, the basis of the modeling approach, the supporting evidence and the assumptions are discussed.

3.2 Numerical modeling (overview)

Numerical models solve mathematical equations describing physical behaviors of the field. Figure 3.1 depicts the major steps involved in building the model. The result of the formulation is a set of coupled non-linear PDE's that describes flow in porous media. The equations derived from this formulation process, if solved analytically (exactly), would give the pressure, saturation and production rates as continuous functions of time and location. Because of the non-linear nature of the equations, analytical techniques cannot be used and solutions must be obtained from numerical methods. Numerical solution gives the pressures and saturations only at discrete points in the reservoir. Discretization is the process of converting the PDE's to algebraic equations. Several numerical methods can be used to discretize the fluid flow equations; however, the most common approach is the finite difference method. Once the model equations have been linearized, one of several linear-equation solving techniques can be used to solve them. The techniques fall into two categories: direct and iterative methods.

There are different methods proposed in literature for approximating the resulting PDE's. These methods differ in the way the functions are treated. The method used in

this modeling work is called the I.M.P.E.S (implicit pressure and explicit saturation method). Other methods include: fully implicit method, Sequential solution method (SEQ) and the Simultaneous Solution method (S.S).

3.3 Physical models

Physical models are used to make direct measurements of flow properties in porous media. Two types of physical models are used in petroleum industry. The first are core flood and sand-pack experiments while the other category uses geometrical-, mechanic- and thermal–similarity concepts.

Core flood, sand-packs and slim tubes experiments generally run on linear cores. They are probably the most common physical models used in the industry today. One detrimental feature of these models is that the experiments are conducted at a scale that is not representative of the actual reservoir scale. Consequently, the results of these experiments must be scaled up to more representative scales. In the second type of physical model, areal geometry, thickness, porosity, and permeability of the model and the fluid properties are scaled so that the shape and dimensions of the model are proportional to those in the reservoir. The drawback about these models is that the mechanism or process being represented may be slightly different from what happens in the field.

This work specifically targets modeling sand-pack experiments, which has been used extensively for investigating solution-gas drive experiment. The modelled system consists of sand packed in a core holder. Flow is assumed to be one-dimensional and two-phase. Gravity effect is negligible. The sand is assumed to be uniform, isotropic, chemically inert and non-deformable.

The sand-pack is originally saturated with live oil above the bubble point pressure of the oil. The live oil, which is in single phase, is then produced from one end of the sand-pack (depletion) until two-phase flow is generated in the system.

3.4 Methodology

The methodology involved in this modeling approach is to set up and solve the material balance and energy balance equations for a one-dimensional multi-phase core depletion problem. The model accommodates for dispersed flow with low gas relative permeability values. The dependence of flow on depletion rate and oil viscosity is introduced into the flow equations by making gas relative permeability and critical gas saturation a function of capillary number. In this model, a base relative permeability function and critical gas saturation function is predefined into the simulator and the simulator is allowed to accommodate for change in flow conditions (capillary or viscous-dominated) by adjusting this base relative permeability functions.

Specifically, the model:

1) Calculates local oil velocity from local flow conditions

2) Determines capillary number from local velocity using the capillary number function

3) Determines relative permeability as function of saturation and capillary number.

4) Calculates pressure, saturation, recovery and production terms.

Figure 3.1 shows the flow diagram for the methodology.

Various input parameter; porosity,
depletion rate, water saturation,
viscosity, pore geometry, bubble
point pressure

SIMULATOR MODEL

$$K_{rg} = f(N_{ca}, S_g)$$

$$S_{gc} = f(N_{ca})$$

OUTPUT
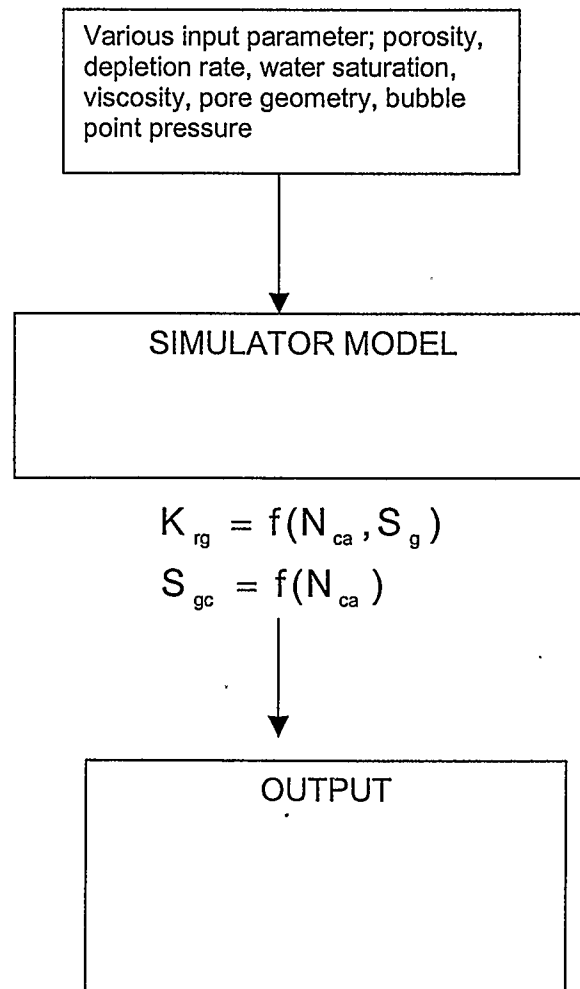
Figure 3.1: Methodology for modeling dependence of viscous forces on gas flow

3.5 Assumptions

The model assumes the following: ·

1) Fluid flow is one-dimensional even on a microscopic scale, no vertical movement and no gravity segregation.

2) Fluid flow obeys Darcy's law regardless of a non-continuous gas phase. Dispersed, intermittent or foamy flow is represented in the model as low gas relative permeability values.

3) Viscous forces do not affect the shape of the relative permeability curve. Only the endpoint value (magnitude) is affected.

4) Viscous forces do not affect oil mobility.

5) The effect of viscous forces on early time non-equilibrium processes is only accounted for by modifying the critical gas saturation. Furthermore, the model assumes equilibrium between the gas and the oil during gas flow.

3.6 Applicability

This modeling work is highly applicable to solution-gas drive in sand-pack depletion experiments. However, the correlation used in the simulator may vary from system to system. Also, since the critical parameters in this modeling work (gas mobility and critical gas saturation) are correlated against a dimensionless capillary number term, with proper up scaling methods, this modeling work may be extended to other cases.

3.7 Model formulation

The one-dimensional two-phase flow equation to be solved is given below.

$$\frac{\partial}{\partial x}(\lambda_o \frac{\partial P_o}{\partial x}) = \frac{\partial}{\partial t}(\frac{\phi S_o}{B_o}) + Q_o \qquad (3.1)$$

$$\frac{\partial}{\partial x}(\lambda_g \frac{\partial P_g}{\partial x}) + \frac{\partial}{\partial x}(R_{so}\lambda_o \frac{\partial P_o}{\partial x}) = \frac{\partial}{\partial t}(\frac{\phi S_g}{B_g} + R_{so}\frac{\phi S_o}{B_o}) + Q_g + R_{so}Q_o \qquad (3.2)$$

Equation 3.1 and 3.2 are non-linear parabolic, partial differential equations. Other equations include the capillary pressure relation

$$P_c = P_g - P_o \qquad (3.3)$$

And the saturation conservation equations;

$$S_o + S_g = 1 \qquad (3.4)$$

Corey type functions (described later) are used for the phase relative permeability.

3.7.1 I.M.P.E.S method

As pointed out earlier, the partial differential equations obtained for two-phase flow in porous media are non-linear. A non-linear finite difference approximation scheme is employed. The I.M.P.E.S scheme is one of the ways to linearize these finite difference equations.

The acronym I.M.P.E.S means Implicit Pressure Explicit Saturation. The basic principle in this method is the elimination of the differences in non-pressure variables from the model's set of *n* conservation equations to obtain a single pressure equation.

This principle was attributed to Stone and Sheldon (1960). Young and Stephenson (1983) and Wattenbarger (1968) have all extended the I.M.P.E.S method to develop compositional simulators. After pressure has been advanced in time, the saturations are updated explicitly. For our two-phase model, there are two coupled, non-linear, parabolic partial differential equations that need to be solved simultaneously with

four other flow equations. Although the I.M.P.E.S formulation is conditionally stable, it is fairly accurate for simulation of multi-phase flow in porous media and moreover, it is not very expensive in terms computational time for multi-dimensional problems (unlike fully implicit methods). However, its stability condition may result in small time steps.

The resulting pressure equation after applying the I.M.P.E.S method is given as

$$\Delta T_o(\Delta P^{n+1}) + A_i \Delta T_{gi} \Delta P^{n+1} + A_i \Delta(R_{so} T_o(\Delta P^{n+1})) = (C_{2p} + A_i C_{3p})\Delta_t P + Q_o + A_i(R_{so} Q_o + Q_g) \qquad (3.5)$$

where

$$A_i = \frac{C_{2o}}{C_{3o} - C_{3g}}$$

$$C_{2p} = \frac{V}{\Delta t}(S_o \phi)b_o{}' + S_o{}^n b_o{}^{n+1} \phi'$$

$$C_{2o} = \frac{V}{\Delta t}(\phi b_o)^{n+1}$$

$$C_{3o} = \frac{V}{\Delta t}R_{so}(\phi b_o)^{n+1}$$

$$C_{3g} = \frac{V}{\Delta t}(\phi b_g)^{n+1}$$

$$C_{3p} = \frac{V}{\Delta t}(R_{so}((S_o \phi)^n b_o{}' + S_o{}^n b_o{}^{n+1} \phi') + S^n{}_g \phi^{n+1} b'{}_g + S^n{}_g \phi' b^{n+1}{}_g + (\phi S_o b_o)^{n+1} R'{}_{so}$$

The above formulation follows that given by Aziz and Settari (1979). When equation (3.5) is expanded for all the grid points, the following matrix is obtained.

T P (n+1) = D [P (n+1) – P (n)] + G + Q

Matrix *T* is a tri-diagonal matrix containing the transmissibilities, matrix *D* contains compressibilities and *G* is a diagonal matrix

When new pressures are obtained, the saturations are updated explicitly using the oil equation below

$$\Delta T_o (\Delta P_o{}^{n+1}) = 1/\Delta t\ \Delta_t (V_p S_o/B_o) + Q_{oi} \qquad (3.6)$$

The derivation of Equation 3.5 is given in Appendix I

3.7.2 Non–linearities

There are two types of non-linearities involved in this scheme: weak non-linearities and strong non-linearities. All variables that are functions of pressure in one phase (B_l and μ_l) are considered weak non-linearities. They can be evaluated at a previous time step. Hence the approximation of $i+1/2$ step is not critical for weak non-linearities. Strong non-linearities are co-efficients that depends on saturation for example relative permeability in each phase (k_{rl}). These non-linearities need a special weighting scheme.

3.7.3 Weighting of transmissibilities

The problem of approximating $i+1/2$ level in space co-ordinate is referred to as the weighting problem. In relation to the I.M.P.E.S method, the weighting problem involves how relative permeability at $i+\frac{1}{2}$ is related to S_{wi} and $S_{w\,i+1}$

There is the mid-point, upstream and the downstream weighting. However, the most commonly used scheme is the upstream weighting defined by

$k_{rwi} = k_{rw}(S_{wi})$ if flow is from i to $i+1$

$k_{rwi} = k_{rw}(S_{wi+1})$ if flow is from $i+1$ to i

The upstream weighting has been observed to produce fairly accurate results.

3.7.4 Relative permeability

Two-phase relative permeability is approximated are by relative permeability models. Models can be used to investigate the effect of other parameters other than saturation. Two-phase models that are commonly used are Corey, Naar and Henderson's two-phase models.

In most relative permeability models, relative permeability curves are often expressed as a function fluid saturation only. These functions are generally characterized by three important parameters, the residual/critical saturations, the end-point values and the relative permeability curvature. Corey's model is a simple model, which accommodates the important features of relative permeability functions. For low values of gas saturation as it occurs in heavy oil systems under depletion Corey-type relative permeability functions ((3.7) to (3.9)) is adequate for representing phase relative permeability.

$$k_{rg} = k_{rg}^0 S^{n_g} \qquad (3.7)$$

$$k_{ro} = k_{ro}^0 (1-S)^{n_o} \qquad (3.8)$$

where

$$S = \frac{S_g - S_{gc}}{1 - S_{gc} - S_{or}} \qquad (3.9)$$

k_{ro}^0, k_{rg}^0 are oil and gas relative permeability endpoints respectively.

3.7.5 Capillary number

As mentioned earlier, the magnitude of viscous forces in a system during flow is often expressed by a dimensionless group called capillary number, $N_{Ca} = \frac{v\mu}{\sigma}$. Capillary number signifies the ratio of viscous forces to capillary forces. A lot of work on the variation of relative permeability with capillary number has been done in gas and gas condensate reservoirs [Pope et al. (1998), Mott et al. (1999), Fulcher et al. (1983)]. Corey function was used for relative permeability and the coefficient was interpolated between miscible and immiscible limits. Others authors explicitly matched a capillary

number dependent correlation for relative permeability by basically fitting empirical correlations to experimental data. Fulcher *et al.* (1987) used linear regression to obtain the best-fit coefficient for equation and statistical parameters to evaluate the function. He represented relative permeability to gas by

$$k_{rg} = AS(B + C \ln \gamma)(\frac{\mu_g}{\mu_w})^D$$

(3.10)

Where A, B, C and D are fitting parameters.

For most two-phase systems, the parameters characterizing Equations (3.7) to (3.9) are constant. In their experimental studies, Kumar *et al.* (2002) varied the critical gas saturation, S_{gc} and end-point value of the gas relative permeability curve, k_{rg}^0 to match the experimental results. A similar approach is adopted in this work but only this time, the model internally adjusts the relative permeability according to the local capillary number. The relative permeability models used in this study have the following features.

1. The relative permeability of oil is not affected by change in N_{Ca}.

2. The relative permeability to gas is reduced with increased N_{Ca}. This is accommodated by expressing k_{rg}^0 as a function of N_{Ca}.

3. The critical gas saturation is increased as N_{Ca} increases.

Equations (3.13) and (3.14) describe the dependency S_{gc} and k_{rg}^0 on N_{Ca}.

$$S_{gc} = S_{gci} + aN_{ca}$$

(3.11)

$$k_{rg}^0 = k_{rgi}^0 - bN_{ca} \qquad N_{Ca} \le N_{Ca}^0$$

(3.12-a)

$$k_{rg}^0 = k_{rg}^0(N_{Ca}^0) - c\left[\ln\left(\frac{N_{Ca}}{N_{Ca}^0}\right)\right] \qquad N_{Ca} \ge N_{Ca}^0$$

(3.12-b)

Equation (3.11) suggests a linear dependence of S_{gc} on N_{Ca}. Equation (3.12-a) also suggests a linear dependence of k_{rg}^0 on capillary number for low values of capillary number ($N_{Ca} < N_{Ca}^0$). The constant N_{Ca}^0 is chosen as an arbitrary low value. For $N_{Ca} \geq N_{Ca}^0$ a logarithmic dependence is expressed by using Equation (3.12-b). Various forms of equations were tried out but only the logarithmic function gave a good match of the experimental results presented later in this chapter. The linear function (Equation (3.12-a)) combined with the logarithmic function (Equation (3.12-b)) was used to cater for the near zero and zero capillary number.

The linear behavior of critical gas saturation and the logarithm behavior of the Corey endpoint relative permeability values with depletion rate have been previously reported in literature [Kumar (2002)].

The advantages of using Corey type models includes:

1) Such functions are based on important aspects of relative permeability like turtuosity and non-conductive saturation. Hence the effect of capillary number can be translated directly to affect the coefficient.

2) It allows a plausible relationship between relative permeability and capillary number if no experimental data is available.

3) The approach allows separate relative permeability characteristic to change independently with capillary number.

3.8 Model development

By combining all the above equations, a one-dimensional two-phase flow simulator was developed. The primary simulation unknowns are pressure and saturation. The I.M.P.E.S formulation described above was used to obtain the unknowns at each time step. The code was developed in the C++ programming language.

3.9 Model validation

Two problems were considered for validating the two-phase flow model of this work. The first problem is a single-phase one and the simulator was validated against a known analytical solution. The second problem is a two-phase solution-gas drive problem and the solutions were compared with those obtained from CMG's black oil simulator IMEX^{TM}.

First Problem: A case of a one-dimensional single-phase flow is considered, where fluid is produced from one end at a constant rate, while the other end is closed. Starting from an initial uniform pressure, constant rate production results in a transient pressure disturbance that propagates through the system. At later times, when the pressure has propagated to the no-flow boundary a pseudo-steady state regime develops. The analytical solution to this problem is given by Ozisik (1993), and is represented by,

$$P(x,t) = P_i + \frac{\mu q}{Lk}\left\{\frac{kt}{\phi c_t \mu} + 2\sum_{m=1}^{\infty}\frac{(-1)^m}{(\frac{m\pi}{L})^2}\cos(m\pi\frac{x}{L}) \times \left[1 - \exp\left(-m^2\pi^2\frac{kt}{\phi c_t L^2}\right)\right]\right\} \qquad (3.13)$$

The derivation of equation 3.13 is shown in Appendix I (Section A.2). Figure 3.2 shows the pressure profile across the core at three different times. Figure 3.2 also shows that the pressure profiles as obtained from the model are in good agreement with the analytical solution.

Second Problem: In the second problem, depletion from a core saturated with live oil at an initial pressure above the bubble point pressure is considered. Fluids are produced at a constant rate of total fluid production under reservoir conditions. The rock and fluid properties are those used in the experiments of Kumar et al. (2002). These

properties are given in Table 3.1. Some of the other input data required for simulation are given in Table 3.2.
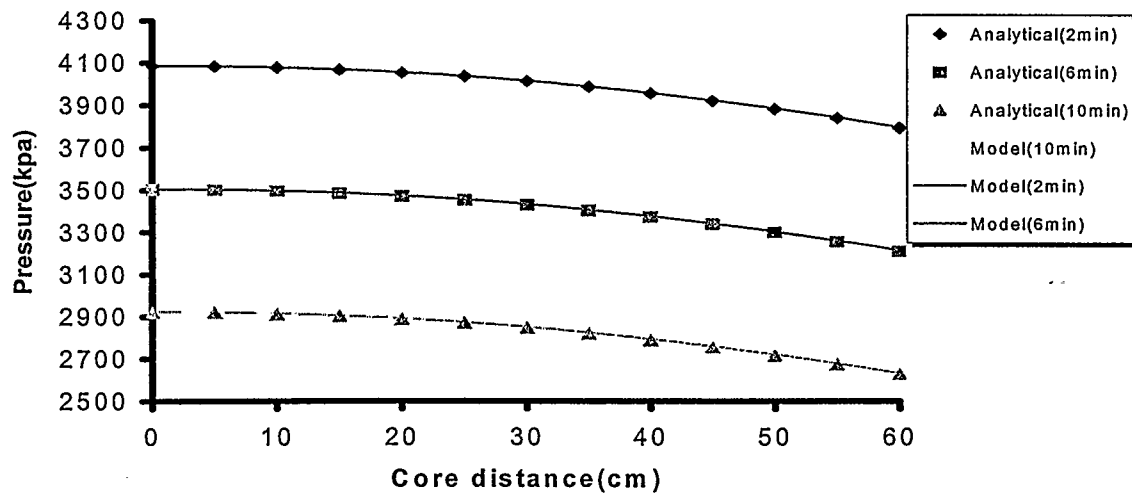
Figure 3.2 Validation with analytical solution

Table 3.1: Rock and Fluid Properties

Property	Value
Sand-pack compressibility	3.34×10^{-6} (kPa^{-1})
Operating temperature	25 Deg C
Specific gravity of oil	0.85
Gas Oil Ratio	15.57 v/v
Bubble point pressure	3962.4 (kPaa)
Connate water saturation	2.10%
Effective permeability	1.18Darcy
Porosity	38.60%
Dead oil compressibility	1.16×10^{-6} (kPa^{-1})

Table 3.2: Simulation parameters

Property	Value
Initial pressure (kPaa)	4275
Initial saturation	1
Formation Volume factor at bubble point (cm/scm^3)	1.046
Number of grids	100
Number of layers	1
Bubble point pressure (kPaa)	3965
Corey exponent, oil	2
Corey exponent, gas	1.5
Interfacial tension (dyne/cm)	25
Critical Capillary Number	5×10^{-7}
Residual oil saturation (%)	20
Core Length (cm)	60

The same input data were used in the model of this study and IMEX[TM]. The results are shown in Figures 3.3 and 3.4. Figure 3.3 shows the average pressure in the system as a function of fluid production or expansion. Figure 3.3 shows that the pressure declines fast initially while the fluid in the core is single-phase liquid. At bubble point pressure, the slope of the pressure decline curve reduces. Figure 3.4 shows the cumulative free gas production. Initially there is no free gas production while the gas saturation is building up to reach the critical gas saturation. Study of Figures 3.3 and 3.4 shows that the results obtained from our model are in close agreement with those obtained from IMEX[TM]. In the following section, we use the numerical model of this study to study the behavior of solution-gas drive in experiments that show rate dependency. These results have been recently reported by Talabi and Pooladi-Darvish (2002).
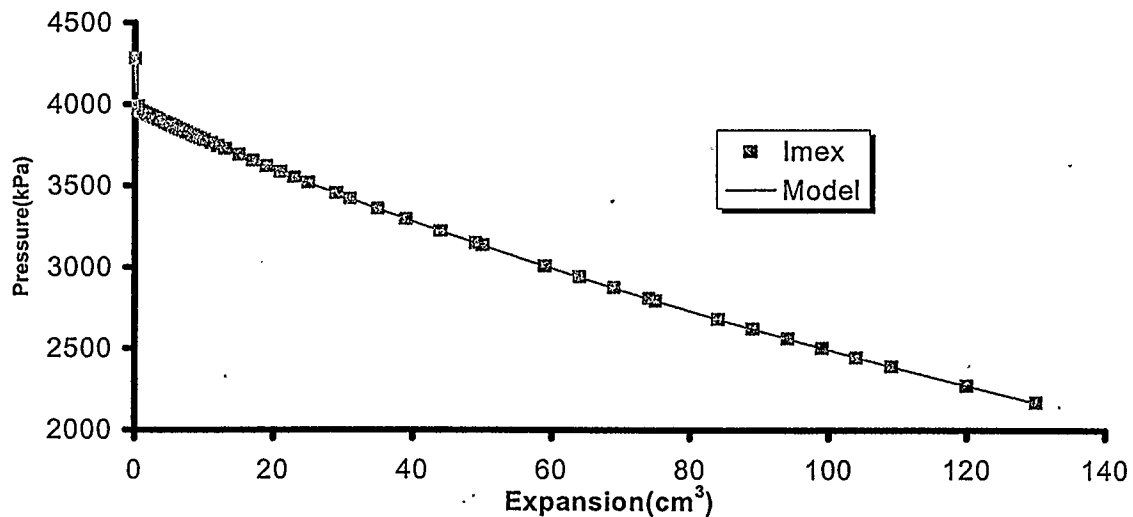
Figure 3.3: Validation with IMEX[TM] (Average pressure)
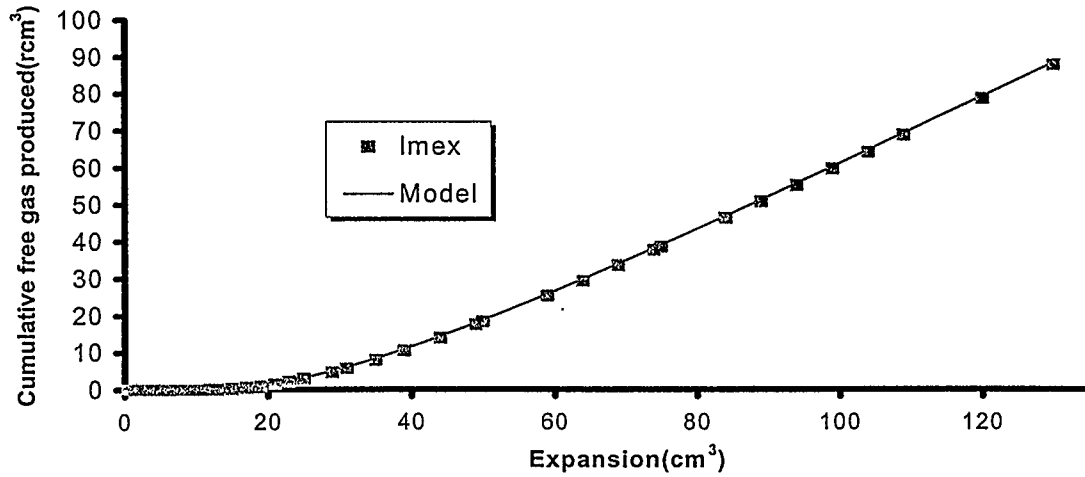
Figure 3.4 Validation with IMEX™ (Cumulative free Gas Produced)

3.10 Modeling solution-gas drive experiments

. In this section, the dependence of gas relative permeability on capillary number, the local velocity is calculated using the pressure and saturation values from the previous time-step. The local velocity and viscosity, along with an interfacial tension of 25 dynes/cm, were used to calculate the local capillary number. This was then used in equations 3.11 and 3.12a to evaluate parameters of a gas relative permeability function.

The developed numerical model was used to simulate depletion experiment where the effect of viscous forces has been reported [Kumar *et al.* (2002)]. The results are shown in Figures 3.5 through 3.7. The data includes the average pressure in the core, cumulative gas production and the average gas saturation in the core. Figure 3.5 shows the experimental and simulated average pressure in the core and the high-pressure separator. This figure indicates that, the average pressure from all the experiments

exhibits the same general characteristics. Pressure initially drops sharply, then rebounds after reaching a pressure minimum, and finally decreases with a small slope. The experimental data of Figure 3.5 shows that the average pressure is affected by the depletion rate. This is because in faster runs, gas evolution is less than the equilibrium values; the gas remains in the oil leading to reduced pressure. The simulation runs however do not show such behavior. The reason is that the model does not account for the supersaturation effects. The model accounts for rate effects on gas mobility, and by doing so will correctly model whether the gas is in the core or has been flown into the high pressure separator, but will not account for the extra gas remaining in the liquid due to supersaturation effects.

Figure 3.6 is a plot of gas saturation in the core as a function of fluid expansion and shows that gas saturation in the core is higher at higher rates. The simulation results predict a similar behavior. At higher rates, the capillary number is larger leading to higher S_{gc} and lower k_{rg}^0 from Equations (3.12) and (3.13). Lower gas mobility leads to higher gas saturation in the core and improved oil recovery. Figure 3.8 and 3.9 show the range of S_{gc} and k_{rg}^0 as a function capillary numbers obtained during the simulation runs. The values of capillary number for the three runs, using the total withdrawal rate, are given in table 3.3. The constant of Equations (3.12) and (3.13) are reported in Table 3.4. The critical gas saturation varied between 0.025 and 0.0365 for all the rates considered. The gas relative permeability was low (1×10^{-4}) even for the fastest local velocity. The Table 3.3 shows the various range of values obtained.

Figures 3.7 show the cumulative free gas produced at different rates. There is good agreement between the experimental and simulation results. Figure 3.10 shows the gas and oil relative permeability curves obtained in the grid-block at the production end for one of the runs. It can be observed that despite the variation of relative permeability with

both saturation and capillary number, the curves are smooth and monotonous functions of gas saturation. Furthermore, Figure 3.10 shows that for gas saturation as high as 9%, the relative permeability to gas is less than 1.2×10^{-4}. Figures 3.5 to 3.7 suggest that the model suggested in this work with a capillary number-dependent relative permeability can match the experimental data and show the rate-dependent behavior of solution-gas drive. In Chapter five, a similar equilibrium model is used to simulate experiments in which oil viscosity and depletion rates are varied. The relative permeability is allowed to vary with a more general term defined later.

Table 3.3: Summary of Results

Expansion rate, (cm^3/hr)	Maximum capillary number	Critical gas saturation, %	End point value
0.08	4.65165E-07	2.53	0.00895
0.37	2.15139E-06	2.63	0.00662
3	1.74437E-05	3.55	0.00453

Table 3.4: Correlation constants

Parameter	Value
N^0_{ca}	5×10^{-7}
S_{gci}	0.025
a	600
b	2.5×10^4
c	0.001
k^0_{rgi}	0.020582
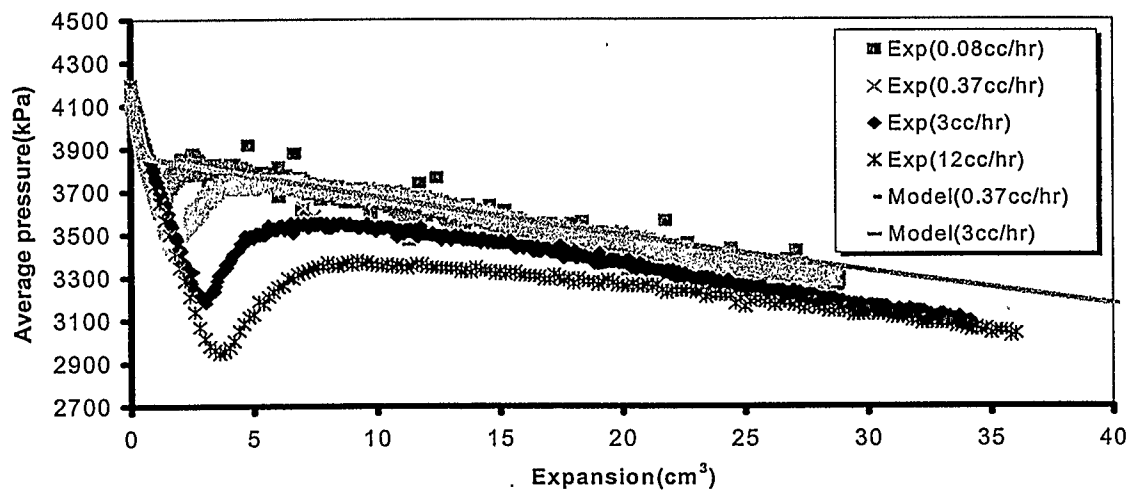
Figure 3.5 Match of Experimental data (Average pressure)
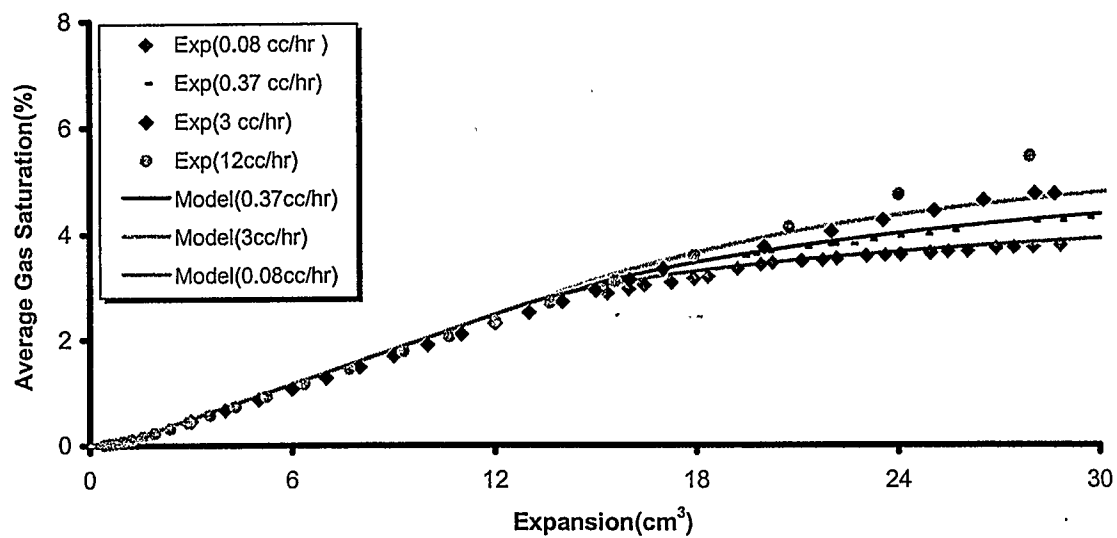
Figure 3.6 Match of Experimental data (Average gas saturation in the core)
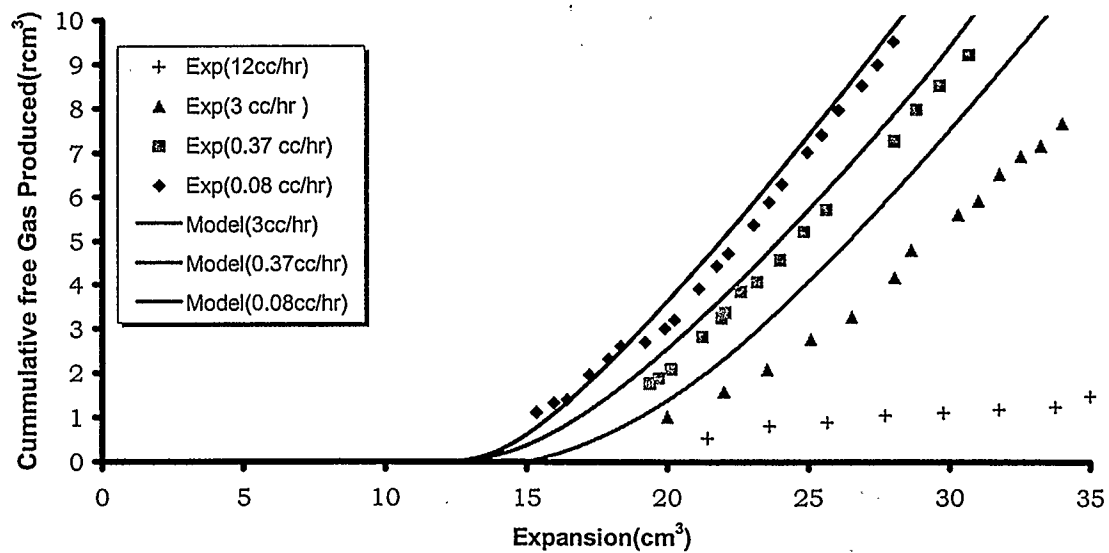
Figure 3.7 Match of Experimental data (Cumulative free gas produced)
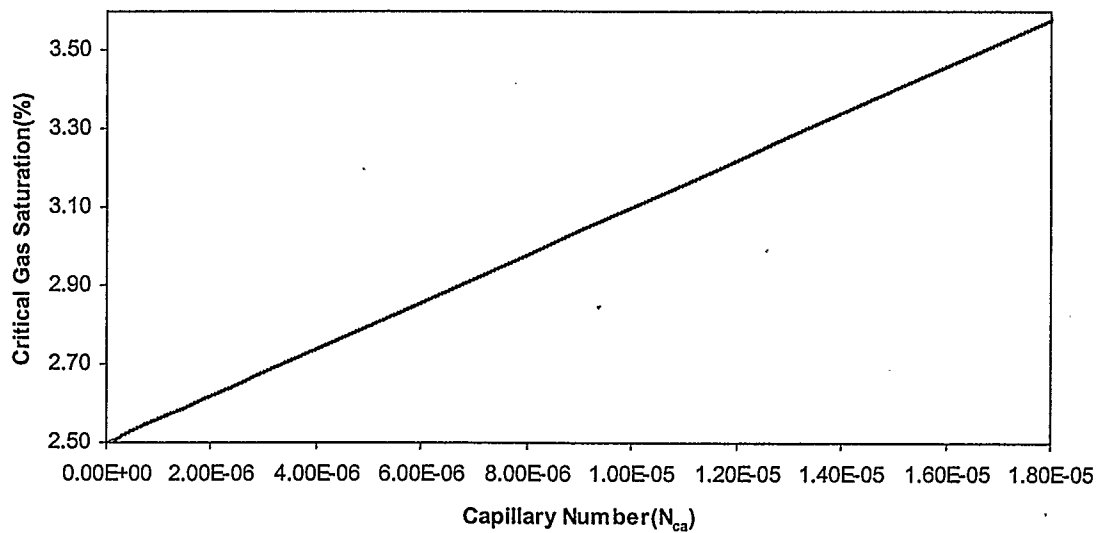
Figure 3.8: Critical gas saturation as a function of capillary number
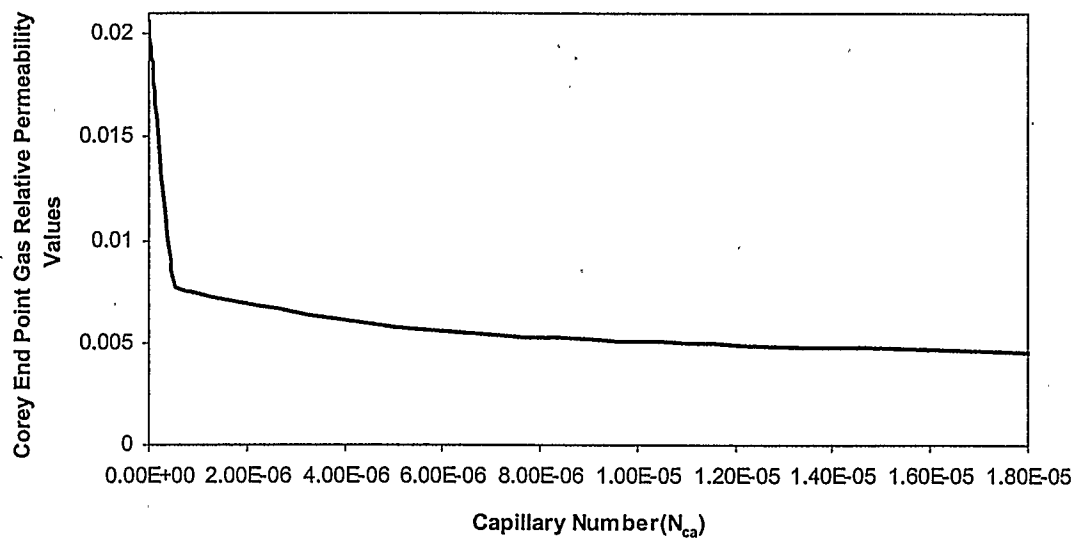
Figure 3.9: Endpoint relative permeability as a function of capillary number
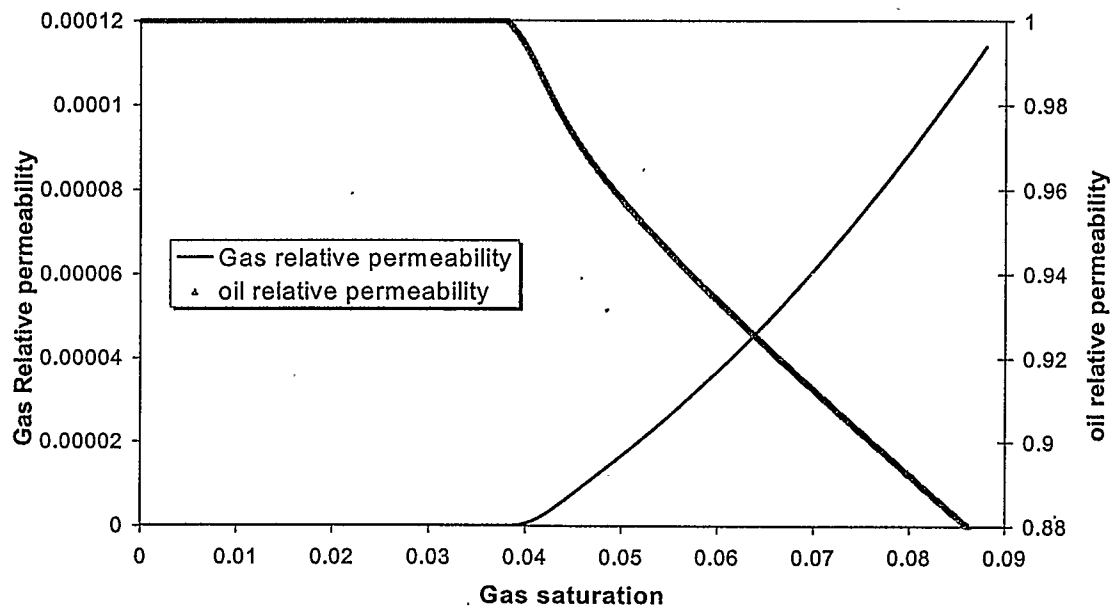
Figure 3.10: Gas and oil relative permeability (expansion rate of 3 cm³/hr)

3.11 Limitations of model

1) The model constants are specific to the systems considered. This constant changes from system to system. These constant are obtained from a match of one of the runs and the other matches are automatically determined from the correlation constants.

2) The experimental data used in this chapter did not consider changes in interfacial tension or oil viscosity. As such, the dependence of gas mobility on capillary number was not fully investigated. In Chapter 5, a more general term will be used to account for the effects of rate and oil viscosity.

3) In the model, the effect of the depletion rate on the early time processes of nucleation and growth was accounted for by allowing the critical gas saturation to vary with depletion rate. A more detailed mechanistic model may be more representative of the system.

GAS MOBILITY MEASUREMENTS

4.1 Introduction

As described earlier, one of the plausible explanations for the high recoveries observed in heavy oil reservoirs is low gas mobility. Depletion experiments were conducted in a sand-pack and the gas mobility was determined. In this section, the experiments involved in the measurements of gas mobility during solution-gas drive in heavy oil are described.

4.2 Experimental setup (Overview)

The experimental setup is similar to that used by Kumar *et al.* (2002). It consists of a multiple pressure port core holder, which encases a sand-pack; a gas separator system and an overburden and axial pressure system. An ISCO pump is used for depleting the core and another one for maintaining a constant overburden pressure on the core. The live oils used in the experiments were prepared using the live Oil Recombination Unit (L.O.R.U.). Fluid was withdrawn from the core through the gas oil separators. A camera system operated by Megawave™ video software was used to record the volumes of fluids in the gas oil separators while a Labtech™ notebook was used to log data from pressure transducers and thermocouple. The core holder was rotated to exclude gravity segregation. The core holder and the gas oil separator were placed in a constant temperature air. The schematic diagram of the experimental setup is shown in Figure 4.1. A more detailed diagram is given in Appendix II. The next section describes in details of the individual components in the setup followed by the experimental procedure.

Differential pressure gauge
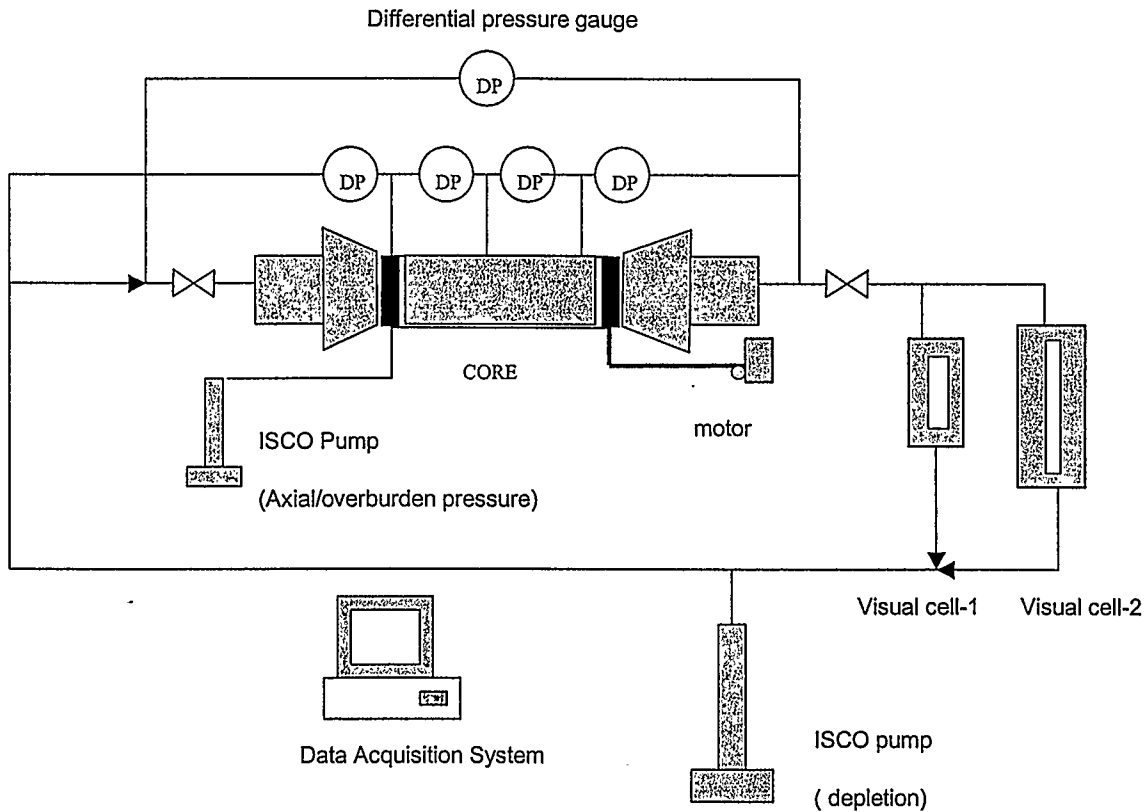
Figure 4.1: Schematic diagram of the experimental setup

4.2.1 Gas oil separators

These are high-pressure titanium vessels with long visual windows on both sides so that the gas oil interface is clearly visible for production measurement. There are two gas oil separators used in these experiment, a small cell with 10 cm^3 volume and a large one with 190 cm^3 volume. Both are connected to a three-way valve to allow switching between the two cells. In the large visual cell, water was used as the withdrawal fluid to minimize the volume of live oil outside the sand pack. This ensures that almost all the gas collected was from the sand-pack (pore volume = 490cm^3) and negligible amount

was generated from the oil in the visual cell (pore volume = $10cm^3$). Figure 4.2 shows the gas-oil separators.
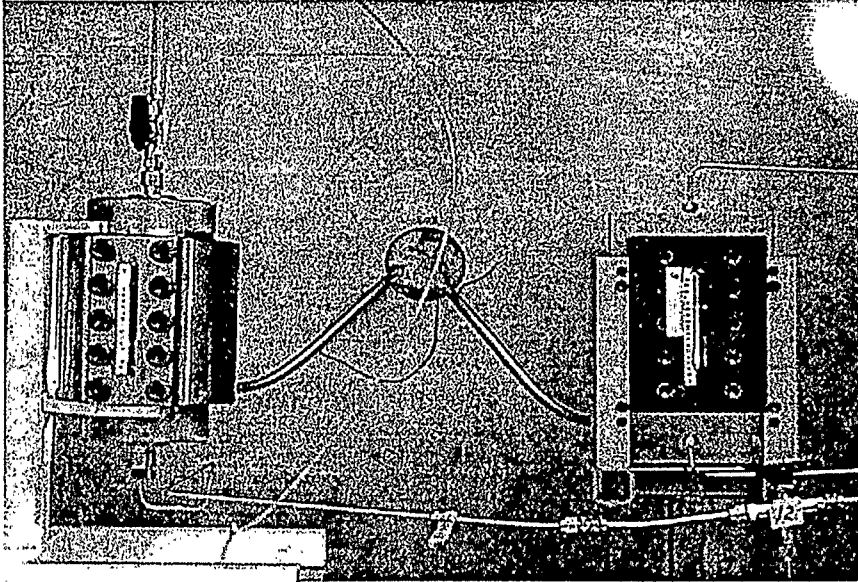
Figure 4.2: Gas oil separators

4.2.2 Live-oil recombination unit (L.O.R.U.)

The live oil recombination unit consists of two oil pressure vessels, a gas pressure vessel and a circulating pump. The two oil vessels have volumes of 1 liter and 4liters while the gas vessel has a volume of 0.5liters. The 1liter-pressure vessel was used as the oil-gas mixing chamber. It was packed with chain to increase the surface area of contact between the oil and the gas. The 4-liter pressure vessel was used as the live oil storage when the live oil recombination was complete. The gas vessel was used to temporarily store gas to be used for the recombination. As a safety feature, the L.O.

R.U. was equipped with pressure relief devices. The principle involved in the recombination is simple; the oil, which is in contact with the gas in the 1-litre-pressure vessel, is circulated in the setup at the desired saturation pressure by the circulating pump until there was no more dissolution of gas in oil. Figure 4.3 shows the "live oil recombination unit". Before the new oil was used, toluene was circulated through the unit in order to clean the L.O.R.U. Nitrogen was later used to dry the unit. The unit was then put under vacuum for 24 hours. The other steps for recombining oil are stated in the manual.
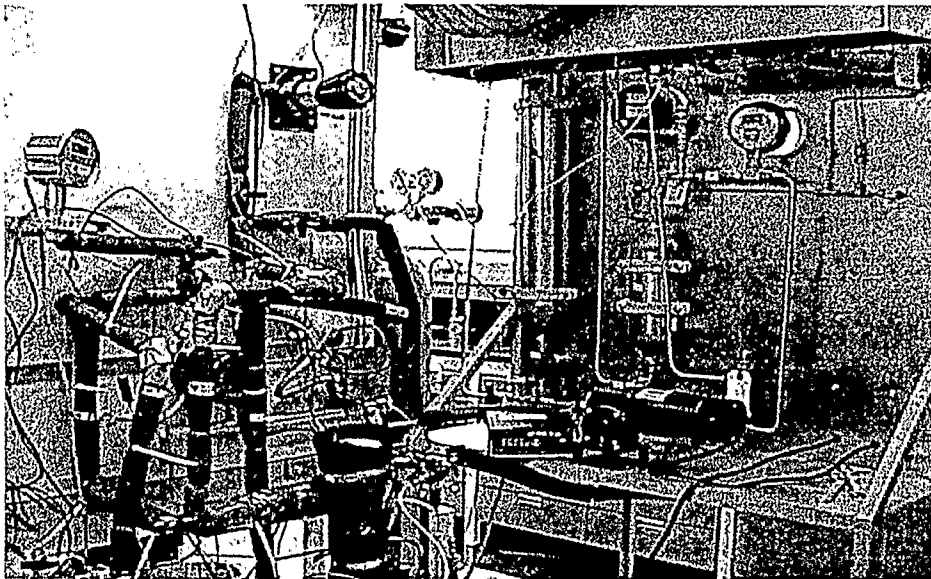
Figure 4.3: Live oil Unit

4.2.3 Axial and overburden pressure

The axial and overburden pressure system comprise of an ISCO pump, a hand pump and a backpressure regulator. The hand pump was used to build up the pressure during start up. Water was used as the overburden / axial pressure medium. By using the hand pump, the pressure was built in steps of 100psi up to the desired overburden / axial pressure. At the desired overburden pressure, the ISCO pump was run at a

constant pressure mode. The ISCO pump adjusted the rate of injected water in order maintain a constant axial and overburden pressure during depletion.

4.2.4 Core properties and sand properties

The sand used for the depletion experiments is white water wet sand. The grain size distribution of the sand was between 50 and 75 μ m. The property of the sand-pack is given in Table 4.1. The core was packed in such a way that a thin layer of coarse grain was used at either end when packing the sand. This was done so that a screen larger than the grain size of the sand-pack can be used and yet migration of the sand into the outlet stream is avoided. The larger screen size prevents buildup of gas at the outlet due to trapping of gas bubbles.

4.2.5 Core holder

The core holder is made of titanium and encases the viton sleeve that contains 60cm long sand-pack. There are 3 pressure taps in the core holder connected to pressure transducers to measure differential pressure in various parts of the sand-pack. The picture of the core holder is shown in Figure 4.4. To avoid any gravity effects, the core was rotated. For this purpose, the core holder is mounted on a swivel joints on both ends. A DC motor with gear box having a gear ratio of 15125:1 was attached to rotate the core holder approximately 180 degrees every 30 minutes.

Table 4.1: Core and sand properties

Length of Sand-pack	60cm
Pore volume	490 cm^3
Porosity	38.85%
Absolute permeability	1.5 Darcy
Effective permeability	1.4-1.45 Darcy
Connate water saturation	3%
Sand grain size	50-75 μm
Overburden / axial pressure	7.96×10^3 kPaa
Total Compressibility of the system with Overburden pressure	25×10^{-6} psi^{-1}
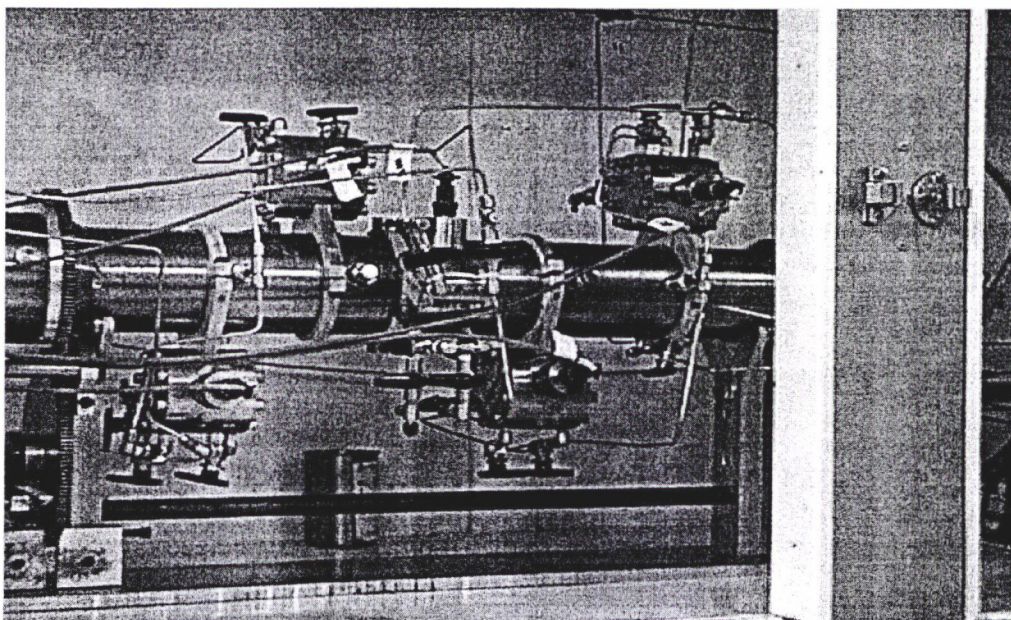
Figure 4.4: Core holder

4.2.6 Over-pressure controls

The system was equipped with proportional relief valves set at various pressures depending on the maximum operating pressure and the design pressure of the equipment and pipefitting. The ISCO pump control software has an inherent feature through which the safety pressure was adjusted. The outlet of the pumps was equipped with pressure relief device to ensure additional safety. All the pressure safety valves were set at proper relieving pressure by flowing fluid through using a Quizix pump. The overburden pressure and recombination system was also equipped with pressure relief valves.

4.2.7 Data acquisition and control

A Labtech™ notebook software was used for temperature and pressure data acquisition from the various pressure transducers and thermocouples. A program was written to acquire required data and display it on the screen in tabular as well as graphical form. This data was also logged into a file. This log file was analyzed using Microsoft Excel.

4.2.8 Temperature controls

The fluids used in this experiment have small compressibility so temperature fluctuations affect the pressure significantly. A constant temperature bath was necessary for the experiment. A big cabinet housing the core holder equipped with temperature controller was used as an air bath. A temperature controller acting on an in-car heater that was placed in the oven controlled the temperature in the smaller blue M oven. Both ovens were equipped with circulating fans to ensure homogeneous temperature across the oven. A similar controller acting on a heating tape wound around the pump barrel is

used to control the temperature of the fluids in the ISCO pumps. The pump barrel was later insulated to prevent heat loss. The lines were all insulated to prevent heat losses. All temperature controllers were equipped with over temperature control, which shuts down the system if the temperature exceeds a set safety temperature.

4.2.9 Pumps

There are four pumps used in this setup altogether. Two ISCO pumps, a circulating pump and a Quizix pump. The ISCO and the Quizix pumps are positive displacement pumps. The Quizix pump was used for water injection while one of the ISCO pump was used for the fluids withdrawal from the core and the other was used for maintaining overburden pressure on the core. The ISCO pumps have a capacity of 500 cm^3 each while the Quizix pump has a volume of 20 cm^3. The circulating pump was used to circulate oil during the recombination of live oil. The circulating pump has a multiple speed controller. The volumetric rate of the circulating pump was calibrated with the pump speed

4.3 Fluid data

The oils used in the depletion experiment are methyl silicone oils of various viscosities. Table 4.2 shows the various properties of the different oils: oil A, B, C. Nye Oils limited provided these oils.

Table 4.2: Oil Properties

Property	Oil A	Oil B	Oil C
Kinematic viscosity at 25°C, cS	1000	10,000	30,000
Specific gravity at 25 °C	0.971	0.975	0.975
Surface tension at 25 °C, dyne/cm	21.2	21.3	21.5
Live oil viscosity at 25 °C, cp	580	5680	21600
GOR scm^3/scm^3	23.2	22.3	22.8

It can be observed that oils have very similar properties except for their viscosities.

4.4 Experimental procedure

This section describes the procedures before and during the experiments. It starts with the preparatory procedures employed before the depletion runs and later describes the steps used while running the actual depletion experiments.

4.4.1 Preparatory steps

4.4.1.1 Vacuuming of pumps /system /sand-pack

After the sand-pack and all the fittings had been connected, a vacuum pump was used to draw vacuum on the whole system. A catch pot, positioned before the vacuum inlet, was kept in dry ice to achieve such a high vacuum.

4.4.1.2 Leak test

Once all the piping and core holder was set in place, the system was leak tested. For the piping, this was done by isolating a section of piping, pressuring it up with water and observing the pressure in each section, under isothermal conditions. No pressure

drop with time will indicate a leak free system. The leak test of the L.O .R .U was done separately from the depletion setup using the same principle.

4.4.1.3 Brine preparation

A sample of NaCl was dissolved in de-ionized, de-aerated water to form the 1-% brine solution. Brine was used for the connate water and also for absolute permeability determination.

4.4.1.4 Hydro-testing

All the vessels and fittings in the recombination unit as well as the depletion unit were tested to 1.5 times the maximum operating pressure in the system. This was done to authenticate the integrity of the vessels and avoid any leakage or failure of the vessels during the experimental run.

4.4.1.5 Calibration of pressure transducers

The absolute pressure transducers and digital pressure gauges were calibrated using a dead weight tester. The Sensotech differential pressure transducer was calibrated using the method described in the manual. The range of measurement of differential pressure transducer is 10-15psi for the smaller gauges and 100-144psi for the large gauge. The differential pressure transducer was designed to operate with liquid on both sides, so it was made sure that both chambers were free of air by filling it with bayol using a hand pump in such a way did this that the bayol displaces any trapped air.

4.4.1.6 Calibration of gas oil separators; Camera calibration

The gas and oil produced from the core was separated in the visual cell. The amount of gas and oil produced was determined by measuring the oil-gas interface. So it was necessary that the visual cells be calibrated. The height of the interface was measured by a camera, which was mounted outside the oven. A Megawave™ software was connected to this camera and the interface at any time was recorded. A high intensity light was thrown from a rear window of the visual cell, which facilitated the measurement of gas–oil interface in the visual cell. The visual cell was then calibrated with the Quizix pump. The calibration was done by recording the level of the interface at different time against the volume of fluids injected by the Quizix pump. Figures 4.5 and 4.6 show the plot of the volume of fluids injected with the height for both visual cells.
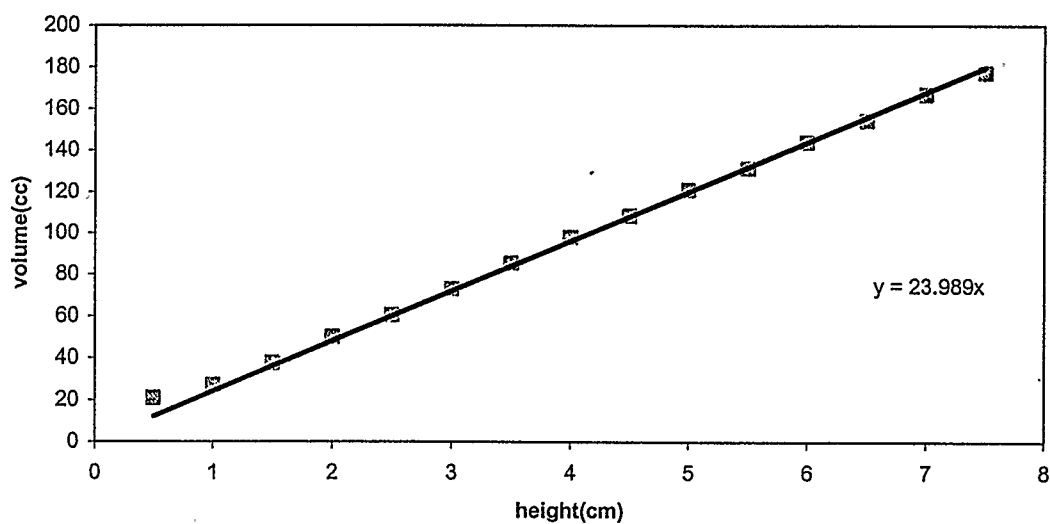
Figure 4.5 Large visual cell calibrations
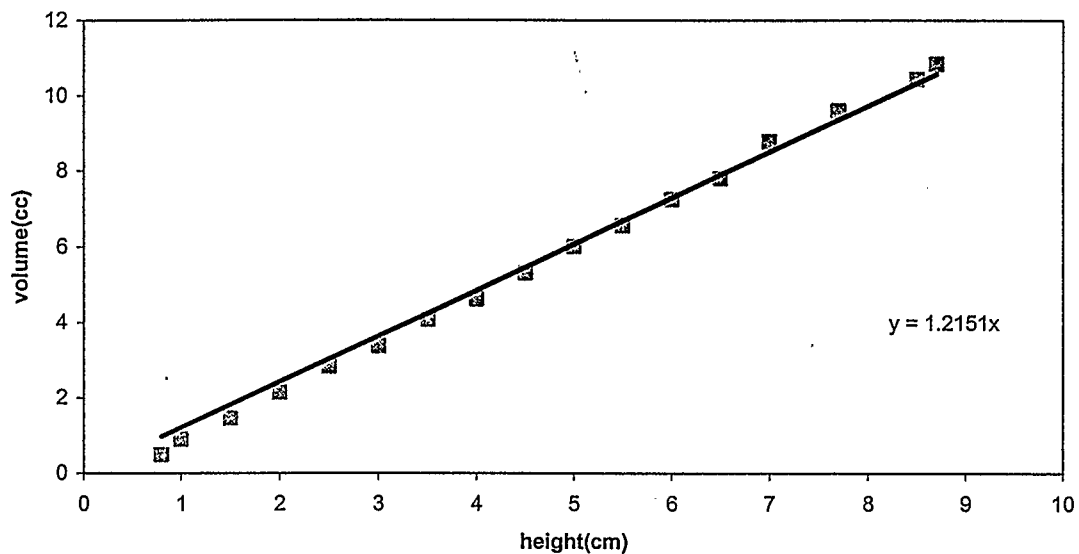
Figure 4.6 Small visual cell calibrations

4.4.2 Other procedures

Other preparatory procedures were also carried out to determine rock and fluid properties beside calibration of equipments. These procedures are discussed below.

4.4.2.1 Volume measurement by water

After the system was put under vacuum for a long time, water was introduced into the system by pumping using the Quizix pump. To measure the volume in each section of piping, water was introduced into the system section by section; isolating a particular section from the rest of the vacuumed system by closing the valve. Once a particular section was filled with water, the pressure was raised to 100psig. The difference in the volumetric reading indicated the volume of that section. The sand-pack was bypassed in this stage.

4.4.2.2 Porosity and absolute permeability measurement (saturating the core)

Next, the vacuumed sand-pack was flooded with brine to measure the pore volume and hence the porosity of the sand-pack. The measured pore volume was 490 cm^3. Once the sand-pack was flooded with brine, the valves connecting the pressure transducers were opened. Brine was flowed through the sand-pack at a known rate and the pressure drop across the core was measured to determine the absolute permeability. This was done at several flow rates. The result is shown in Figure 4.7 The Darcy
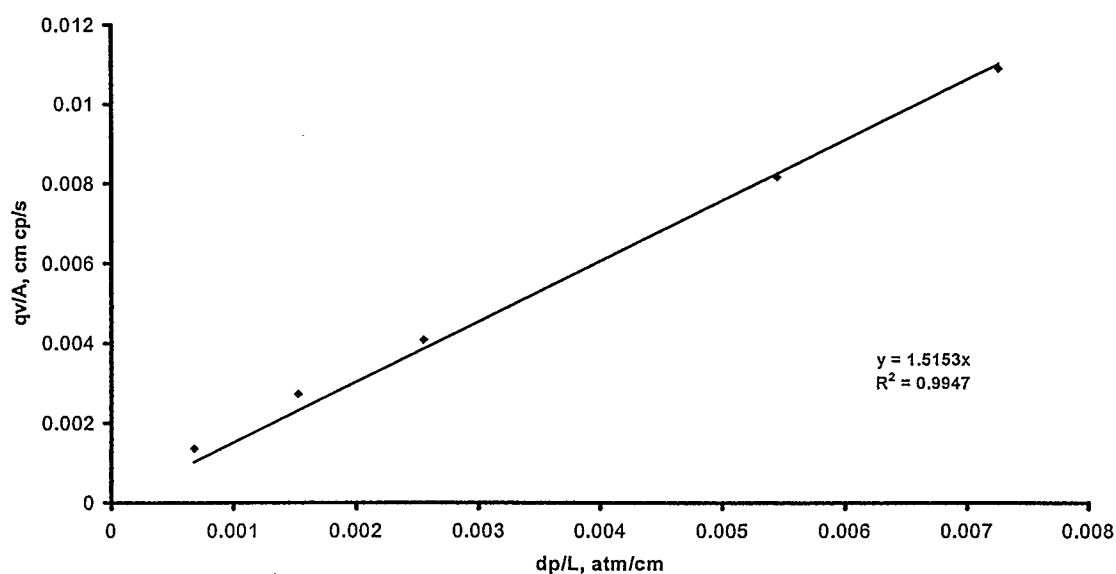
Figure 4.7: Absolute permeability with brine

equation was used to determine permeability value. The absolute permeability was about 1.5 Darcy.

4.4.2.3 Connate water saturation and effective permeability measurements (flooding with dead oil).

Once the sand-pack was flooded with brine and the absolute permeability determined, dead oil A of 1000cS viscosity was initially used to displace the water. The dead oil was injected until no additional water was produced. The oil and the water volumes were measured and the connate water saturation in the sand-pack was determined from material balance calculations. Once the inlet piping into the core holder and the sand-pack was flooded with dead oil, the dead oil was flowed through the sand-pack at a known flow rate and the differential pressure across the core was measured to determine the effective permeability of the sand-pack. This was done at various rates to get an average permeability value. This is repeated for all the three oils used in the study. The sequence for determination of effective permeability was displacing the lower viscosity oil with one of higher viscosity. An about two-pore volume of the displacing oil was needed for each displacement process. Figures 4.8 and 4.9 show the results of the effective permeability measurements. It was observed that the higher the viscosity, the higher the permeability observed.
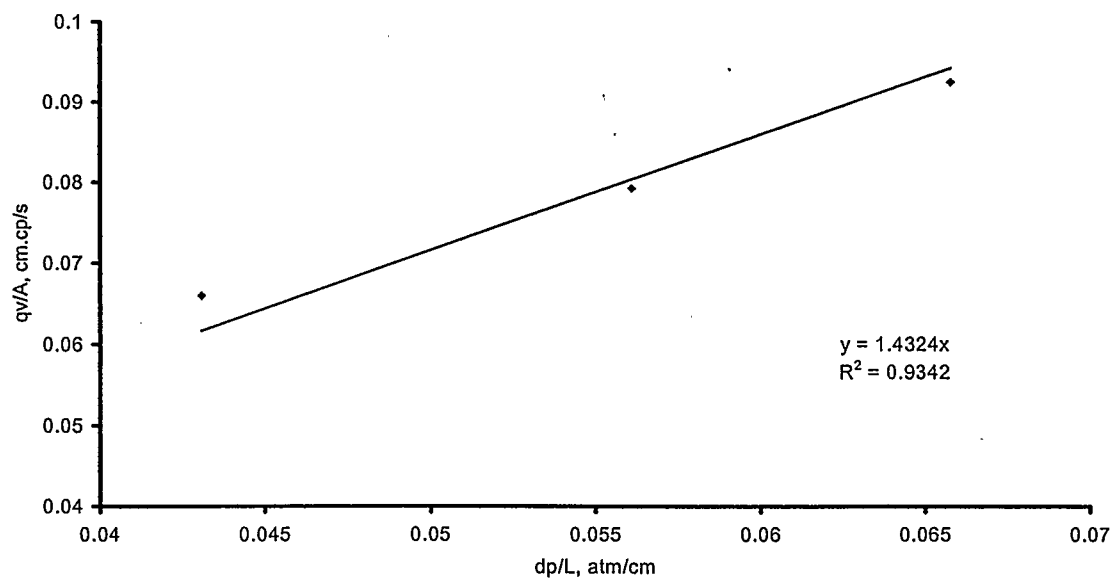
Figure 4.8: Effective permeability Dead oil = 1000cS
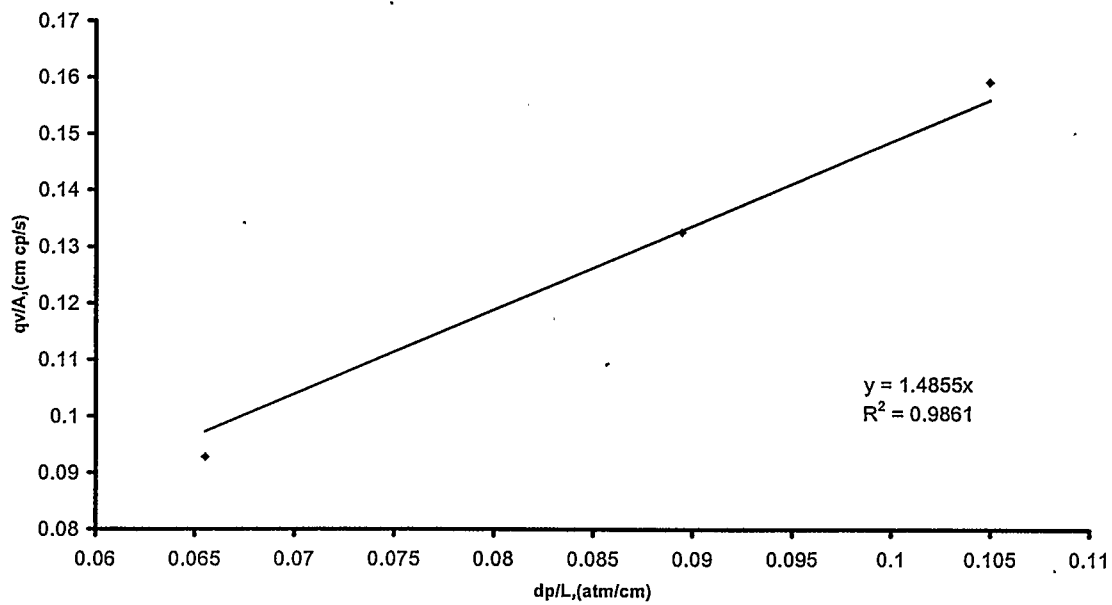
Figure 4.9: Effective permeability Dead oil = 10000cS

4.4.2.4 Gas oil ratio measurement

The GOR of the live oil from the L.O.R.U. and the outlet of the core need to be determined. The gas oil ratio of the live oil was determined by taking live oil sample through a backpressure regulator into a flask whose outlet was connected to an inverted glass graduated cylinder filled with water. This was done to collect the gas produced in the inverted cylinder by bubbling it over water. The weight of the flask was measured to determine the oil volume. More time was allowed for equilibrium for the higher viscosity oils. The quantities were then brought to standard conditions to calculate the gas oil ratio. Figure 4.10 shows the setup.
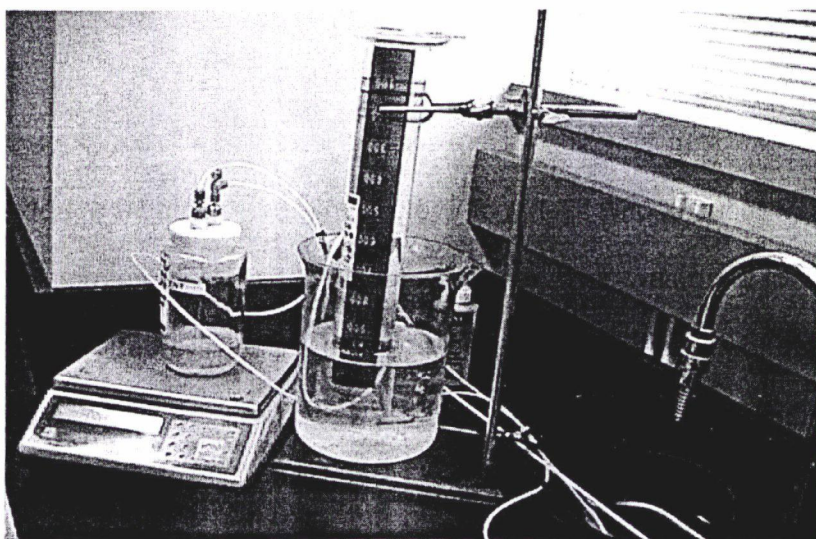
Figure 4.10: GOR measurement setup

4.4.2.5 Gas oil ratio curve

A setup was prepared to obtain the Rso curve for the oil and is shown in Figure 4.11. The cylinder was first filled with methane gas to a pressure equal to the bubble point of live oil. A know volume of dead oil was then injected into the cylinder with the ISCO pump. The dead oil and the gas were then thoroughly mixed at the desired bubble point pressure. The system was then stabilized for 24 hours. The pressure in the cylinder was then lowered, by bleeding off methane into the gas cylinder. The pressures in both cylinders were allowed to stabilize. The resultant pressure in the cylinders was an indication of the gas left in respective cylinders. This value was then used to calculate the solution gas oil ratio at various pressures. The Rso curves obtained for the different oils are shown in Figure 4.12 and demonstrates similar values for oils A and B. Due to the high viscosity of Oil C, it was difficult to use this setup to obtain the bubble point curve for this oil.
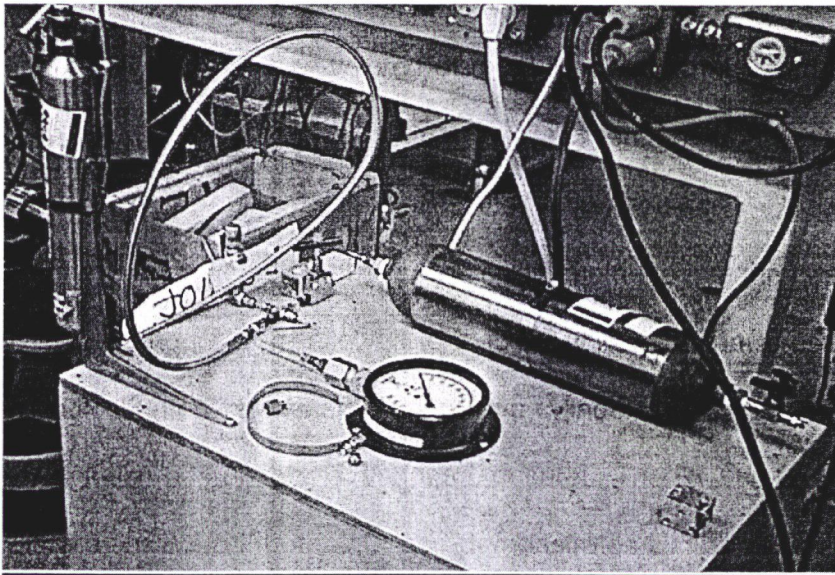
Figure 4.11: Rso setup
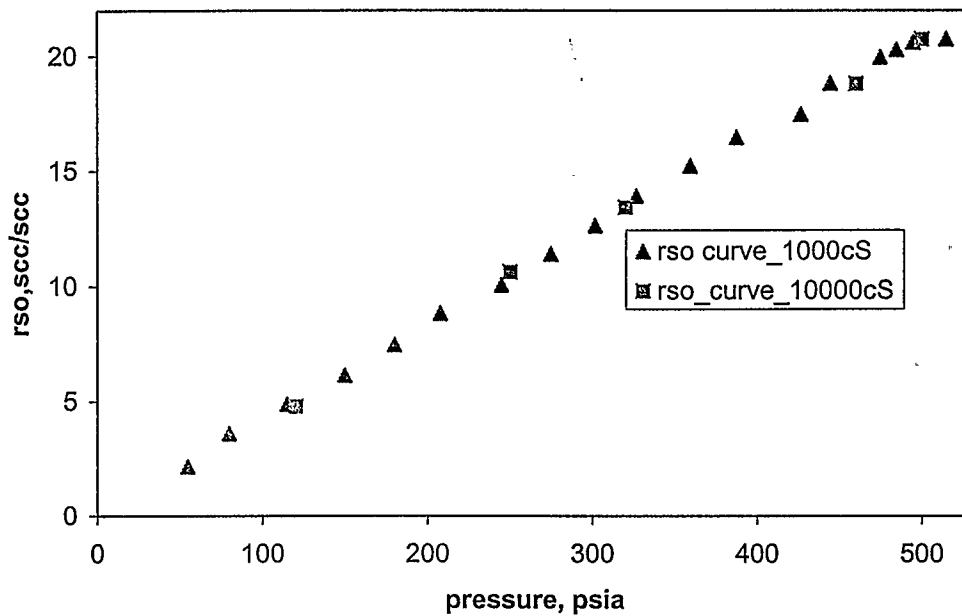
Figure 4.12: Bubble point curves

4.5 Viscosity measurements

4.5.1 Viscosity loop calibration

The viscosity of the live oil was measured inline during floods. This was done by measuring the pressure drop in a certain section of a coiled tube and then calculating viscosity using the Hagen-Pouislle equation [McCabe, Smith and Harriot (1990)] for flow through pipes which is expressed as

$$\Delta P = \frac{4\rho L f u^2}{2D}$$

(4.1)

where f is the friction factor. For laminar flow, $f = \dfrac{16}{Re}$. Re is the Reynolds's Number and

$$Re = \frac{Du\rho}{\mu}.$$

(4.2)

Substituting this in equation 4.1 and simplifying we get

$$\mu = \left(\frac{\pi D^4}{128L}\right)\frac{\Delta P}{q} \qquad (4.3)$$

Here, the initial part of the RHS in the bracket is a constant and depends on the geometry of the flow loop (geometric factor). This constant was determined by calibrating the flow loop with fluid of known viscosity viz: water and the three dead oils. These were flowed through the loop and the pressure drop across the loop was measured. Knowing the viscosity, this data was then used to determine the geometric constant of the loop for the oils of different viscosity at the experimental temperature. Figure 4.13 shows the calibration of the viscosity loop with dead oil A to obtain the geometric factor. The geometric factor obtained from the three oils A, B, and C was 0.0525, 0.06 and 0.08 for oils A, B and C respectively.
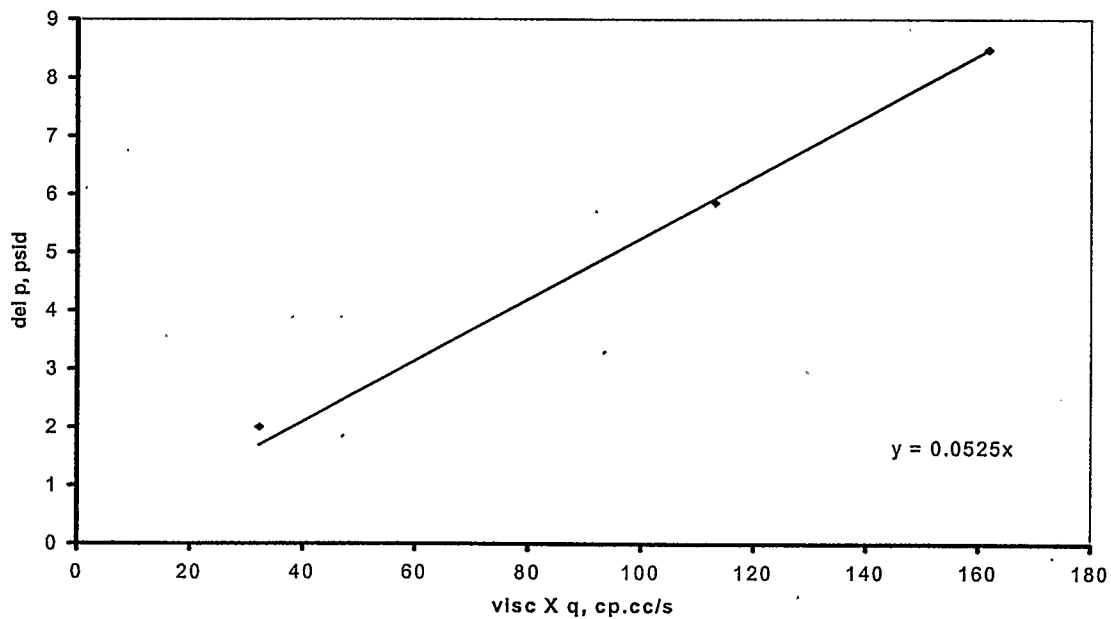
Figure 4.13: Calibration of viscosity loop (dead oil A) at 25C

4.6 Dead oil compressibility

Compressing the oil in the ISCO pump cylinder and recording the pressure vs. volume data was used to determine the compressibility of the dead oil. The data was then plotted on a graph and the slope of the line was used to calculate the compressibility using the formula. The P-V curve for the determination of the dead oils is shown in Figure 4.14. The average of dead oil compressibility value was about 9×10^{-6} psi^{-1}
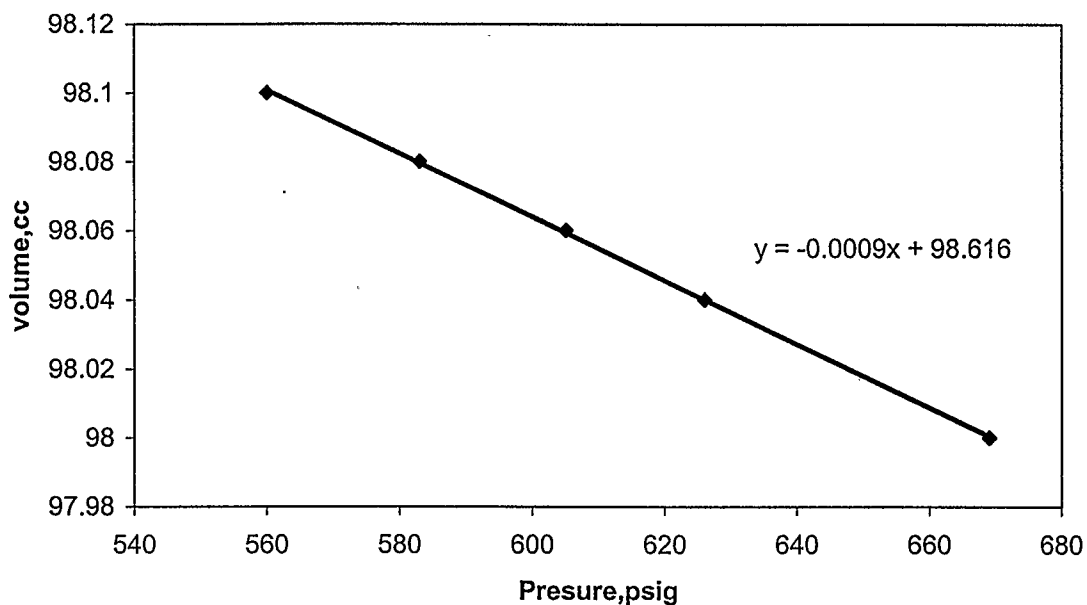
Figure 4.14:Oil A dead oil compressibility

4.7 Live oil compressibility

Once the live oil was prepared, it was transferred into a transfer vessel and later transferred into the ISCO pump. The compressibility of the live oil was measured using a similar procedure as the as that used for the dead oil. The average value was about 10×10^{-6} psi^{-1}.

4.8 Sand-pack compressibility

The compressibility of the sand-pack was measured using dead oil in a similar way. The inlet of the core was connected to a pump and the outlet was closed. The fluid was then injected into the core and the pressure versus volume injected was recorded and plotted. The slope as usual gave the compressibility of the system (sand-pack and live oil).
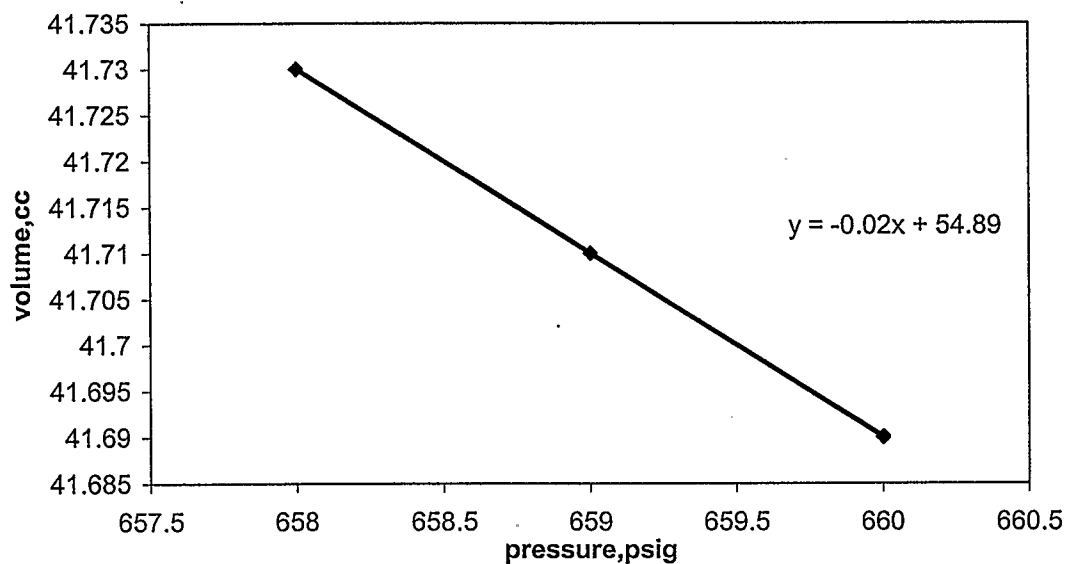
Figure 4.15: Total compressibility of the sand-pack and oil

Figure 4.15 shows the combined sand-pack and oil compressibility. The calculated sand-pack compressibility using oil A is about $25 \times 10^{-6} psi^{-1}$.

4.9 Live oil injection

Once the system was flooded with dead oil and the ISCO pump was charged with live oil, the next step was to inject live oil into the system. Injecting live oil into the

core displaced the dead oil. The displaced oil was produced through a backpressure regulator. The pressure of the backpressure regulator was set above the bubble point pressure of the live oil. This was done to ensure that pressure is above the bubble point pressure and a second phase is not generated in the system. Samples were drawn from the produced oil periodically and GOR was measured. It was assumed that all of the dead oil was displaced when the GOR of the produced oil became equal to the GOR of the live oil being injected. This required flooding of about 1.5 to 2.5 pore volumes of live oil.

4.10 Running experiments

4.10.1 Depletion runs.

Once the sand-pack is filled with live oil and pressurized, it was ready for depletion. The ISCO pump was operated at constant flow refill mode. The oil was withdrawn initially into the pump through the smaller visual cell. The inlet to the visual cell is from the top and the outlet is from the bottom. When the smaller visual cell is half filled up with gas, the withdrawal was conducted through the larger visual cell. The depletion was done at rates of 0.37 and 3 cm^3/hr for each of the oils. Before the start of a new run, the core was thoroughly flushed with about 2 pore volumes of dead oil and then two pore volumes of live oil at pressure higher than the bubble point. This was done, to guarantee complete dissolution of the gas into the oil. Once this was done, the system was left for 24 hours and pressure was recorded to ensure that there was no free gas dissolving into the oil. Presence of free gas is reflected by fall in pressure in sand-pack. The compressibility of the sand-pack was also measured before start of run to ensure single phase in the sand-pack.

4.10.2 Production measurements

The critical gas saturation is marked by sustained gas production in the visual cell. After reaching critical gas saturation, produced free gas starts to accumulating at the top of the visual cell. The small size of the small visual cell minimizes the dead volume and ensures that the gas being accumulated is coming from the sand-pack rather than being generated from the oil in the visual cell. The amount of free gas produced was measured with the camera by recording the oil-gas interface. The run was stopped after depleting the sand-pack to a certain volume. All other parameters were recorded viz: temperatures, pressures, differential pressures etc. were recorded on the Labtech™ notebook.

RESULTS

As discussed in Chapter 1, solution gas drive in heavy oils has shown high recovery and one of the possible explanations for this abnormal high recovery is low gas mobility. This chapter reviews the results of the gas mobility experiments conducted in the last chapter particularly, studying the effect of depletion rate and viscosity on gas mobility.

5.1 Introduction

As described in Chapter 4 depletion experiments were conducted on a linear sand-pack. Oil A (1000 cS) was used in Runs 1 and 2, Oil B (10,000 cS) in Runs 3 and 4, and Oil C (30,000 cS) in Runs 5 and 6. Odd-numbered and even-numbered Runs were performed at depletion rates of 0.37 and 3 cm^3/hr, respectively. Run 3-b is reproducibility Run using Oil B (10,000 cS) at 0.37 cm^3/hr. The gas production and pressure drop across the core were measured. From these measured values, gas mobility and critical gas saturation were estimated. This chapter examines the experimental observations and analysis of these results. The experimental data examined includes the average pressure in the core, cumulative gas production, the average gas saturation in the core and the pressure drop across the core. Table 5.1 shows the summary of results for the various runs.

Table 5.1. Summary of experimental results

Run #	S_{gc}, %	Final recovery, %	Depletion index $\times 10^8$ $m^2 s^{-1.5}$
1	0.2	3	0.12
2	2.5 ± 0.5	5.5	0.97
3	1.8 ± 0.2	3.2	0.37
4	5 ± 1	12.6	3.02
5	2 ± 0.5	5.1	0.73
6	5 ± 1	14.8	5.89

The next section looks at the reproducibility run followed by the discussion of the overall pressure and production response for all the runs. Sections 5.4 through 5.6 examine the effect of viscosity and the effect of depletion rate. Section 5.7 discusses a methodology for analyzing the combined effect of rate and viscosity. The last section describes the simulation of experimental results using commercial reservoir simulator software as well as the one-dimensional numerical model discussed in Chapter 3.

5.2 Reproducibility

Run 3-b was conducted to check the reproducibility of the runs. The reproducibility Run was found to duplicate the data of the original Run quite well. Figure 5.1 shows the differential pressure and the gas saturation as obtained from the two runs. While the differential pressure data match well, the difference between the gas saturation results of the order of 0.5% indicates the extent of error in the data. The average pressure response for the runs is discussed in next section.
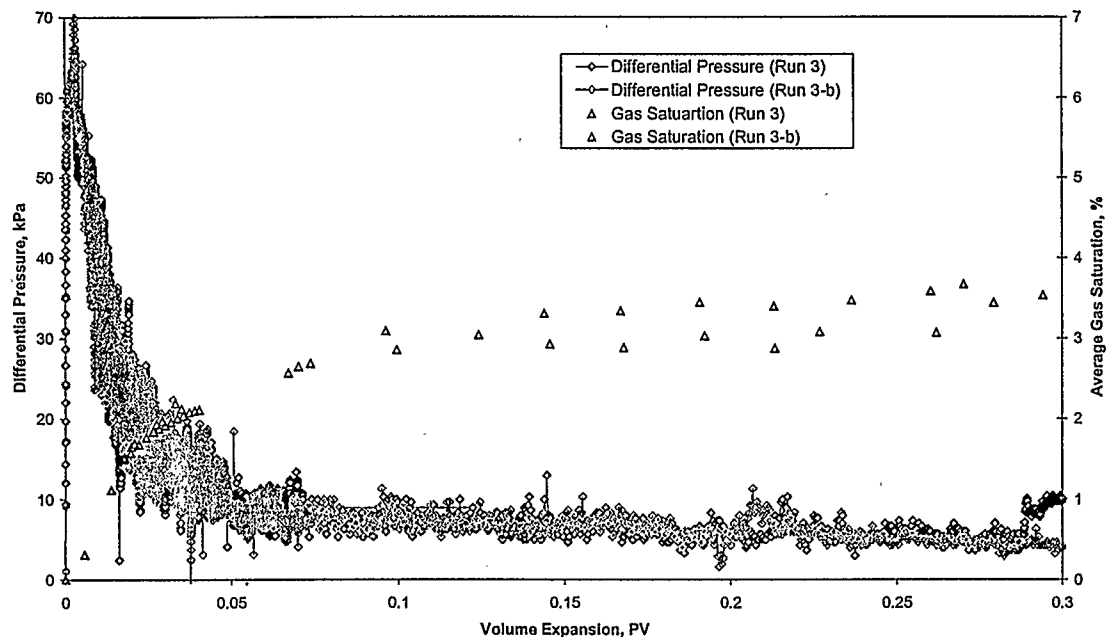
Figure 5.1 Reproducibility (Run 3-b)

5.3 Pressure

In Figure 5.2, the average pressure in the sand-pack is plotted against the volume of the fluid withdrawn and demonstrates the P-V behavior for some of the runs. The volumetric average pressure was calculated using a linear combination of pressures at different points along the sand-pack weighted with the lengths corresponding to each pressure. As the differential pressure in the sand-pack increases, the accuracy of this method reduces. Hence for the runs with a very high differential pressure in the sand-pack, a two-point average was used which further reduced the accuracy of averaging process. This was because the individual differential pressure gauge had a maximum 10psid value. For the high differential pressure runs (high viscosity and depletion rate); the individual differential pressure gauges were isolated. The average initial pressure for all the runs was 555 psig.

Kumar *et al.* (2002) reported this pressure trend in a previous experimental study. The data for all runs followed a similar trend starting with a sharp pressure decline above the bubble-point pressure. The slope of the P-V data at this stage is representative of single-phase compressibility. The pressure declined below the bubble-point pressure and reached a local minimum. The fluid at this stage is supersaturated and has a tendency to approach equilibrium. Therefore, the pressure bounced back, reducing supersaturation, before the pressure started to decline again with a much smaller slope. The data suggests that some oils remained supersaturated throughout the run. This was confirmed by measuring supersaturation at the end of each experiment, where a rise in average pressure would indicate supersaturation.

The experimental data of Figures 5.2 (a) and (b) show that the average pressure is affected by the depletion rate and viscosity. Figure 5.2(a) shows the pressure comparison for oil A and shows that at a particular oil viscosity, the higher the depletion rate, the higher the supersaturation and the lower the pressure minima. This is because in faster runs, gas evolution is less than the equilibrium values; the gas remains in the oil leading to reduce pressure. Figure 5.2(b) shows the pressure comparison for two of the oils at a 3 cm^3/hr depletion rate. From Figure 5.2 (b) it can be observed that the higher the viscosity, the lower the pressure. This effect was less pronounced for the slow 0.37 cm^3/hr depletion rate. The lower pressure at high viscosity can also be explained using a similar explanation used for high depletion. Kumar and Pooladi-Darvish (2002) have previously demonstrated that, when the diffusion coefficient is low, e.g. in high viscosity oils, or when depletion rate is fast, the evolved gas does not have enough time to grow to its equilibrium quantity and therefore, the mixture remains supersaturated.
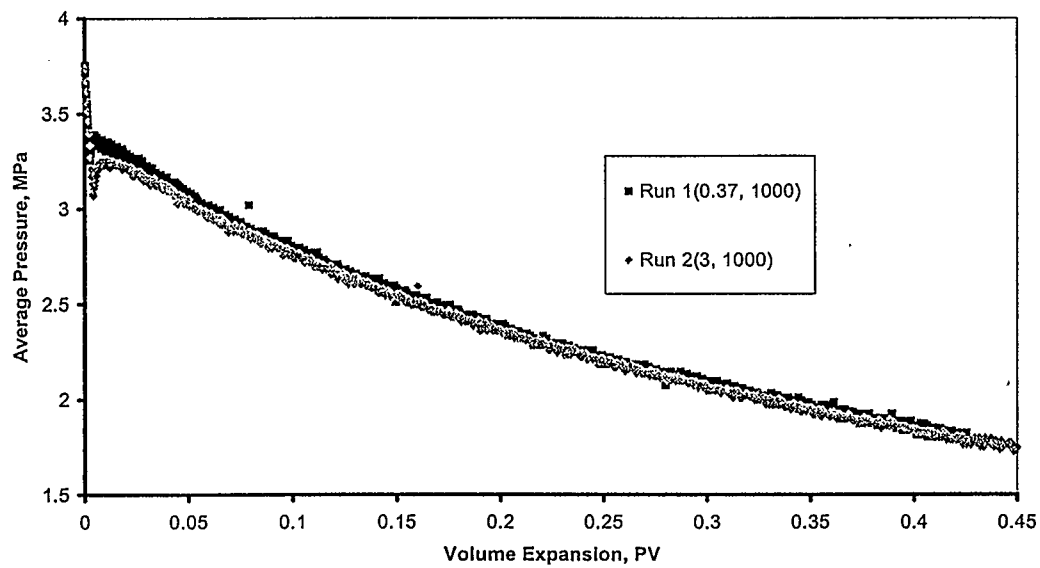
Figure 5.2(a) P-V curves for oil A.
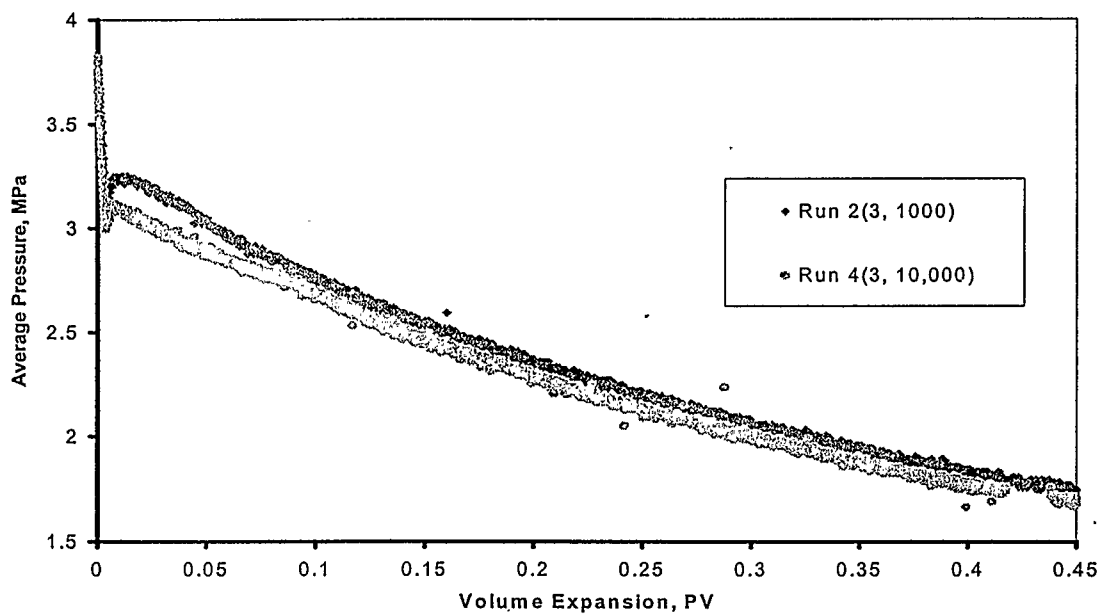
Figure 5.2(b) P-V curves for oil A and B.

Run 6 was omitted in Figure 5.2 (b) due to the large errors in the pressure averaging techniques.

The average pressure- expansion curve is not affected by flow properties and analysis of these curves may give very little information about late time flow properties. For this reason, and because the two-phase flow properties are the major focus of this work, we do not offer any further analysis of these P-V curves.

It is important to note that the attention of this research work is beyond the details of the early time phenomena of supersaturation, nucleation and growth. Instead, this work specifically looks at the two-phase flow behavior. Therefore, gas production and the differential pressure during two-phase flow were studied and the effects of viscosity and depletion rate on these factors were investigated. The effect of depletion rate and oil viscosity on early time mechanisms is introduced in the modeling by allowing the value of value of critical gas saturation to vary with depletion rate. Further work needs to be done to investigate the details of the effect of depletion rate and oil viscosity on the early time mechanisms.

5.4 Gas production and average gas saturation

The gas accumulated in the visual cells was determined by measuring the height of the oil gas interface. It is assumed that all the gas collected in the gas oil separator is from the core and the gas is at core conditions. For Run 1, steady gas production started after 2.8 cm^3 of depletion. This corresponds to 0.2% average gas saturation. This Run like all the slow runs was stopped after 3 weeks of depletion. For Run 3, steady gas production started at 9.8 cm^3 (1.7% average gas saturation). For Run 5, gas production started at 10.7 cm^3 (1.7% gas saturation). For Run 2, steady gas started accumulating in the visual cell after 14.3 cm^3 of depletion (2.3% gas saturation). For Runs 4 and 6, steady gas production started at 14.1 cm^3 (2.5% gas saturation) and 3.8 cm^3 (0.5% gas

saturation) respectively. Critical gas saturation was defined as the point of sustained production of gas. From Figures 5.3a and 5.3b show the gas produced at core conditions for all the runs. In general, a low gas production indicates that gas mobility is low or critical gas saturation is high.

5.4.1 Average gas saturation

The average gas saturation was determined by finding the difference between free gas produced and the total volumetric depletion divided by the pore volume. This calculation is based on the assumption that the produced oil does not contain gas bubbles. For slow runs and those with lower oil viscosity where pressure and saturation gradient across the core is small, the actual gas saturation in the core is believed to be close to the average gas saturation determined. However for the high-pressure drop Runs (4 and 6) the average gas saturation as calculated from material balance may not represent the actual average gas saturation in the core.

Figure 5.4 shows a typical curve for the observed average gas saturation in the core. Initially at the start of depletion, the oil was above the bubble point pressure and there was no gas in the system. As expansion continues and pressure falls below the bubble point pressure of the oil, gas is formed and the gas saturation increases linearly. This corresponds to the linear part of the average gas saturation curves in Figure 5.4, when the evolved gas remains in the sand-pack, before critical gas saturation (S_{gc}) is reached. When gas starts to flow, the slope of the line changes. Critical gas saturation is represented by a break in the gas saturation plot. The value of critical gas saturation under solution-gas drive is very important, as it sets the minimum possible value of recovery, and has therefore received considerable attention. For a constant oil viscosity,

the slope of the new line/curve after critical gas saturation is an indication of gas mobility. The larger the slope, the lower the gas mobility.

In the next section, the experimental results are discussed in terms of the effect of rate and viscosity on critical gas saturation and gas mobility.

5.5 Effect of viscosity

In this section, the effect of changing the oil viscosity on gas production, critical gas saturation and average gas saturation is described. As discussed earlier, the oil viscosity was changed by a factor of 30. For this analysis, either odd number Runs (1, 3 and 5) 0.37 cm^3/hr-depletion rate or the even number Runs (2, 4 and 6) 3 cm^3/hr-depletion rate are compared.

5.5.1 Gas production

Figures 5.3(a) and 5.3 (b) show the volume of the free gas collected in the visual cells as a function of the volume expansion for all three oils at the two depletion rates. Figure 5.3(a) shows the data for the slow 0.37 cm^3/hr Runs and Figure 5.3(b) shows the results for the fast 3 cm^3/hr Runs. From Figures 5.3(a) and (b), it can be observed that the volume of gas produced is a function of oil viscosity.

A possible explanation for the low gas production during depletion of the high viscosity oil is that gas mobility is reduced due to delayed coalescence and increased breakup, which are caused by increased viscous forces and low diffusion coefficient.
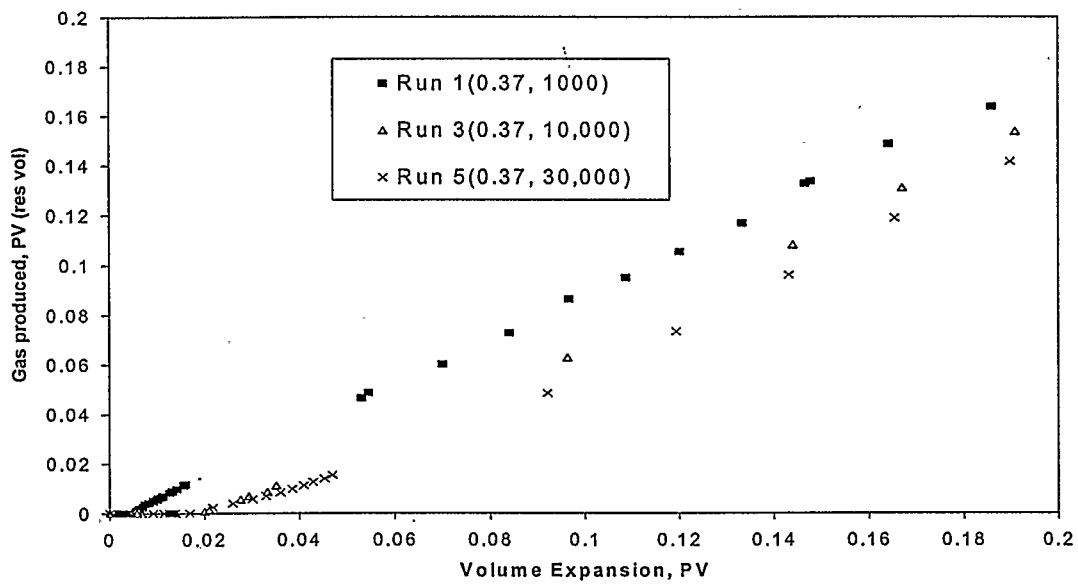
Figure 5.3(a) Effect of viscosity: Cumulative gas produced for a depletion rate 0.37 cm³/hr
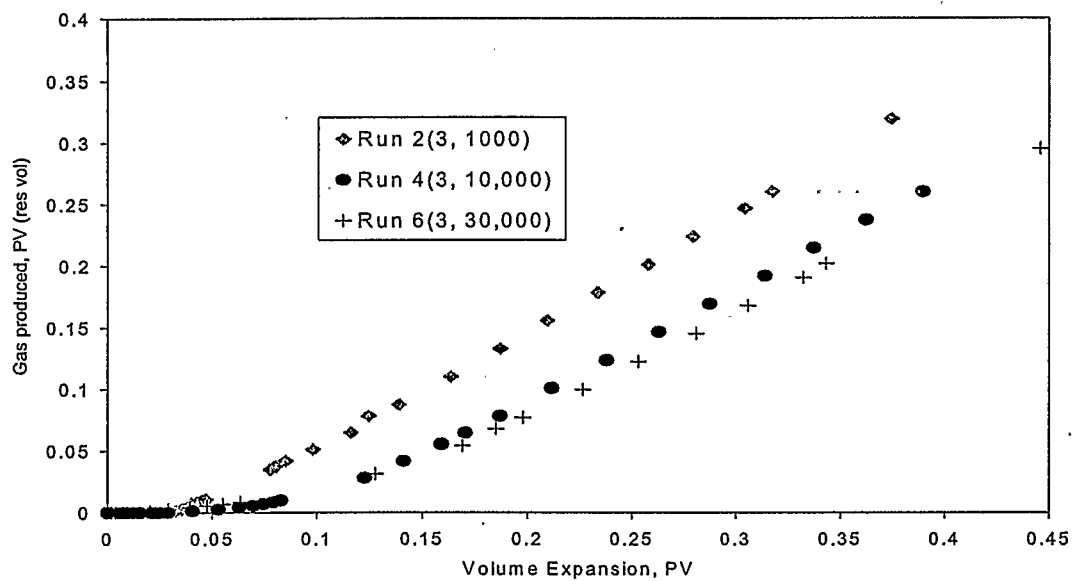
Figure 5.3(b) Effect of viscosity: Cumulative gas produced for a depletion rate of 3 cm³/hr

5.5.2 Average gas saturation

Figures 5.4(a) and (b) are plots of gas saturation in the core as a function of fluid expansion and shows that gas saturation in the core is higher at higher viscosity. Lower gas mobility leads to higher gas saturation in the core and improved oil recovery.

As discussed earlier, Figures 5.4(a) and (b) exhibit a linear portion at early times followed by a curved line. The slope of the curve after the breakpoint represents the effectiveness of oil recovery. The higher the slope, the better the oil recovery after critical gas saturation. Figure 5.4 (a) and (b) suggests that oil recovery improved with an increase in oil viscosity, which is in line with the reduced gas mobility.

5.5.3 Critical gas saturation

Figures 5.4 (a) and (b) suggest that critical gas saturation (S_{gc}) for Run 1 (1000 cS) is very low, about 0.2%. The critical gas saturation for Run 3 (10,000 cS) is 1.8±0.2%. For Run 5 (30,000 cS) the recovery data did not define S_{gc} very precisely (2±0.5%). Therefore, a thirty-fold increase in dead-oil viscosity from 1000 cS to 30,000 cS resulted in a ten-fold increase in S_{gc} in the live oil from 0.2 to about 2%. Focusing now on the fast Runs, Figure 5.4(b) suggests that S_{gc} for Run 2 is about 2.5±0.5%. An increase in depletion rate of about eight times (as compared to Run 1) resulted in an increase in S_{gc} from 0.2 to 2.5%. It appears as if S_{gc} is affected more strongly by depletion rate than by viscosity. The effect of rate on critical gas saturation will be discussed later.

As suggested earlier, the onset of gas flow may not be representative of the critical gas saturation over the whole length of the sand-pack especially for the higher viscosity and higher depletion rates. Nevertheless, a comparison between Figures 5.4(a) and (b) show that sustained gas flow started at a higher gas saturation for the fast runs. This is

represented by a break in the recovery at 5±1%. The S_{gc} and final recovery for all of the runs are given in Table 5.1.
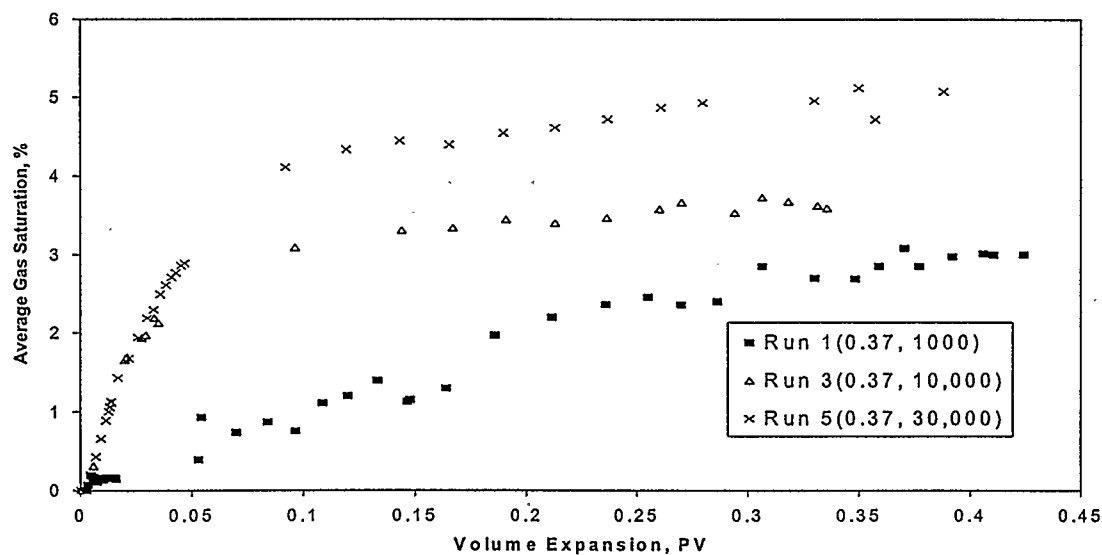
Figure 5.4(a) Effect of viscosity: Average gas saturation for a depletion rate 0.37
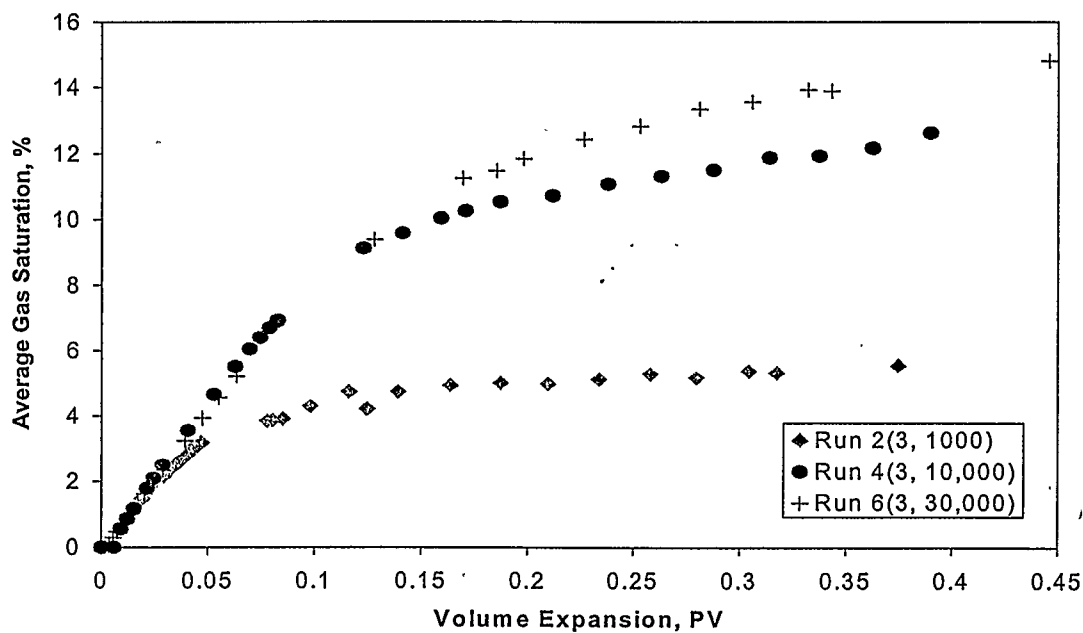
Figure 5.4(b) Effect of viscosity: Average gas saturation for a depletion rate of 3 cm³/hr

5.5.3.1 Error in critical gas saturation values

Critical gas saturation can be obtained from two sources; the recovery curve, which shows the average saturation in the core vs. expansion and the cumulative gas production curve, which represents the directly measured volume of the produced gas. As mentioned earlier, on the recovery curve, the break in the curve is representative of critical gas saturation. The average gas saturation that corresponds to the onset of gas flow into the visual cell may not be representative of the average critical gas saturation throughout the core. This "error" or uncertainty in the reported value increases as the differential pressure across the core increases. Hence, in this work, the critical gas saturation values are reported with error bounds to account for this uncertainty. From Table 5.1, the error bound varied from 0.2-1% and increases as the differential pressure increases.

5.5.4 Differential pressure

Figures 5.5(a) and (b) show the differential pressure across the sand-pack for the three oils at 0.37 and 3 cm^3/hr, respectively. The data exhibited a large value at early times followed by a decline in differential pressure as expansion continues. The experiments were conducted at a constant total volume withdrawal rate; the large early-time value is obtained during single-phase oil flow. With the start of gas flow, total mobility increases, and differential pressure decreases. The early-time behavior of the differential pressure data is affected by the initial stages of gas formation, and has been explained previously for similar experiments [Kumar (2002)]. Here, the focus is on the declining portion of data, where two-phase flow is present.

Figure 5.5c shows the expanded version of the differential pressure-volume expansion for oils at 0.37 cm^3/hr depletion rate. Once the critical gas saturation is

reached, differential pressure became more chaotic and fluctuates with greater frequency and higher amplitude. This indicates that gas is flowing out intermittently rather than continuously. This has been previously observed in other works [Pooladi-Darvish and Firoozabadi (1999), Kumar and Pooladi-Darvish (2002)]. From Figure 5.5c, as the viscosity increases, the pressure fluctuations also increase. This suggest that the higher the viscosity, the more intermittent or discontinuous the flow becomes.

5.5.5 Relative permeability to gas

A number of studies of solution-gas drive in heavy oils refer to the slugs of gas being produced and intermittent gas flow [Sheng *et al.* (1999), Pooladi-Darvish and Firoozabadi (1999), Kumar and Pooladi-Darvish (2002), Tang and Firoozabadi (2003)]. The concept of relative permeability is invalid for flow of a discontinuous gas phase. In the absence of mathematical models that account for the intermittent flow of gas, current simulation models use the relative permeability to characterize the two-phase flow of gas and oil. In the past, the concept of relative permeability has been successfully used for other forms of discontinuous flow of the phases [Vassenden and Holts (2000)]. For these cases however, relative permeability may be a function of other parameters in addition to phase saturation. Here, we assume that the concept of relative permeability applies to solution-gas drive in heavy oils, and examine the dependency of the relative permeability functions to gas saturation, withdrawal rate and oil viscosity. Tang and Firoozabadi (2003) recently suggested a simple mathematical model for the estimation of gas and oil relative permeability from 1-D depletion experiments that are under two-phase pseudo-steady state conditions and exhibit a small capillary pressure gradient (This equation was described in Chapter 2).
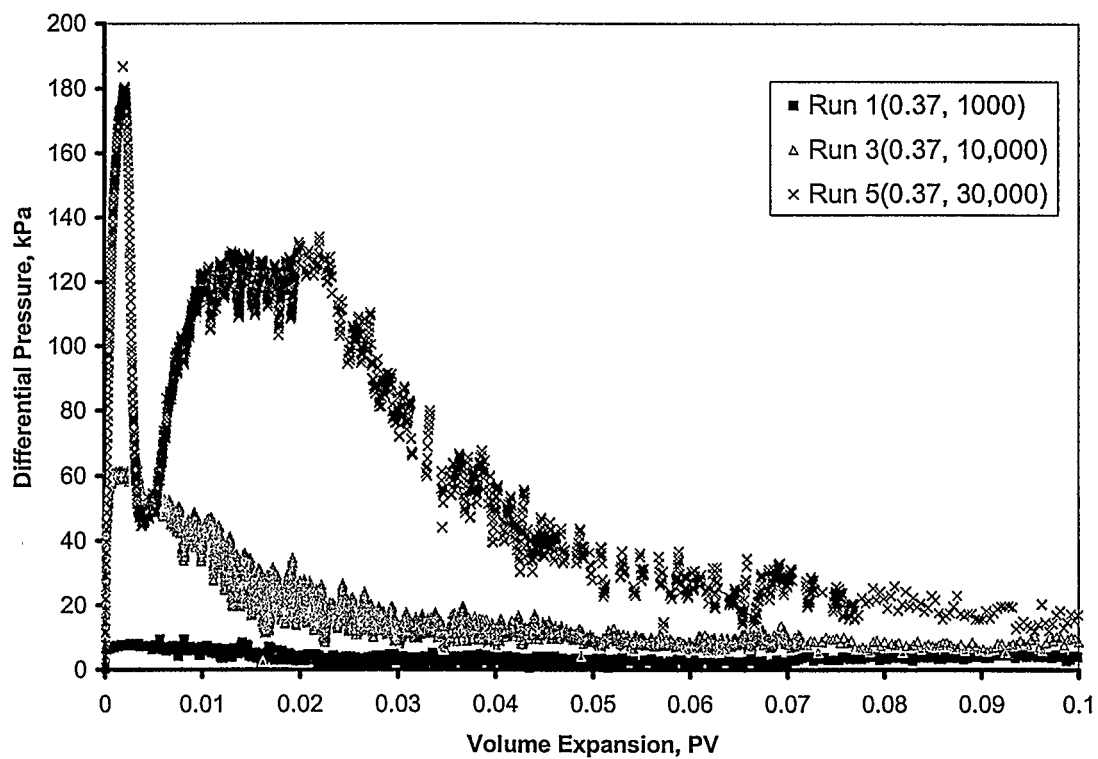
Figure 5.5(a) Effect of viscosity: Differential pressure across the core for a depletion rate of 0.37 cm³/hr
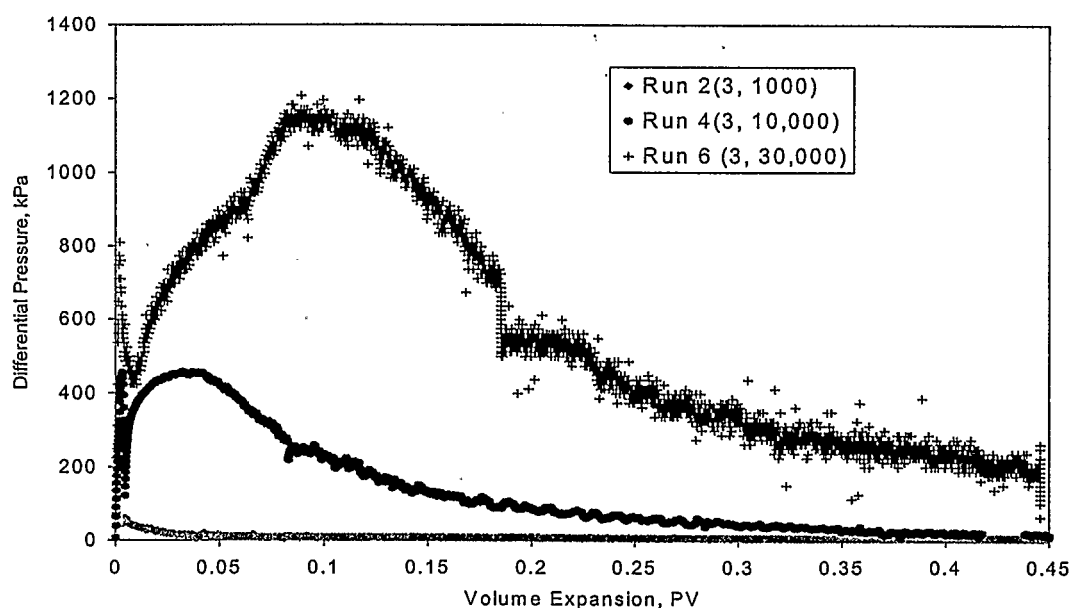
Figure 5.5(b) Effect of viscosity: Differential pressure across the core for a depletion

rate of 3 cm³/hr
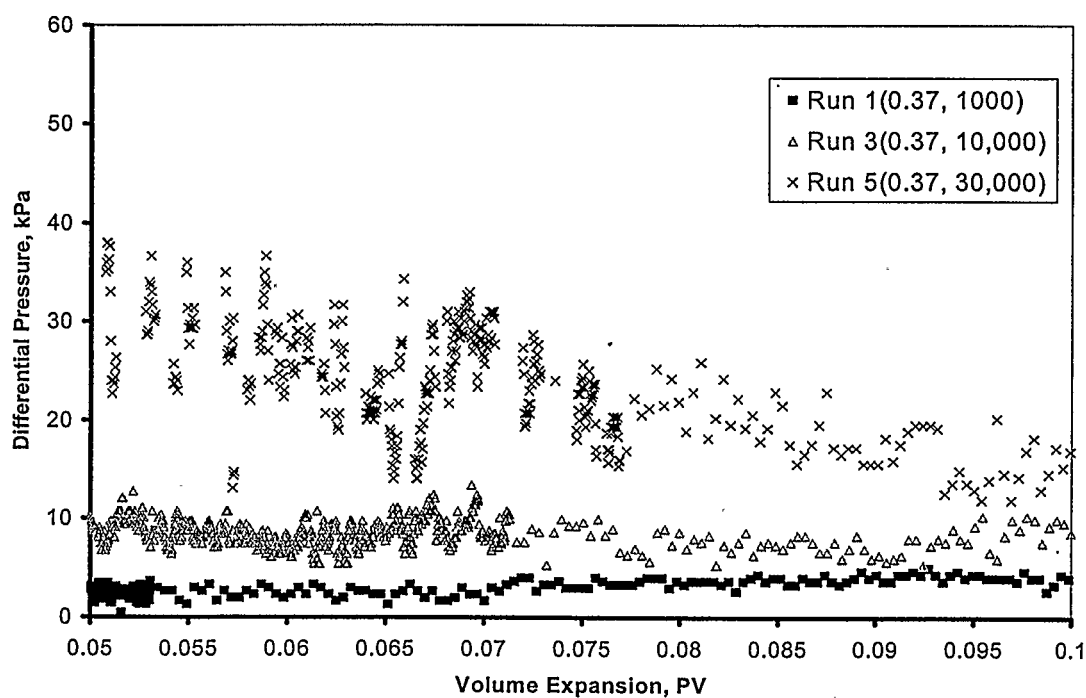
Figure 5.5(c) Effect of viscosity: Differential pressure across the core for a depletion

rate of 0.37 cm³/hr (Expanded version)

The flow in this set of experiments is predominantly one-dimensional, as vertical flow is minimized by continuous rotation of the core holder. Furthermore, pseudo-steady state is assumed similar to the assumption made in similar studies [Tang and Firoozabadi (2003)]. The condition of negligible capillary pressure gradient also holds for all the experiments. In the slow and/or low viscosity experiments, the small pressure drop along the sand-pack suggests the uniform possibility of gas nucleation and growth across the length. The result is uniform gas saturation, leading to a negligible capillary pressure gradient. In runs exhibiting a large differential pressure, it is expected that the magnitude of the capillary pressure gradient would be negligible as compared with the viscous pressure gradient, because of the high permeability and low capillary pressure of the sand.

The previously described model of Tang and Firoozabadi (2003) was used to estimate relative permeability to oil and gas. The oil and gas rates used in equation 2.7 were obtained from the cumulative volumes by dividing the volume of gas and oil produced over the duration of production. Due to intermittent gas flow, the rates calculated from the original data may lead to negative values. Hence, calculating relative permeability values (from equation 2.7) using the original data lead to negative relative permeability. Therefore, the oil and gas rate calculated from the original cumulative production data was smoothened. This was done by averaging the oil and gas rates over a longer length of time such that the effect of intermittent flow that results negative rates was minimized. Figures 5.6 (a) and 5.6 (b) show the relative permeability values for all of the runs, where the solid symbols are for oil and open symbols for gas. The following observations are evident.

1. Relative permeability to oil remains primarily between 1 and 0.1. In some cases, relative permeability values larger than 1 were obtained.

2. As expected, the relative permeability to gas increases with an increase in gas saturation. Run 1 appears to be exceptional. Over the whole saturation range of 0 – 15% gas saturation, relative permeability to gas is low and varies between 10^{-7} and 10^{-4}.
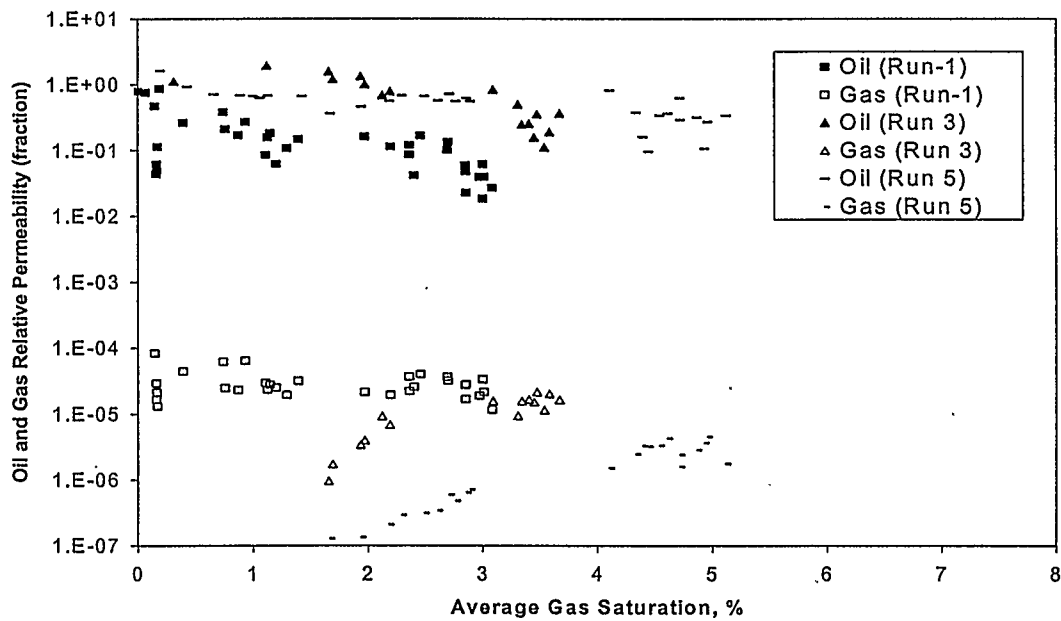
Figure 5.6(a) Effect of viscosity: Gas Relative permeability for a depletion rate of 0.37 cm³/hr
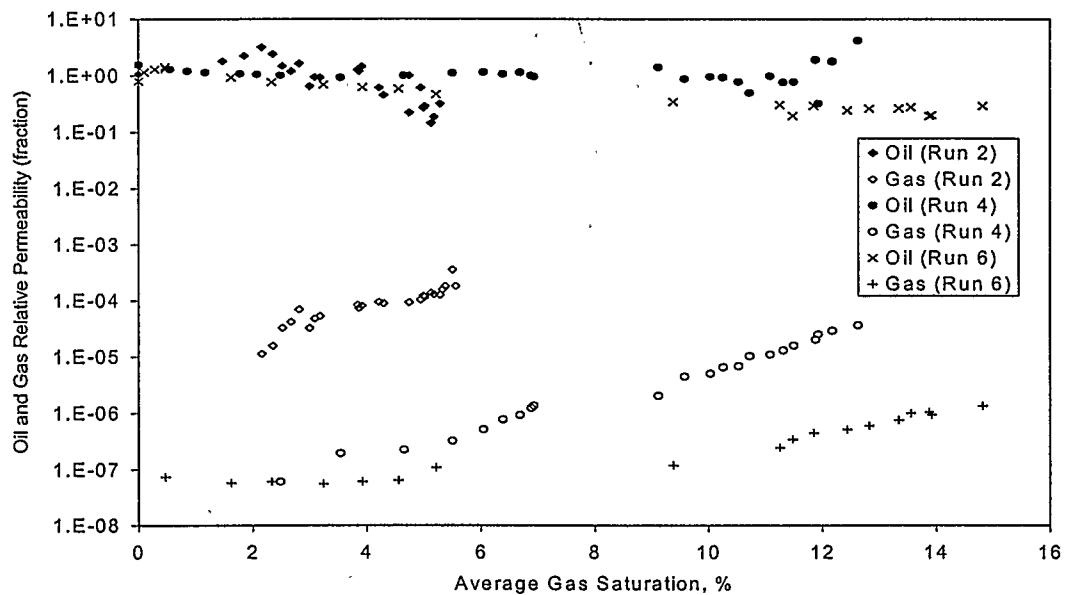
Figure 5.6(b) Effect of viscosity: Gas Relative permeability for a depletion rate of 3 cm³/hr

Figures 5.6(a) and (b) show the comparison of the calculated relative permeability for different oil viscosity. As the viscosity increases from Runs 1 to Run 3 and Run 5, the gas mobility decreases from 10^{-5} and 10^{-4} to 10^{-7} and 10^{-5}.

Relative permeability to gas appears to be a function of both gas saturation and oil viscosity. From Figures 5.6(a) and (b), it is observed that as oil viscosity increases, relative permeability to gas decreases at the same gas saturation. The high-pressure differentials along with low gas volumes from Figures 5.3 and 5.5 had already suggested this.

5.6 Effect of depletion rate

Figures 5.7 through 5.10 uses the same data to demonstrate the effect of depletion rate as opposed to viscosity. For brevity, the effect of depletion rate in Oil B is discussed only. A detailed study of the effect of depletion rate on gas mobility was previously reported by Kumar *et al.* (2002).

5.6.1 Gas production

Figure 5.7 show the gas produced for oil B, and suggests that as depletion rate increases less gas is produced. Also the onset of gas production is delayed.

5.6.2 Differential pressure

Figure 5.8 shows the differential pressure across the sand-pack for oil B, and indicate that as oil viscosity increases, the single- and two-phase pressure drop increases.

An increase in two-phase pressure differential from Figure 5.8, along with a decrease in gas production from Figure 5.7, suggests lower gas mobility and improved oil displacement as depletion rate increases. The fluctuation in differential pressure increases when gas starts to flow. This fluctuation also increases with an increase in depletion rates. This suggest that the higher the depletion rates, the more intermittent or discontinuous the flow becomes.

5.6.3 Average gas saturation

Figure 5.9 shows the average gas saturation in the core as the rate increases ten folds for oil B. The final gas saturation increases by 4 times.

5.6.4 Relative permeability

Figure 5.10 presents the relative permeability data for oil B, and demonstrates that relative permeability to gas decreases as depletion rate increases for particular oil.
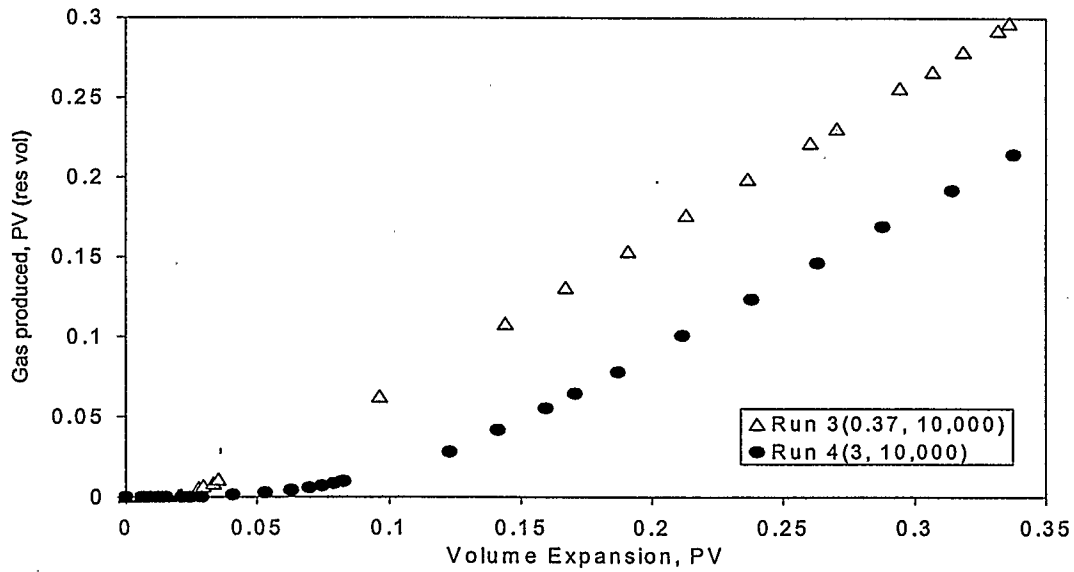
Figure 5.7 Effect of Rate: Gas production for a depletion rate for Oil B
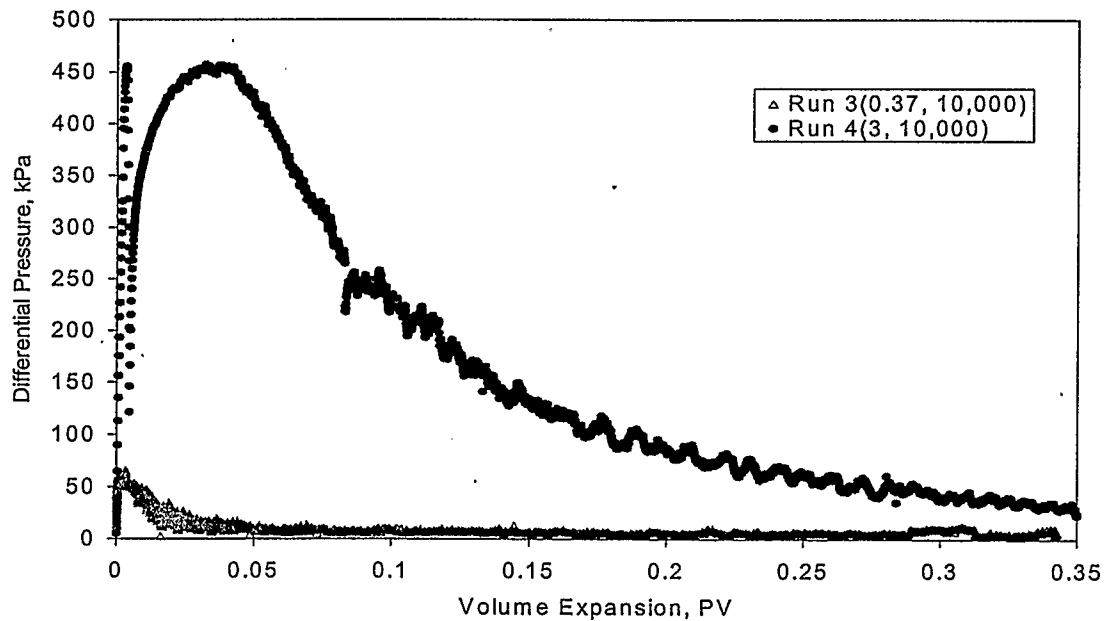
Figure 5.8 Effect of Rate: Differential pressure across the core for Oil B
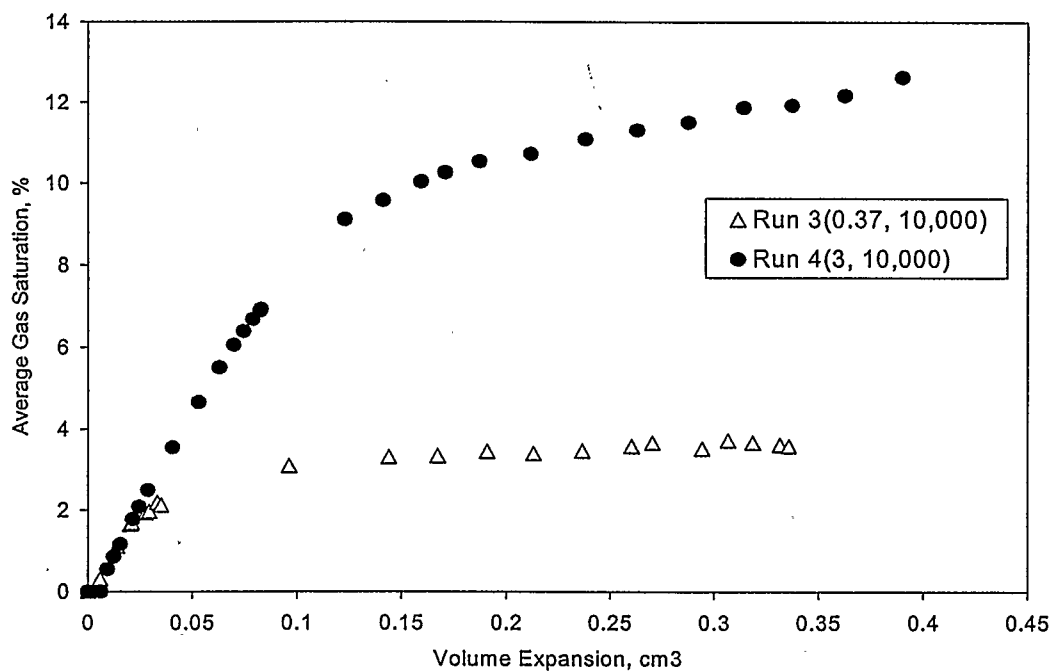
Figure 5.9 Effect of Rate: Average gas saturation in the core for Oil B
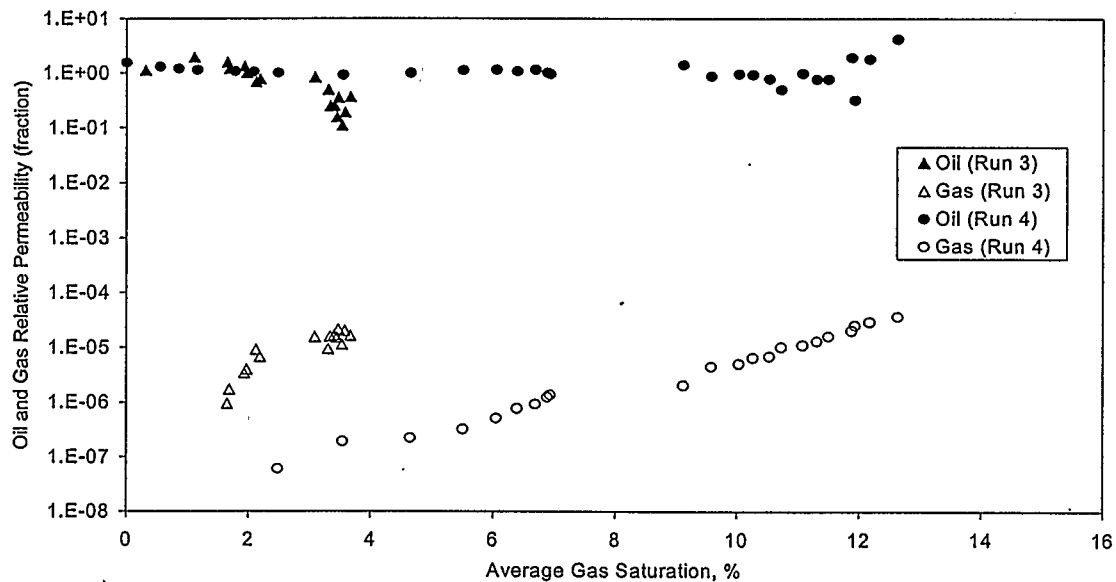
Figure 5.10 Effect of Rate: Gas relative permeability for Oil B

In summary, the faster experiments resulted in lower gas mobility, lower free gas production and higher average gas saturation in the sand-pack. These results are consistent with those of Kumar *et al.* (2002).

5.7 Analysis and Discussion

The proposed mechanisms for the observed phenomena are as follows. At the early time, the reduction of pressure causes the nucleation and evolution of gas bubbles, initially they are very small, then they start to grow in size due either to further reduction of pressure or to coalescence. At the early stage, grown gas bubbles are trapped at the pore throats constituting immobile gas saturation. Further growth in size results in the formation of an independent passage for the gaseous-phase flow. The independent gas flow bypasses the oil during the late time and does not contribute to the oil recovery. As discussed earlier, once a mobile gas phase has formed, it may continue to flow as a continuous gas phase, or it may break up into several smaller clusters leading to dispersed-gas flow. A faster withdrawal rate provides less chance for the coalescence of the gas bubbles and formation of the independent gas flow; therefore, it should result in lower gas mobility, higher critical gas saturation and higher oil recovery. On the other hand, a higher oil viscosity slows down the coalescence, increases the break-up of the flowing gas clusters and restricts the formation of independent gas flow; therefore, at a given withdrawal rate, higher viscosity oil is expected to show lower gas mobility and a higher critical gas saturation. This is consistent with the experimental observation.

From the experimental results, it seems that rate and viscosity affects gas mobility to different degrees. For example, if the rate of depletion for oil B (Run 3) is increased about 8 times (Run 4) the final gas saturation in the core is increased four times. However, if the viscosity is increase ten times from oil A (Run 1) to oil B (Run 3)

the final gas saturation increases about 4 times at higher rates and at lower rates, increases about 1.33 times. Hence it may be important to combine the effect of the rate and viscosity and find out how the combined effects of viscosity and depletion on solution-gas drive in heavy oils.

In the next section, a methodology is proposed for combining the effect of rate and viscosity.

5.7.1 Index for effect of withdrawal rate and oil viscosity

In this work, the capillary number term defined in equation 2.10 is generalized and a new parameter referred here as depletion index is introduced. As was discussed earlier, withdrawal rates (favorable for oil production) and rates of coalescence of gas bubbles and formation of the independent gas flow (unfavorable) are two competing factors. Therefore, a ratio of these rates can be used as a depletion index characterizing the process, that is

$$I = \frac{v}{\frac{dV_{CG}}{dt}} \tag{5.1}$$

where I is the depletion index, v the linear withdrawal rate per unit cross-sectional area or velocity and V_{CG} the volume of continuous gas per unit volume.

As explained previously, rate of gas coalescence decreases and bubble breakup increases with increased viscosity. Furthermore, oils of higher viscosity have lower diffusion coefficient, which can affect the early-time processes of nucleation and growth. Here we expressed the effect of oil viscosity through a combination of the above processes by noting that the rate of formation of the continuous-gas phase should be inversely related to some power of oil viscosity; thus,

$$\frac{dV_{CG}}{dt} \propto \frac{1}{\mu^\alpha} \qquad\qquad (5.2)$$

where μ is the oil viscosity and α the adjustable exponent to oil viscosity. A substitution of Equation (5.2) into Equation (5.1) gives

$$I \propto v \cdot \mu^\alpha \equiv I' \qquad\qquad (5.3)$$

Unlike I, I' is not a dimensionless index; nevertheless, it may be a valid index for a series of tests done in the same sand-pack of the same dimension using live oils of similar chemical characteristics. With the use of kinematic viscosity instead of μ, I' has the unit of $m^{1+2\alpha} sec^{-(1+\alpha)}$.

Assuming interfacial tension does not change, capillary number $(\frac{\mu v}{\sigma})$ is proportional to depletion index ($I' = v \times \varphi^\alpha$) when the exponent $\alpha = 1$

The depletion index parameter is a first attempt at combining the effects of rate and viscosity. The depletion index is calculated for all the runs using the total fluid withdrawal rates and the live oil kinematic viscosity. The task is to determine what value of the exponent gives a correlation between depletion index and critical gas saturation, gas mobility or oil recovery. Various values of alpha were tried.

A value of 0.5 for α appears to give good correlation between the depletion index I' and the average gas saturation at the 0.3 PV withdrawal as well as the critical gas saturation as shown in Figure 5.11.

Figure 5.12 shows the trend between depletion index and the average gas saturation in the sand-pack. The legend is ordered with an increase in the depletion index, where I' is used in place of I. This suggests that the higher depletion index, the higher the recovery or gas saturation. Another way of demonstrating the effectiveness of oil

displacement is by the use the fractional flow curve. A high displacement efficiency would result in a fractional flow curve for gas that is shifted towards the right and rises smoothly. Figure 5.13 shows the effect of the depletion index on the fractional flow curve as calculated using the gas production data. Figures 5.12 and 5.13 show that average gas saturation increases and displacement becomes more effective as the depletion index increases. This is also shown in Table 5.1, which shows increasing final recovery with an increase in the depletion index. Calculating the fractional flow of gas from the original data did not give a smooth fractional flow curves for the same reason given earlier for the calculated relative permeability. In order to obtain a smooth curve, the fractional flow was calculated by dividing the produced gas volume by the total produced volume over considerable length of time therefore minimizing the effect of intermittent flow.

In the next section, experimental results are simulated in order to obtain gas relative permeability endpoints as a function of depletion index.
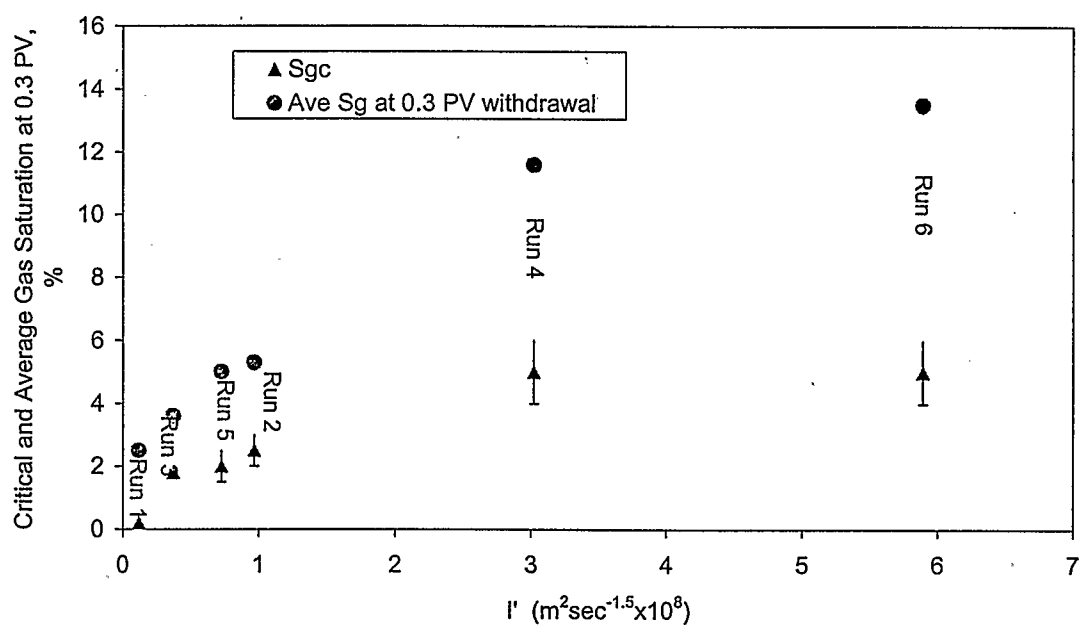
Figure 5.11 Correlation of critical gas saturation with depletion index
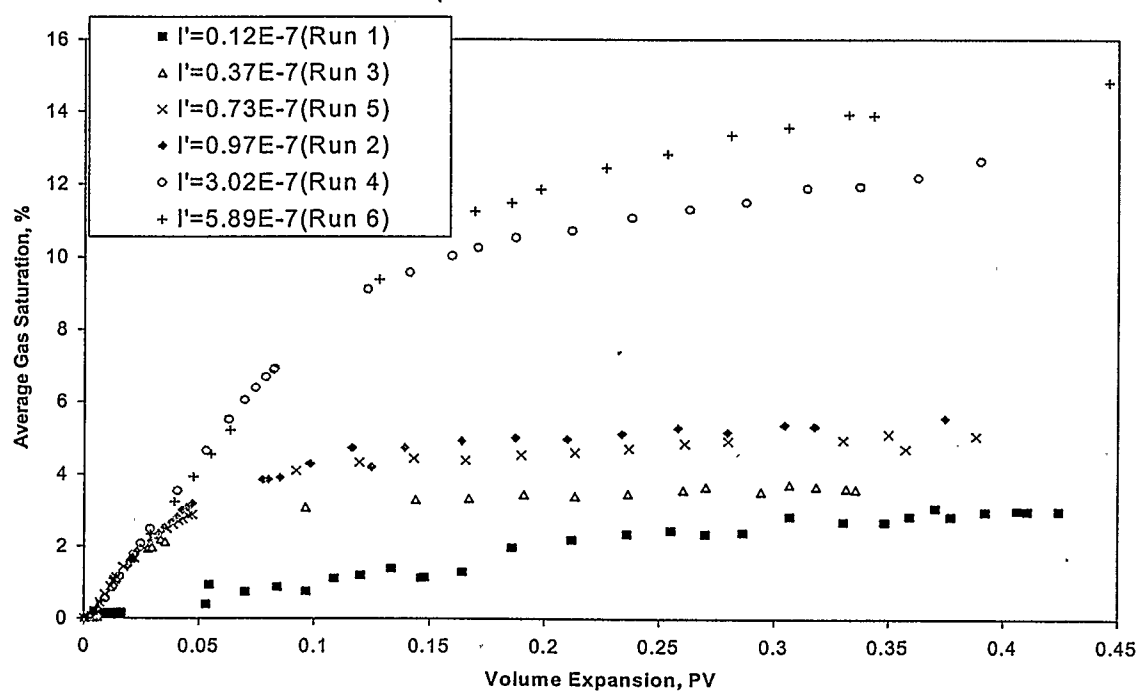
Figure 5.12 Correlation of average gas saturation with depletion index
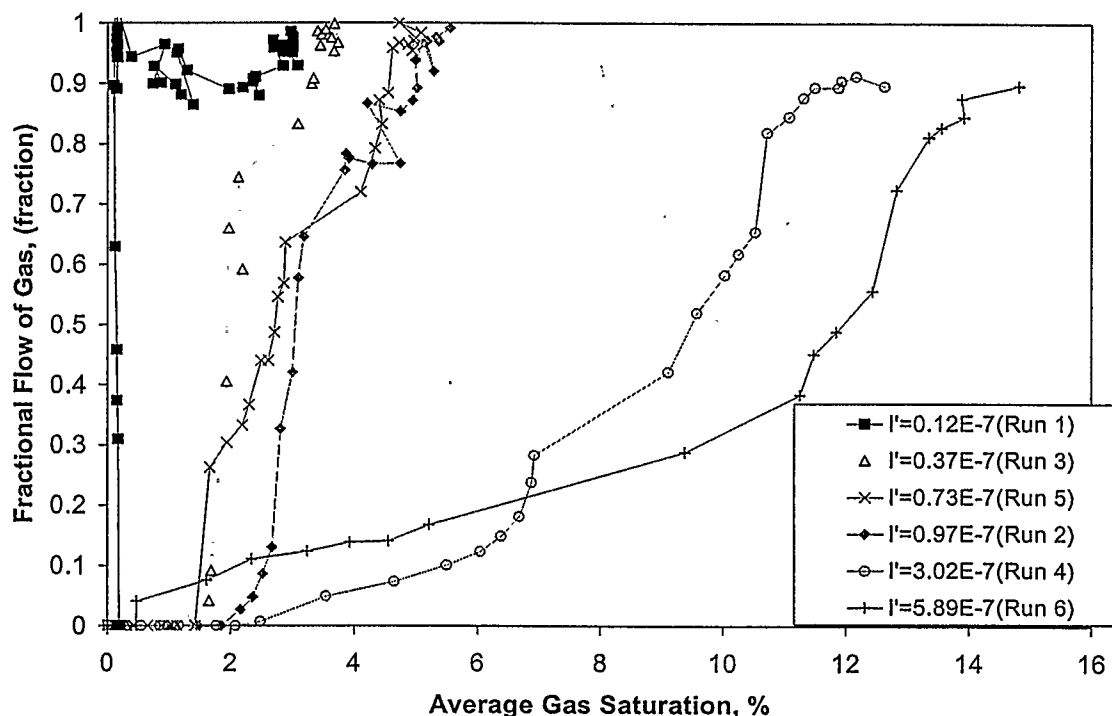
Figure 5.13 Correlation of fractional flow with depletion index

5.8 SIMULATION

5.8.1 Introduction

In the previous section the experimental results were analyzed and recoveries and critical gas saturation were correlated with depletion index. There are many processes that contribute to recovery during solution-gas drive. These processes include: Early time processes like nucleation and growth and late time processes of gas mobility, coalescence and flow. As discussed in Chapter 2, both the early time and late time processes are affected by depletion rate and oil viscosity hence; it may be worthwhile to correlate a more fundamental flow parameter like gas relative permeability endpoint with depletion index. The correlation will be beneficial because relative

permeability is an input into simulators. This correlation will be relative permeability may be helpful for more accurate modeling of solution-gas drive in heavy oils.

In order to achieve this objective, the experimental results were simulated using CMG IMEX™ simulator. The calculated relative permeability from the mathematical model proposed by Tang and Firoozabadi (2003) described above, were smoothened by fitting a Corey type model through. As a first trial, the Corey model that fits the calculated relative permeability data is used in the simulator. By ·varying the gas relative permeability endpoint value, the average gas saturation, the gas production and the differential pressure across the core are matched. After matching the experiment, the endpoint relative permeability was obtained and correlated with depletion index. The known variables are the fluid properties, sand-pack properties, average gas saturation, average pressure in the sand-pack and the free gas produced.

The capillary pressure used was that by Hagoort (1980) type function was used to represent the capillary pressure.

$$P_c = 0.005 + 0.02\frac{(1.01 - S)^{0.2} - (0.01)^{0.2}}{S^{0.3}}$$

A sensitivity on capillary pressure during simulation shows that the results are slightly affected by capillary pressure.

After the correlation between gas relative permeability endpoint is obtained by matching with a commercial simulator, a similar correlation was used in the one-dimensional two-phase simulator (discussed in Chapter 4) only this time, the depletion index is calculated from local parameters.

5.8.2 RELATIVE PERMEABILITY

Figures 5.13 and 5.14 show the calculated values as determined by the Tang and Firoozabadi model for oil B at the two depletion rates. As discussed earlier, a Corey type model was fitted

$$k_{rg} = k^0_{rg} S^{n_g}$$

$$k_{ro} = k^0_{ro} (1 - S)^{n_o}$$

$$S = \frac{S_g - S_{gc}}{1 - S_{gc} - S_{org}}$$

Table 5.2 shows some of the data used in the simulation. As described above, K^0_{rg} is adjusted until the Corey model matches the experimental data. The parameter n_g *is kept constant.* Table 5.3 shows the comparison between the initial (fits the calculated permeability curves) and the final values of gas endpoint relative permeability after the match of the experimental data.

Table 5.2. Data used in Simulation

No of Grid blocks	100
Live oil viscosity, cp	585, 5680, 21600
Oil FVF at bubble point, rm^3/sm^3	1.04
Bubble point pressure, kPaa	3542
n_o, n_g	2, 1.5
S_{org}	40%

Table 5.3. Variation of critical gas saturation and gas endpoint relative permeability with simulation.

Runs		Critical gas saturation, %		End point relative permeability	
	Initial	Initial	Final	Initial	Final
Run 1	0.2	0.19		0.05	0.05/0.1
Run 2	2.5	2		0.03	0.015
Run 3	1.8	1.6		0.003	0.0035
Run 4	5	7.5		0.0029	0.0015
Run 5	2	2		0.0015	0.00075
Run 6	5	12		0.00017	0.000275

5.8.3 Analysis of simulation results

The match of the experimental data for all six runs is shown in Figure 5.16 to Figure 5.19. Figures 5.17 and 5.19 show the differential pressure matches for all the runs. The dip, early in the depletion process, in the differential pressure in all cases is an indication of gas being formed at the outlet end, whereas there is still single phase at the no-flow boundary. This results in a sudden decrease of differential pressure. This phenomenon happens in the simulator at the bubble point pressure since an equilibrium assumption is considered in the simulator. This does not match experimental data where the bubbles nucleate after achieving a certain supersaturation.

Figure 5.16 and Figure 5.18 show the match of the gas saturation in the sand-pack. For Runs 5 and 6, we needed to use a high critical gas saturation in the model in order to match the experiments. For Run 6 the simulation data did not match very well with experimental data. Run 6, with the highest viscosity and depletion rate is characterized by high supersaturation values, so the free gas is expected to be less than the equilibrium value. The quality of the match is seen in Figures 5.16 and 5.18.

The depletion index for all the runs were calculated and correlated with the Corey endpoint relative permeability value used to match the experiments. Figure 5.20 shows the correlation obtained for the critical gas saturation and depletion index. After trying a number of values for alpha (exponent in the depletion index term), a value of 0.5 was used to correlate critical gas saturation with depletion index. Figure 5.21 shows the correlation obtained for the gas relative permeability endpoint and depletion index an alpha of 2.8 was used to correlate gas relative permeability endpoint. A linear trend was observed for the critical gas saturation while a power law trend was observed for the gas endpoint relative permeability with depletion index. The endpoint value for Run 1 was not included in the correlation of Figure 5.21. The reason for this is that the average gas saturation curve for Run 1 has an unusual behavior demonstrating significant oil recovery after critical gas saturation. This makes it very difficult to match.

From Figure 5.20, it seems that the lower rate runs all have lower critical gas saturation while the higher rate runs have higher critical gas saturation. Whereas, in the endpoint correlation, the higher the viscosity, regardless of the rates, the lower the endpoint relative permeability value and vice versa. This somewhat suggests that the endpoint relative permeability is a stronger function of viscosity while the critical gas saturation is a stronger function of the depletion rates confirming the experimental observation, and this is also reflected in the values of $\alpha = 2.8$ and $\alpha = 0.5$ for the endpoint relative permeability and critical gas saturation respectively. There may be a physical meaning but this is not further studied in this work.
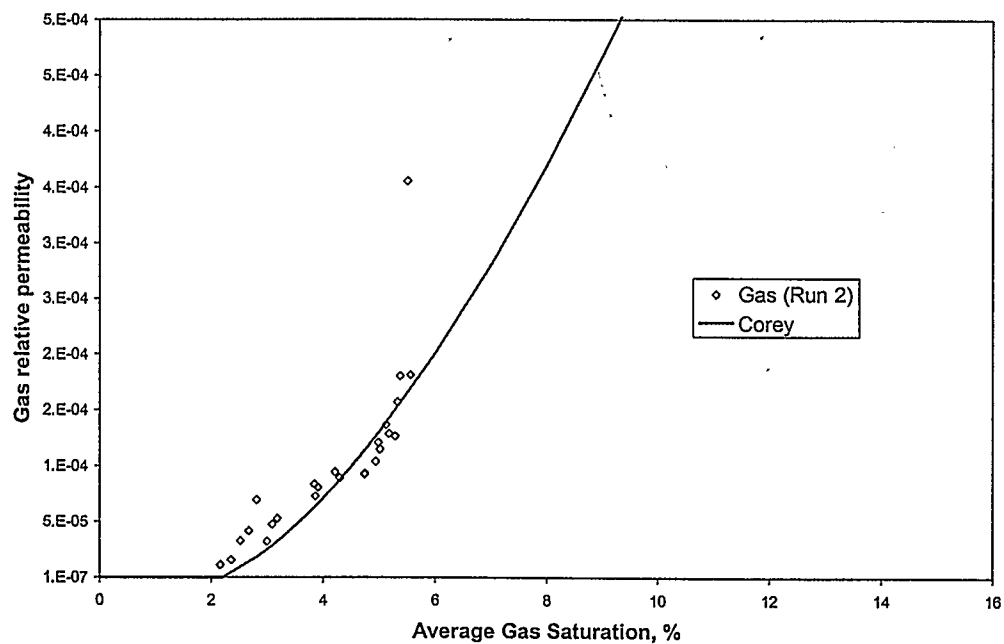
Figure 5.14 Corey relative permeability curve (Run 2)
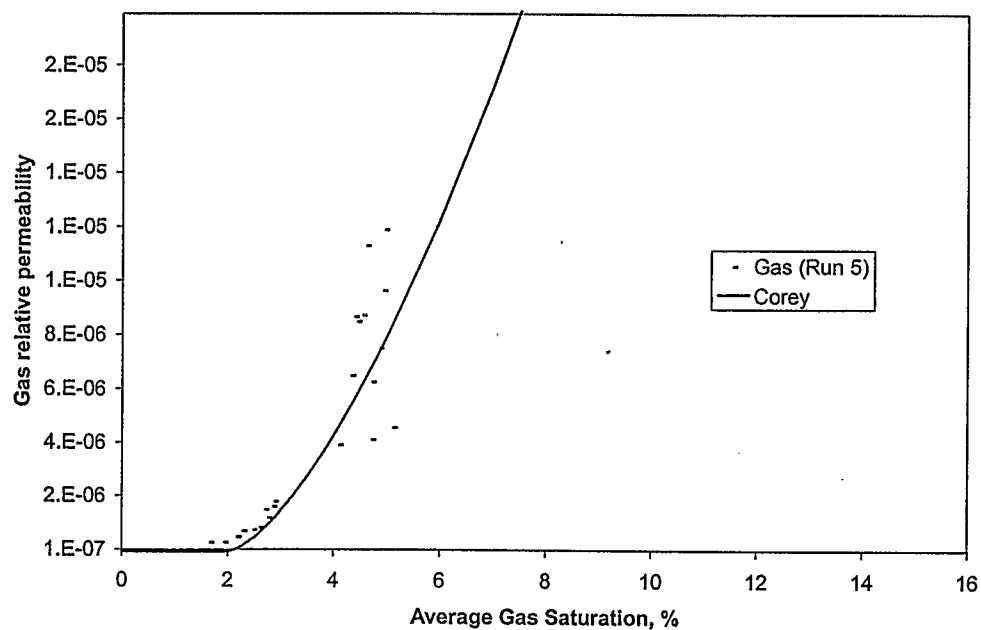
Figure 5.15 Corey relative permeability curve (Run 5)
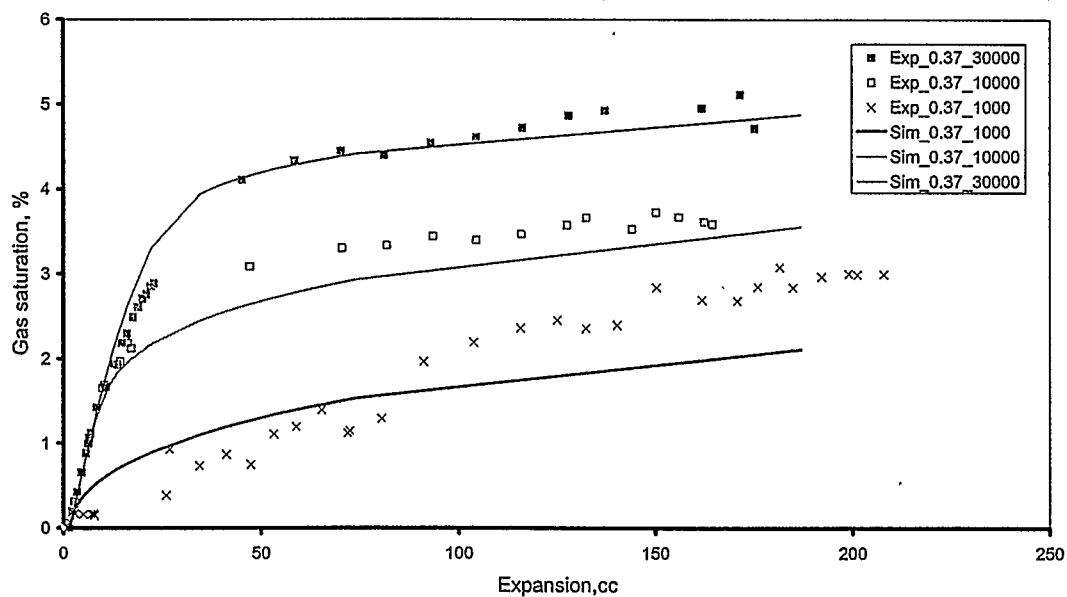
Figure 5.16 Simulation of Gas saturation using IMEX™ (Depletion rate = 0.37 cm³/hr)
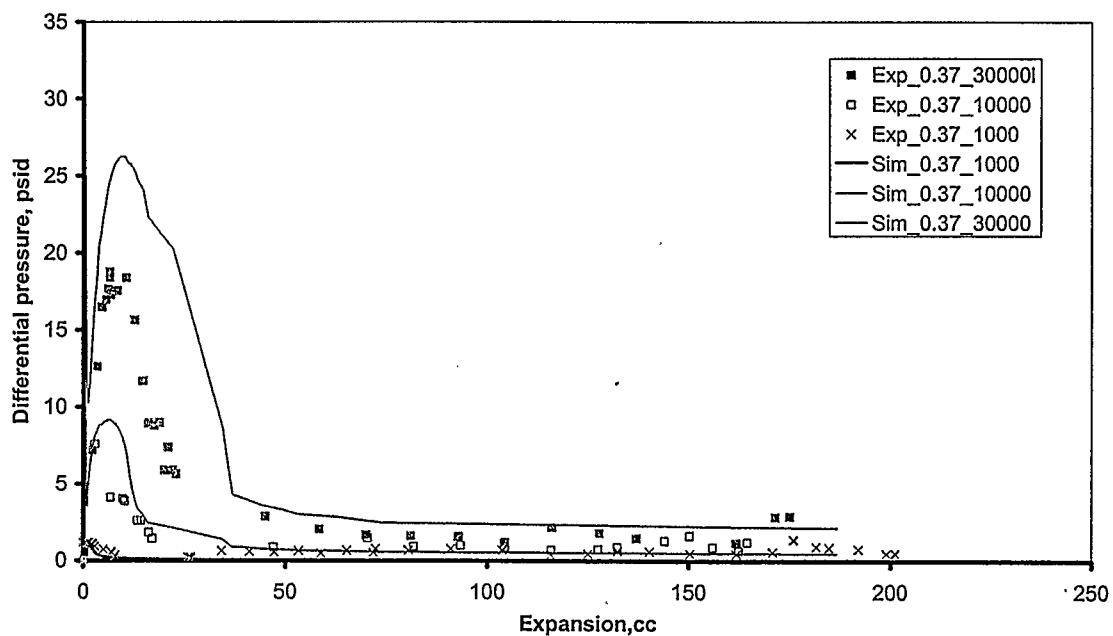
Figure 5.17 Simulation of differential pressure using ™ (Depletion rate = 0.37 cm³/hr)

Figure 5.18 Simulation of Gas saturation using IMEX™ (Depletion rate = 3 cm³/hr)
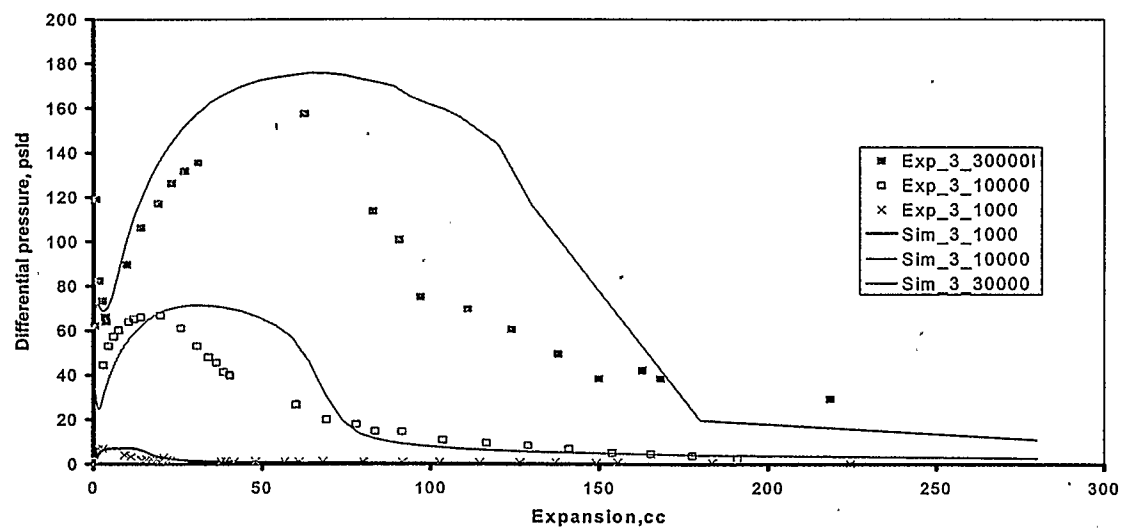
Figure 5.19 Simulation of Differential pressure using IMEX™ (Depletion rate= 3 cm³/hr)
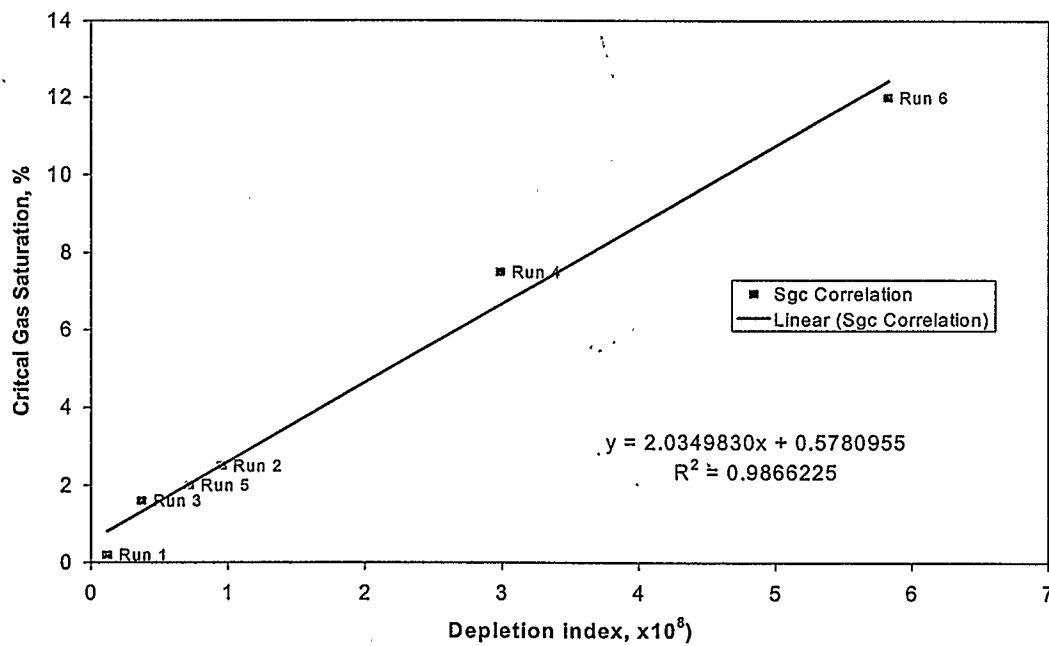
Figure 5.20 Correlation of Critical Gas Saturation with Depletion index, Alpha = 0.5
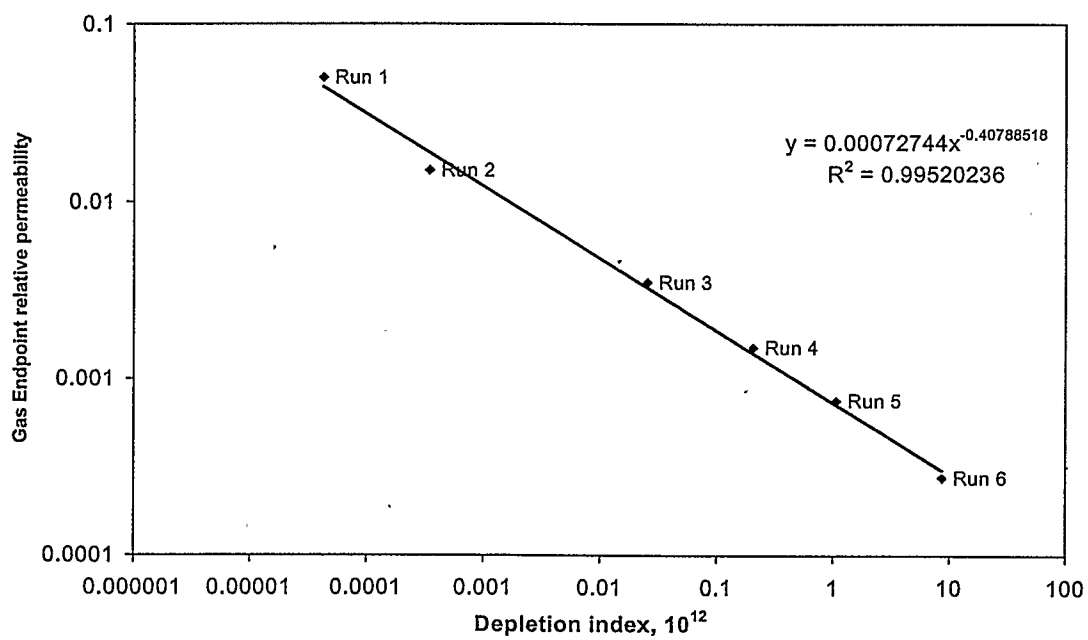
Figure 5.21 Correlation of Endpoint relative permeability with Depletion index, Alpha =

2.8

5.8.4 MATCHES BASED ON LOCAL PARAMETERS

In the previous section, the depletion index was calculated using the total fluid withdrawal rates. In order to investigate how the local depletion index correlates with gas endpoint relative permeability, the one-dimensional simulator described in Chapter 4 is used to simulate the experiment. As a first pass, the correlations obtained in section 5.8.3 were used in the simulator. As discussed in Chapter 4, the simulator internally calculates relative permeability values from local parameters. Sequence of event used in the simulator is as follows.

1) Calculates local velocity.

2) Calculate local depletion index from local velocity and local viscosity.

3) Calculate gas endpoint relative permeability from depletion index- Endpoint correlation.

4) Calculate Critical gas saturation from depletion index- Critical gas saturation correlation.

5) Calculate gas relative permeability values.

Figures 5.26 and 5.27 show the correlation for endpoint relative permeability and critical gas saturation respectively. Alpha was 0.5 for the critical gas saturation and 2.8 for the gas endpoint relative permeability. Figure 5.24 and Figure 5.25 show the match of the Average gas saturation while Figures 5.22 and 5.23 show the match of the pressure drop. The quality of the matches can be assessed from Figures 5.22 to 5.25.
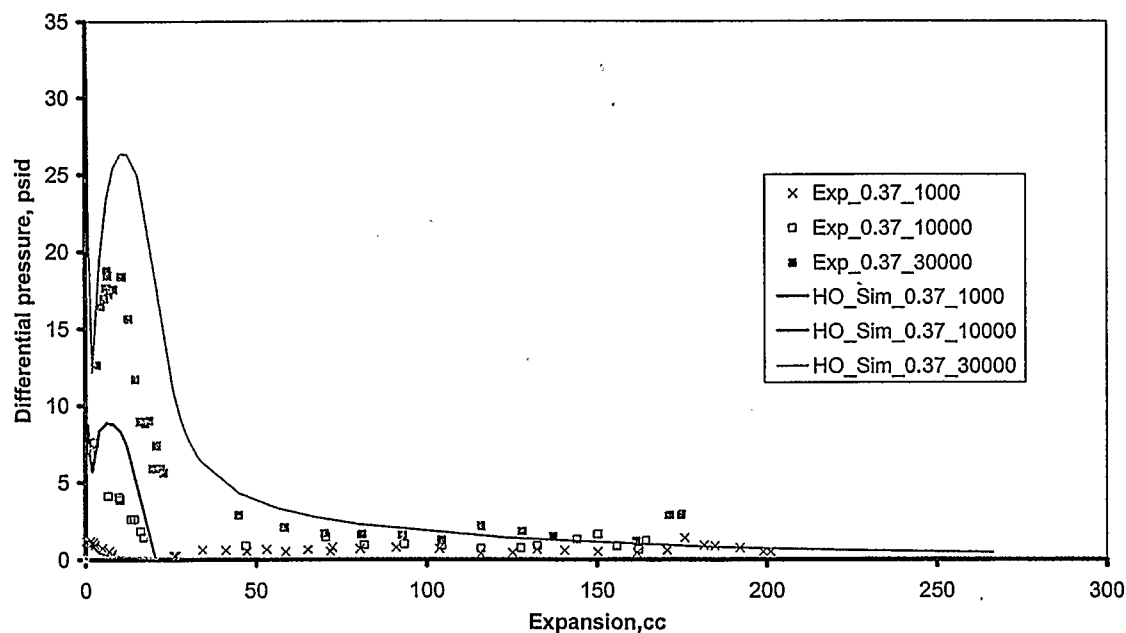
Figure 5.22 Simulation of Differential pressure using numerical model (0.37 cm³/hr)
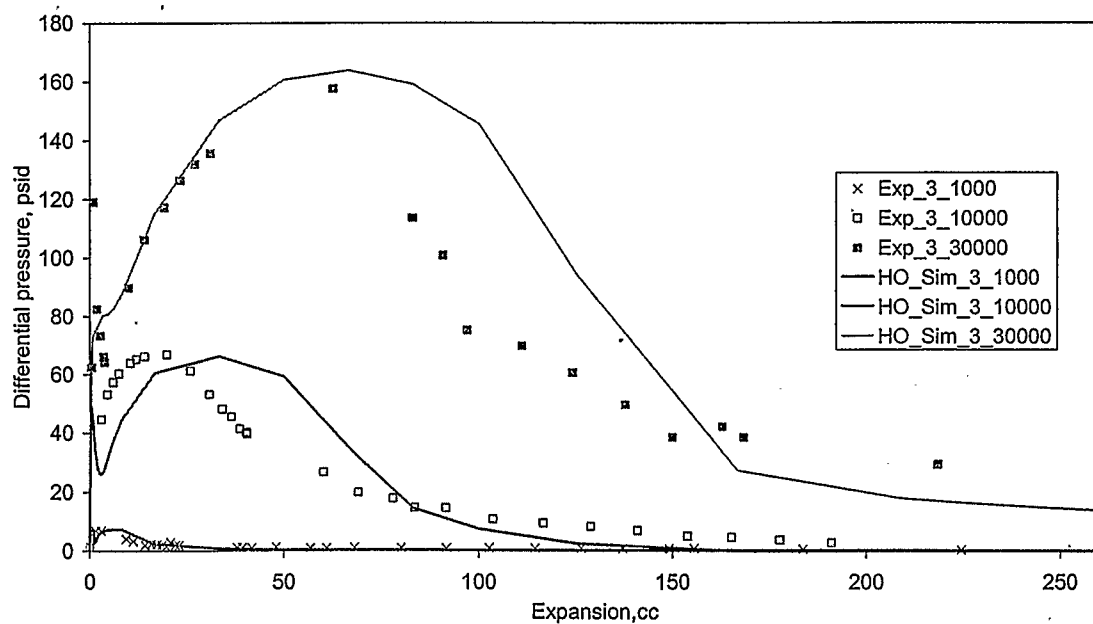
Figure 5.23 Simulation of Differential pressure using numerical model (3 cm³/hr)
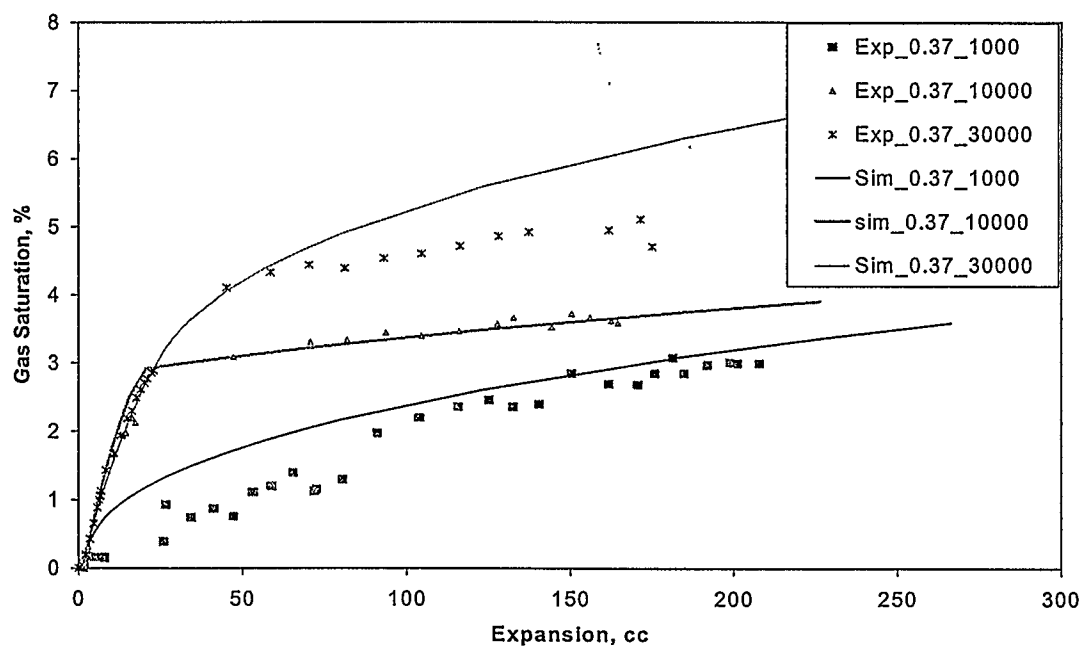
Figure 5.24 Simulation of average gas saturation using numerical model (0.37 cm³/hr)
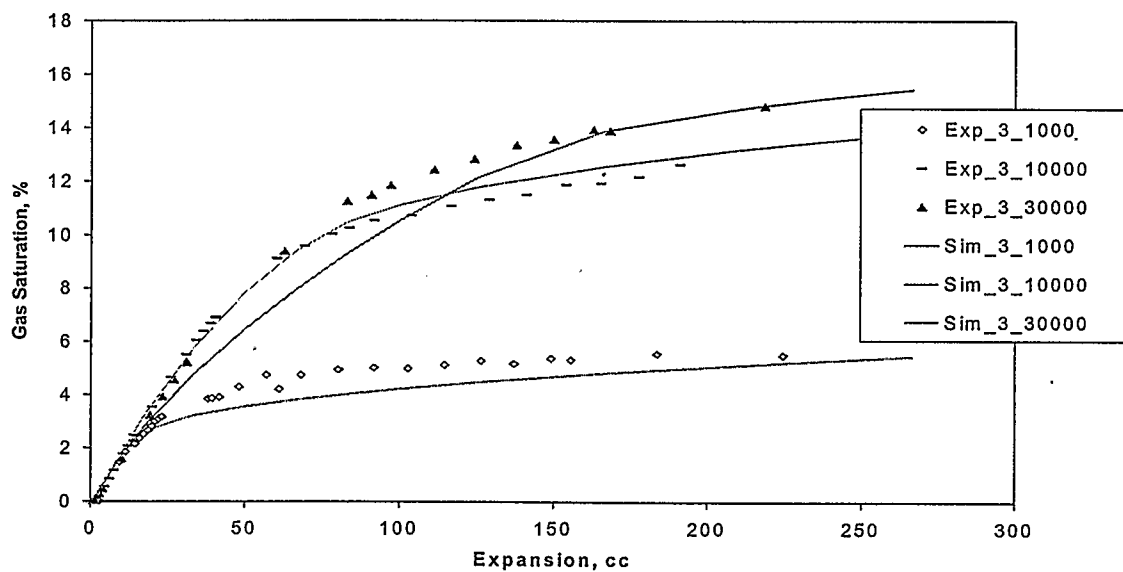
Figure 5.25 Simulation of average gas saturation using numerical model (3 cm³/hr)
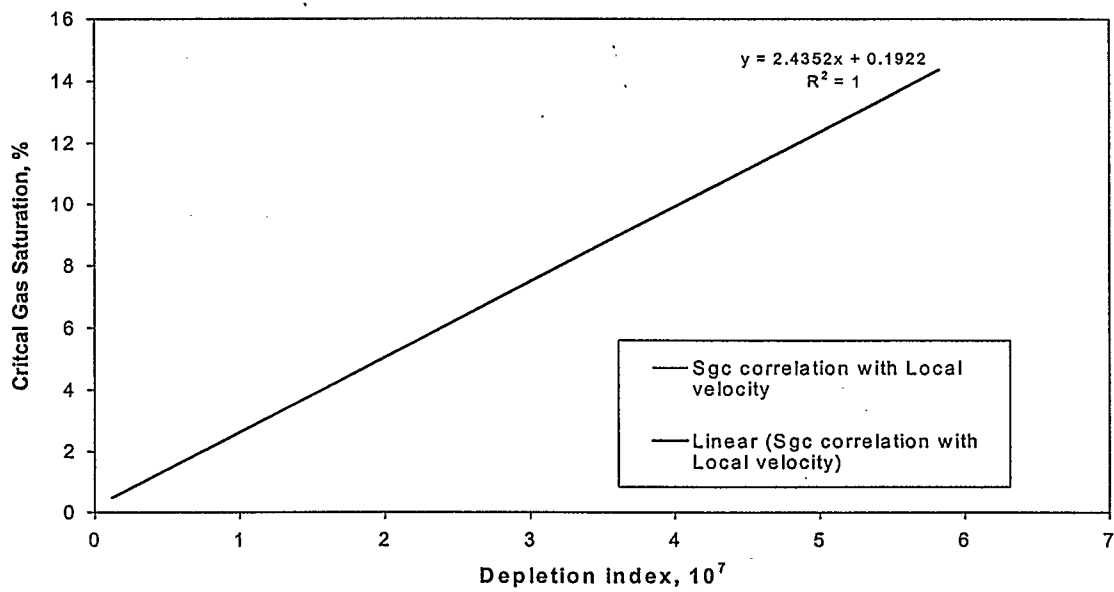
Figure 5.26 Correlation of Critical gas saturation with Depletion index, Alpha = 0.5
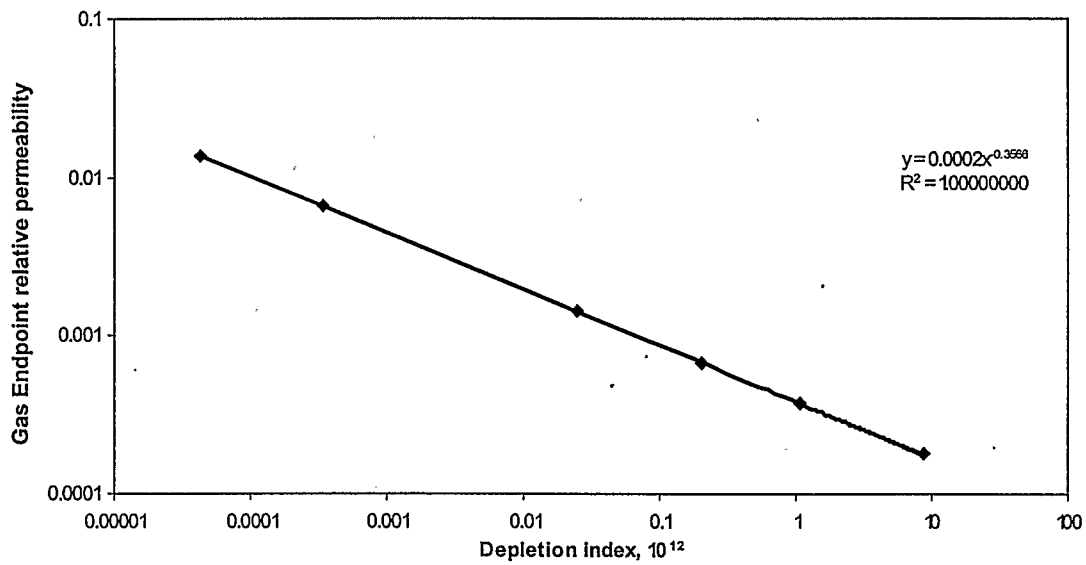
Figure 5.27 Correlation of gas endpoint relative permeability with depletion index, Alpha=2.8

5.8.5 Comments on modeling work

In Chapter 3, we used gas mobility as a function of capillary number to match experiments that included the effect of rate. There, relative permeability was a function of capillary number. The capillary number was chosen because it is a known dimensionless group that affects two-phase flow. In this chapter, we found that in order to match data of experiments where both rate and viscosity vary, a correlating factor (i.e. depletion index) other than capillary number need to be defined. In this section, we will show that with the correlating factor of depletion index, one could have matched the experiments of Chapter 3.

Equation 3.11 can be written as

$$S_{gc} = S_{gci} + a\frac{v\mu}{\sigma} = S_{gci} + \frac{a\mu^{0.5}v\mu^{0.5}}{\sigma}$$ (5.4)

Therefore,

$$S_{gc} = S_{gci} + a'I'$$

where

$$a' = \frac{a\mu^{0.5}}{\sigma}$$

Similarly, Equation 3.12a can be written as ·

$$k^0{}_{rg} = k^0{}_{rgi} - b\frac{v\mu}{\sigma} = k^0{}_{rgi} - b\frac{v\mu^{-1.8}\mu^{2.8}}{\sigma}$$

Therefore,

$$k^0{}_{rg} = k^0{}_{rgi} + b'I'$$ (5.5)

where

$$b' = \frac{b\mu^{-1.8}}{\sigma}$$

The above derivation shows that the match obtained in Chapter 3 with the capillary number term can also be obtained with the depletion index term by just changing the constants of equations 3.11 and 3.12a.

SUMMARY AND RECOMMENDATIONS

6.1 Summary and conclusions

Overall, a study of the effect of oil viscosity and depletion rate on gas mobility was done. This work is divided into two parts: the gas mobility experiments and numerical modeling. The following are the main findings from the study.

A)   Experiments were carried out to investigate factors leading to the favorable behavior of heavy oil solution-gas drive. Effect of both depletion rate and oil phase viscosity was studied. A complete set of pressure, pressure differential, and production data are reported. Observations from experiments showed that:

- Average gas saturation increased in the sand-pack as the depletion rate and oil phase viscosity increases.

- Critical gas saturation increased slightly with depletion rate and oil viscosity. For the system studied in this work, it seems that depletion rate is a major contributor to the value of critical gas saturation.

- Gas mobility was found to be low, and decreased with an increase in oil viscosity or depletion rate. In all the cases, gas relative permeability was low and the low gas phase mobility was presented as one of the reasons contributing to the favorable behaviors of heavy oil reservoirs.

- The effect of depletion rate and oil viscosity was successfully combined into a depletion index term and this parameter was correlated with gas relative permeability, oil recovery and critical gas saturation. It was observed that as the depletion index increases, gas mobility decreases, critical gas saturation increases and oil recovery increases. In this work,

combining oil viscosity and depletion rate in the "capillary number" term was not sufficient to give a good correlation with oil recovery, critical gas saturation or gas mobility.

It is important to note that the experiments of this study were conducted at a constant withdrawal rate and showed higher recoveries when oil viscosity increased. The observation of higher recovery for more viscous oils is not a general rule, especially in the field where often the total driving force (pressure differential) is fixed. Although solution-gas drive in more viscous oils may result in reduced oil recovery; however, there seems to be sufficient evidence to suggest that gas mobility decreases as oil viscosity increases. This partly compensates for the inefficient displacement that one would expect from a displacement with very unfavorable viscosity ratios.

B) The experimental results were successfully simulated using a commercial simulator and a one-dimensional simulation model. From the modeling work, an equilibrium numerical model was developed to incorporate the effect of oil viscosity and depletion rate. The gas relative permeability was allowed to be a function of saturation and a depletion index. Two depletion parameters: Capillary number and Depletion index were investigated in this study. Two experimental works were successfully simulated using these parameters. The capillary number dependent gas relative permeability was adequate in modeling a previous experiment where the rate-dependent behavior of solution-gas drive in heavy oil was investigated while depletion index dependent gas relative permeability curves better modeled the experiments in this work where the combined effect of rate and viscosity on heavy oil solution-gas drive was investigated. In both cases, the endpoint relative permeability curves decreased as the value of the capillary number or depletion index increases. In

general, the modeling work presented in this work showed that traditional two-phase flow formulation with viscous parameter-dependent relative permeability functions could be used for modeling solution-gas drive in heavy oils. All the data were matched satisfactorily. The results from the simulation indicated that

- Gas phase relative permeability decreased with increased depletion rate and viscosity.

- Gas phase relative permeability in heavy oil under study was low (10^{-4} and 10^{-7}) for gas saturation up to 15%.

- Critical gas saturation was observed to vary linearly with depletion index.

- A power law empirical model was developed to correlate the gas relative permeability as a function of depletion index for the system studied.

- A similar correlation suggested above was observed between critical gas saturation and gas relative permeability endpoint when the depletion index was calculated from local parameters.

6.2 RECOMMENDATIONS

The present work is a small contribution to understanding and modeling the complex phenomenon of solution-gas drive in heavy oil reservoirs. Some work still has to be done to deal with other issues not addressed by this work. Some recommended future works are as follows:

1. The idea of correlating gas mobility with dimensionless groups should be further investigated, whether these dimensionless groups are already established ones such as capillary number or viscosity ratio, or new ones such as depletion index.

2. It is expected that the effectiveness of solution-gas drive in heavy oils and gas-mobility would depend on other factors such as oil type, etc. The relative permeability data of this study are for the type of oil used and under the conditions specified in this work. Other factors should be investigated apart from oil type includes: interfacial tension, GOR, oil bubble point pressure. Interfacial tension, in particular is an important parameter during solution-gas drive and it may be necessary to investigate its contribution to viscous flow. The results of the proposed study and the results from the current study will help develop a more general depletion parameter which will help develop a more accurate model to predict gas phase relative permeability.

3. Earlier in this work, it was suggested that an increase in depletion rate and oil viscosity would alter the early-time phenomena of supersaturation, nucleation and growth as well as the late-time phenomena of coalescence and flow, leading to reduced gas mobility and improved oil recovery. It was then showed that the effects of oil viscosity and withdrawal rate could be combined in the form of a depletion index, such that oil recovery increased as the depletion index increased. The depletion index suggested in this work is a first attempt at combining the effect of depletion rate and oil viscosity on the effectiveness of solution-gas drive in heavy oils, and does not explain how rate and viscosity interact with the above phenomena. Further mechanistic modeling and microscopic experiments are needed to quantify how these factors alter gas mobility. In the mechanistic modeling, depletion index should be correlated with early time parameters like supersaturation, nucleation and rate of bubble growth.

4.   The ideas in this work need to be extended to the field applications such that field cases can be modeled depending on a previously determined depletion index correlation and probably a correlation for sand production. Once again, scaled experiments simulating the field operating conditions should be performed. In general, proper up-scaling methodology needs to be developed to extend experimental and modeling that show viscous dependence results to field scale.

5.   Last but not least, the one-dimensional experiments and model presented in this work needs to be extended to two-dimensional model experiments and simulation. This will improve our understanding of the spatial effect of oil viscosity and depletion rate on the overall solution-gas drive process in heavy oils.

REFFERENCES

AEUB: " Alberta's Energy Resources-1996 in Review, Alberta Energy and Utilities Board, (1997) 6-7.

AKIN, S. and KOVSCEK, A., Heavy Oil Solution-gas drive: A Laboratory Study. Journal of Petroleum Science and Engineering Vol 35, pp 33-48, 2002.

ALBARTAMANI, N.S., FAROUQ ALI, S.M., and LEPSKI, B. Investigation of Foamy Oil Phenomena in Heavy Oil Reservoirs, paper *SPE* 54084 presented at the 1999 *SPE* International Thermal Operations and Heavy Oil Symposium, Bakersfield, California, March 1999.

ANDARCIA, L. HENRY, C. and RICO, A. Experimental Study on Production Performance of Two Different Heavy Oil in Venezuela, paper CIM 2000-43 presented at the 2000 Canadian International Conference, Calgary, AB, June 2000.

ARORA P., KOVSCEK A.R, Mechanistic Modeling of Solution-gas drive in Viscous Oils, paper presented at the *SPE* international Thermal Operations and Heavy Oil Symposium, Porlamar, Venezuela, March 2002.

AZIZ, K and SETTARI, A. Petroleum Reservoir Simulation, Applied Science Publishers Ltd., London pp 99-123 1979.

BAIL, P.T. and MARSDEN, S.S., Saturation Distribution in a Linear System During Oil Displacement; Producers Monthly, pp.22-32, June 1957.

BATYCKY, J.P., LEAUTE, R.P., and DAWE, B.A., A mechanistic model of Cyclic Steam Stimulation, paper *SPE* 37550; Presented at the international Thermal Operations and heavy Oil Symposium, Bakersfield, CA February 1997.

BENTSEN, R. G., Conditions Under which the Capillary Term may be Neglected, *Journal of Canadian Petroleum Technology*, pp. 25-30, Cot-Nov 1978, Montreal.

BORA, R., Cold Production of Heavy oil – An Experimental Investigation of Foamy Oil in Porous Media: Ph. D Dissertation, University of Calgary, 1998.

BORA, R., MAINI, B.B., and CHAKMA, A, Flow Visualization Studies of Solution-gas drive Process in Heavy Oil Reservoirs Using a Glass Micro-model; *SPEREE* pp 224–229 June 2000.

BOYER, R.L., MORGAN, F., and MUSKAT, M., A New Method for Measurement of Oil Saturations in Core; TP 2124 in Petroleum Technology, January 1947.

BRENNEN, C. E., Cavitation and Bubble Dynamics, Oxford University Press, 1995.

BUTLER, R, M., Thermal Recovery of Oil and Bitumen, Prentice-Hall Inc., 1991.

CARMAN, P.C., Fluid Flow Through Granular Beds. *Trans. inst. Chem. Eng.*, Vol. 15, 150-166, 1937.

CARSLAW, H.S. and JAEGER, J.C. Conduction of Heat in Solids, 2nd ed. Oxford University Press, London (1959).

CHARDAIRE, C., Simultaneous Estimation of Relative Permeabilities and Capillary Pressures; presented at the 64th Annual Technical Conference and Exhibition of the *SPE* held in San Antonio, TX, October 8-11, 1989.

CIVAN F. and DONALDSON E. C., Relative Permeability from Unsteady State Displacements: An Analytical Interpretation *SPE* 16200 presented at the *SPE* Production Operation Symposium held in Oklahoma city, Oklahoma March 8-10, 1987.

CLARIDGE E. L. and PRATS M. A. A proposed model and mechanism for anomalous foamy heavy oil symposium held in Calgary AB Canada June, 1995

COLES R. Boiling Nucleation Advance Heat and Mass Transfer, 10 pp. 24-26, 1974

COOMBE, D. and MAINI, B. Modeling Foamy Oil Flow, presented at the Workshop on Foamy Oil Flow held at the Petroleum Recovery Inst., Calgary, 27 April 1994.

DU, C. and YORTSOS Y.C. A Numerical Study of the Critical Gas Saturation in a Porous Medium," Transport in Porous Media 35, pp 205, 1999.

DUMORE, J.M., Development of Gas Saturation During Solution-gas drive in an Oil Layer Below the Gas Cap; *Society of Petroleum Engineers Journal*, pp. 221-218, September 1970.

DUPREY, E. R. LEVREBVE, Factors affecting Liquid-liquid Relative Permeabilities of a Consolidated Porous media, *SPE Journal*, Vol 13, pp 39-47, 1973.

DUSSEAULT, M.B. and EL-SAYED, S. Heavy-Oil Production Enhancement by Encouraging Sand Production; paper *SPE* 59276 presented at the 2000 *SPE/DOE* Improved Oil Recovery Symposium, Tulsa, Oklahoma, April 2000.

EGERMANN, P. and VIZIKA, O. Critical Gas Saturation and Relative Permeability During Depressurization in the Far Field and Near-Wellbore Region, paper *SPE* 63149 presented at the *SPE* Annual Technical Conference and Exhibition, Dallas, TX, 1–4 October, 2000.

EHLIG-ECONOMIDES, C.A., FERNANDEZ, B.G., and GONGORA, C.A. Global Experience and Practices for Cold Production of Moderate and Heavy Oil, paper *SPE* 58773 presented at the 2000 *SPE* International Symposium on Formation Damage Control, Lafayette, Louisiana, February, 2000.

EHRLICH, E., HASIBA, H., RAIMONDI, P., Alkaline Waterflooding for Wettability Alternation Evaluating Potential Field Application, *JPT*, pp 1359-1352, 1974.

ELKINS, L.F., MORTON, R., and BLACKWELL, W.A. Experimental Fireflood in a Very Viscous Oil-Unconsolidated Sand Reservoir, S.E. Pauls Valley Field, Oklahoma, paper *SPE* 4086 presented at the 1972 *SPE* Annual Meeting, San Antonio, Texas, 8-11 October.

FIROOZABADI, A. and AROSON, A., Visualization and Measurement of Gas Evolution and Flow of Heavy and Light Oil in Porous Media paper *SPE* 71499 *SPERE* Volume 2, No 6, pp. 550-553, December 1999.

FIROOZABADI, A. Mechanism of Solution-gas drive in Heavy Oil Reservoirs, J. Cdn. Pet. Tech., pp 40, No. 3 March 2001.

FOULSER R.W.S, GOODYEAR S.G and SIMS R.J. Two-Phase and Three-Phase Relative permeability Studies at High Capillary Numbers, paper *SPE* 24152 presented at the 1992 *SPE/DOE* Symposium on Enhanced Oil Recovery, Tulsa, Oklahoma, April 1992.

HAGOORT, J., Oil Recovery by Gravity Drainage; *Society of Petroleum Engineers Journal*, pp. 139-150, June 1980.

HANDY, L.L., A Laboratory Study of Oil Recovery by Solution-gas drive; Trans AIME, Vol. 213, pp. 310-315, 1958.

HELSET, H. M., NRODTVEDT, J.E., SKJOEVELAND, S.M., and VIRNOVSKY, G.A., Relative Permeabilities from displacement Experiments with Full Account for Capillary Pressure; *SPE Reservoir Engineering Evaluation, pp. 92-98, April 1998.*

HEMMINGSEN, E. A., Cavitation in Gas-Saturated Solutions; Journal of Applied Physics, 46,1, January 1975.

HENDERSON, G.D., DANESH, A., TEHRANI, D.H., AL-SHAIDI, S. and PEDEN, J.M. Measurement and Correlation of Gas Condensate Relative Permeability by the Steady-State Method *SPE* Journal 191 – 201, June 1996.

HEPTER, L.,G. HIS, C. AOSTRA Technical Handbook on Oil Sands, Bitumen and Heavy Oil; AOSTRA Technical Publication Series #6, 1989.

HONARPOUR, M., KOEDERITZ, L., and HARVEY, A.H., *Relative Permeability of Petroleum Reservoirs,* Society of Petroleum Engineers Inc. Publication, 1994

HOYOS, M., MOULU, J.C., DEFLANDRE, F., and LENORMAND, R., Ultrasonic Measurements of Bubble Nucleation Rate During Depletion Experiments in a Rock Sample. *SPE* 20525, presented at the 65th Annual Technical Conference and Exhibition of the *SPE* held in New Orleans, LA, September 23-26, 1990.

HUANG, W.S. *et al.* Cold Production of Heavy Oil from Horizontal Wells in the Frog Lake Field, paper *SPE* 37545 presented at the 1997 *SPE* International Thermal Operations and Heavy Oil Symposium, Bakersfield, California, February 1997.

HUERTA, M., TICO, A., JIMENEZ, I., MIRABAL, M. DE., and ROJAS, G., Understanding Foamy Oil Mechanism for Heavy Oil Reservoirs During Primary Production; *SPE* 36749, presented at the 1996 *SPE* Annual Technical Conference and Exhibition, Denver, CO, October 6-9, 1996.

IMEX USER'S MANUAL, Computer Modeling Group, Calgary, October 1995.

ISLAM, M. R. and CHAKMA, A., Mechanics of Bubble Growth in Heavy Oil Reservoirs; *SPE* 20070 Presented at the 60th California Regional Meeting, Ventura, CA, April 4-6, 1990.

JAVADPOUR, F. and POOLADI-DARVISH, M. Network Modeling of Gas Relative Permeability in Heavy Oil, paper CIM-148 presented at the 2001 CIM Annual Technical Meeting, Calgary, Canada, June, 2001.

JOSEPH, D.D., KAMP, A.M., and BAI, R. A New Modeling Approach for Heavy-Oil Flow in Porous Media, paper *SPE* 69720 presented at the *SPE* International Thermal Operations and Heavy Oil Symposium, Porlamar, Margarita Island, Venezuela, March, 2001.

KALAYDJIAN, F. J. M., dynamic Capillary Pressure Curve for Water/Oil Displacement in Porous Media: Theory Vs. Experiment; *SPE* 24813, presented at the 67th *SPE* Annual Technical Conference and Exhibition, Washington, DC , October 4-7, 1992.

KAMATH, J., and BOYER, R.E., Critical Gas Saturation and supersaturation in Low Permeability Rocks; *SPE* 26663, *SPE Formation Evaluation*, pp 247-253, December 1995.

KAMP, A.M., JOSEPH, D.D., and BAI, R. A New Modeling Approach for Oil Flow In Porous Media, paper *SPE* 69720 presented at the *SPE* International Thermal Operations and Heavy Oil Symposium, Venezuela, March, 2001.

KASHCHIEVE, D., and FIROOZABADI, A., Kinetics of Initial Stage of Isothermal Gas Phase Formation; J. of Chem. Phys., 98,6,pp. 4690-4699, March 5,1993.

KENNEDY, H. T., and OLSON, C. R., Bubble Formation in Supersaturated Hydrocarbon Mixtures; *Trans AIME*, Vol. 195, pp. 271-278, 1952.

KOVSECK, A. R., and RADKE, C., Fundamentals of Foam Transport in Porous Media; Chapter 3 of Foams Fundamentals and Application in the Petroleum industries'" Schramm, L.L., Ed.; Advances in Chemistry Series 242, American Chemical Society, Washington D.C., 1994.

KRAUS, W.P., MCCAFFREY, W.J., and BYOD, G.W. Pseudo-Bubble-point Model for Foamy Oils, paper CIM 93-45 presented at the 44th Annual Technical Conference of the Petroleum Society of CIM Calgary, AB, May 9-12,1993.

KUMAR R., POOLADI-DARVISH M. and T. Okazawa, An investigation into Enhanced Recovery under Solution-gas drive in Heavy Oil Reservoirs, paper *SPE* 59336, in press in *SPEJ*, 2002.

KUMAR R. and POOLADI-DARVISH, M. Solution-gas drive in Heavy Oil: Viscosity Effect on Gas Relative Permeability, paper CIM-152 presented at the 2001 CIM Annual Technical Meeting, Calgary, Canada, June, 2001.

KUMAR R., POOLADI-DARVISH, M. Solution-gas drive in Heavy Oil: Field Prediction and Sensitivity Studies Using Low Gas Relative Permeability, *Journal of Canadian Petroleum Technology*, Vol **41**, pp. 26 – 32 March 2002.

KUMAR, R. and POOLADI-DARVISH, M. Effect of Viscosity and Diffusion Coefficient in the Kinetics of Bubble Growth in Solution-gas Drive in Heavy Oil Reservoirs", JCPT, Vol **40**, pp 30 March 2001.

KUMAR, R., Solution-Gas drive in Heavy Oils – Gas Mobility and Kinetics of Bubble Growth: M.sc. Thesis, University of Calgary, 2000.

LABTECH, User Guide, Laboratory Technologies Corporation; 1994.

LAGO, M., GOMES R., and HUERTA, M. Visualization Study During Depletion Experiments of Venezuelan Heavy Oils using Glass Micromodels, Paper 2000-56 presented at the 51st Annual Technical Meeting of the Petroleum Society of CIM, in Calgary Alberta June , 2000.

LEBEL, J. P. Performance Implications of Various Reservoir Access Geometries, paper presented at the 11th Annual Heavy and Oil sands Technical Symposium, March 2,1994.

LI. A and YORTSOS, Y. C. Theory of Multiple Bubble Growth in Porous Media by Solute Diffusion; *Chem Engg. Sci.*, Vol **50**, pp. 1247-1271, 1995.

LOUGHEAD, D.J. and SALTUKLAROGLU, M. Lloydminster Heavy Oil Production: Why So Unusual? presented at the Ninth Annual Heavy Oil and Oil Sands Symposium, Calgary, 11 March 1992.

MAINI, B.B. Foamy Oil Flow in Heavy Oil Production, JCPT, Vol **35**, pp 21, June 1996.

MAINI, B.B. Foamy Oil Flow in Primary Production of Heavy Oil Under Solution-gas drive, paper *SPE* 56541 presented at the 1999 *SPE* Annual Technical Conference and Exhibition, Houston, 3-6 October.

MAINI, B.B., SARMA, H.K., and GEORGE, A.E. Significance of Foamy-Oil Behaviour in Primary Production of Heavy Oils," JCPT, Vol **32**, No. 9 Nov. 1993.

MCCABE, SMITH and HARRIOT; Unit Operation in Chemical Engineering; McGraw Hill Publications, 1990.

MCCAFFREY, W.J., and BOWMAN, R.D., Recent Success in Primary Bitumen Production, paper No. 6 presented at the 8th Annual Calgary U. *et al.* Heavy Oil & Oil Sands Technical Symposium, Calgary, March 1991.

MEGAWAVE™ Software, User Guide, 2000.

METWALLY, M., and SOLANKI, S., Heavy Oil Reservoir Mechanism, Lindbergh and Frog Lake Fields, Alberta, Part I: Field Observations and Reservoir Simulation, presented at the 46th Annual Technical Meeting of CIM, Banff, Canada, May 1995.

MORGAN, F., MCDOWELL, J. M., DOTY, E. C., Improvements in the X-ray Saturation Techniques of Studying Fluid Flow, *Trans AIME, Vol 189,* pp. 183-194, 1950.

MOULU, J. C., Solution-gas drive: Experiments and Simulation *Journal of Petroleum Science and Engineering,* 2, pp. 379-386, 1989.

OAK, M. J., and EHRLICH, R., A New X-ray Absorption Method for Measurement Three-Phase Relative Permeability; *SPE Reservoir Engineering*, pp.199-206, February, 1998.

OAK, M. J., BAKER, L.E and THOMAS, D. C., Three Phase Relative Permeability of Berea Sandstone; *Journal of Petroleum Technology*, pp.1054-1061, August 1990

ODEH, A. S, Effect of Viscosity Ratio Relative Permeability; *Trans AIME*, Vol. 216, pp. 346-353, 1959.

OSABA, J. S., RICHARDSON, J. G., KERVER, J. K., HAFFORD, J. A., and BLAIR, P. M., Lab Measurement of Relative Permeability; *Trans AIME*, Vol. 192, pp 47-56, 1951.

Ozisik, M. N., Heat Conduction, 2nd ed. John Wiley and Sons, Inc, USA 1993

PARSONS, R. W., Microwave attenuation – A New Tool for Monitoring Saturations in Laboratory Flooding Experiments; *Society of Petroleum Engineers Journal*, pp. 302-310, August 1975.

PATEL, R. D., Bubble Growth in Viscous Newtonian Liquid; Chemical Engg. Sci., Vol. 35, pp 2352-2356, 1980.

POOLADI-DARVISH, M., and FIROOZADI, A., Solution-gas drive in Heavy Oil Reservoirs, *Journal of Canadian Petroleum Technology (JCPT)*, April 1999, Vol 38, (4) pp. 54 – 61.

POPE G., WU W., NARAYANASWAMY G., DELSHAD M., SHARMA M., WANG P., Modeling Relative Permeability Effects in Gas Condensate Reservoirs With a New Trapping Model *SPEREE* 171 – 179, April 2000.

RAPPORT, L. A., and LEAS, W. J., Relative Permeability to Liquid in Liquid Gas systems; Trans AIME, Vol. 192, pp. 83-98, 1951.

RICHARDSON, J. G., KERVER, J. K HAFFORD, J. A., and OSABA, J. S., Laboratory Determination of Relative Permeability; *Trans AIME*, Vol. 195, pp. 187-196, 1952.

SAHNI, A., GADELLE, F., KUMAR, M., KOVSCEK, A. and TOMUTSA, L.: Experiments and Analysis of Heavy Oil Solution-gas drive, papers *SPE* 71498 presented at the 2001 *SPE* Annual Technical Conference and Exhibition, New Orleans, Louisiana, September 3 – October 3.

SARMA H. K and BENTSEN, R. G., A New Method For Estimating Relative Permeabilities From Unstabilized Displacement Data; *Journal of Canadian Petroleum Technology*, Vol 28, No 4, pp. 118-128, July- Aug 1989.

SARMA H. K and BENTSEN, R. G., Further Experimental Validation of the External-Drive Technique; *Journal of Canadian Petroleum Technology*, Vol 29, No 4, pp. 75-83, July- Aug 1990.

SARMA H. K and MAINI, B., Role of Solution Gas in Primary Production of Heavy Oils; *SPE* 23631, presented at the Latin American Petroleum Engineering Conference, Caracas, Venezuela, March 8-11, 1992.

SCRIVEN, L. E., On the Dynamics of Phase Growth; *Chem. Engg. Sci.,* Vol. 10, pp. 1-13, 1959.

SHEN, C. and BATYCKY, J.P. Some Observations of Mobility Enhancement of Heavy Oils Flowing through Sand-pack under Solution-gas drive, paper CIM 96-27 presented at the 47th Annual Technical Conference of the Petroleum Society of CIM, Calgary, 10-12 June 1996.

SHENG, J. J., MAINI, B. B., HAYES, R.E., and TORTIKE, W.S., Critical Review of Foamy Oil Flow, *Transport in Porous Media*, pp 35, 1999.

SHENG, J.J., HAYES, R.E., MAINI, B.B., and TORTIKE, W.S. Modeling Foamy Oil Flow in Porous Media, *Transport in Porous Media,* Vol **35**, pp 227–258 1999.

SMITH, G.E., Fluid Flow and Sand Production in Heavy Oil Reservoirs under Solution-gas drive, *SPEPE*, pp. 169-177, May 1998.

SOLANKI, S. and METWALLY, M., Heavy Oil Reservoir Mechanism, Lindbergh and Frog Lake Fields, Alberta, Part II: Geomechanical Evaluation, paper *SPE* 30249 presented at the 1995 International Heavy Oil Symposium, Calgary, 19-21 June 1995.

STEWARD, C. R. *et al.*, The Role of Bubble Formation in Oil Recovery by Solution-gas drives in Limestones, *Trans AIME*, Vol **201**, pp. 294, 1954.

SZEKELY, J. and MARTINS, G. P., Non equilibrium Effects in the Growth of Spherical Gas Bubbles due to Solute Diffusion; *Chem. Engg. Sci.*, Vol. 26, pp. 147-159, 1971.

SZEKELY, J. and MARTINS, G. P., Non equilibrium Effects in the Growth of Spherical Gas Bubbles due to Solute Diffusion-II; *Chem. Engg Sci.*, Vol. 28, pp. 2127-2140, 1973.

TALABI, O. and POOLADI-DARVISH, M., A simulator for solution gas drive in heavy oil reservoirs, paper CIM 165 presented at the 53rd Annual Technical Meeting of the Petroleum Society, Calgary, 10-12 June 2002.

TANG, G. and FIROOZABADI, A., Effect of GOR, Temperature and Initial Water Saturation on Solution-Gas Drive in Heavy Oil Reservoirs, paper *SPE* 71499

presented at the 2001 *SPE* Annual Technical Conference and Exhibition, New Orleans, Louisiana, 30 September – 3 October, 2001.

TANG, G. and FIROOZABADI, A., Gas and Liquid-phase Relative Permeabilities for Cold Production from Heavy Oil Reservoirs, paper *SPE* 56540 presented at the 1999 *SPE* Annual Technical Conferences and Exhibition Houston, TX, 3-6 October 1999.

TREINEN, R.J. *et al.:* Hamaca: Solution-gas drive Recovery in a Heavy Oil Reservoir, Experimental Results, paper *SPE* 39031 presented at the Fifth Latin American and Caribbean Petroleum Engineering Conference, Rio de Janeiro, 30 August-3 September 1997.

TREMBLAY, B., SEDGWIK, G., and VU, D., CT Imaging of Sand Production in a Horizontal Sand-pack Using Live Oil, paper CIM 98-78 presented at the 49th Annual Technical Meeting of the Petroleum Society, Calgary, 8-10 June 1998.

URGELLI, D. *et al.*, Investigation of Foamy Oil Effect From Laboratory Experiments, paper *SPE* 54083 presented at the 1999 *SPE* International Thermal Operations and Heavy Oil Symposium, Bakersfield, California, 17-19 March 1999.

VASSENDEN, F., and HOLT, T., Experimental Foundation for Relative Permeability Modeling of Foam, *SPEREE*, pp 179 – 185, April 2000.

WALL, C. G., and KHURANA, A. K., The Effects of Rate of Pressure Decline and Liquid Viscosity on Low-Pressure Gas Saturations in Porous Media", *JCPT*, pp 335 November 1977.

WATSON, A. T., RICHMOND, P.C., KERIG, P. D., and TAO, T. M., A Regression Based Method for Estimating Relative Permeabilities From Displacement Experiments; *SPE* Reservoir Engineering, pp. 953-958, August 1988.

WONG, R. C., GUO, F., WEAVER, J. S., and BAR, W. E., Heavy Oil Flow Under Solution-gas drive: Pressure Depletion Experiments;, *Journal of Canadian Petroleum Technology*, pp. 31-37, April 1999.

YORTSOS, Y.C. and PARLAR, M.: "Phase Change in Binary Systems in Porous Media: Application to Solution-gas drive," work performed under Contract No. FG18-87BC14126, U.S. Dept. of Energy, Washington, DC, (October 1989).

APPENDIX I

A1.1 Formulation of problem

The problem solved in the numerical model is a one-dimensional two-phase flow in porous media. Figure A1.1 is a diagrammatic representation of the system. The system was initially fully saturated with live oil above its bubble point pressure. Flow is through one side of the core and the other side is a no flow boundary. As pressure drop in the
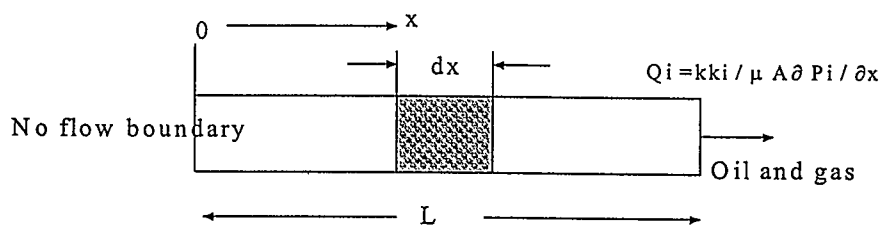
Figure A1.1: Schematic diagram for the one-dimensional two-phase problem

sand-pack, gas is generated and flow moves from single phase to two-phase flow.

The system is assumed to always be in equilibrium and the relative permeability is allowed to be a function of gas saturation as well as other depletion parameters.

A1.2 Initial and boundary conditions

There are two boundary conditions incorporated in the model. For the depletion experiments conducted in this work, the constant flow Neumann boundary condition on both boundaries is applied with flow rate of zero for the no flow boundary.

A1.3 Derivation of the two-phase flow equations

The flow equations in this model were derived from the laws of conservation of mass and momentum, Darcy's law and compressibility equations. The equation for one-dimensional oil-gas flow is given as

$$\frac{\partial}{\partial x}\left[\lambda_o\left(\frac{\partial P_o}{\partial x}-\gamma_o\frac{\partial z}{\partial x}\right)\right]=\frac{\partial}{\partial t}\left(\frac{\phi S_o}{B_o}\right)+q_o \quad \text{(Oil phase)} \tag{A1.1}$$

$$\frac{\partial}{\partial x}\left[\lambda_g\left(\frac{\partial P_g}{\partial x}-\gamma_g\frac{\partial z}{\partial x}\right)\right]+\frac{\partial}{\partial x}\left[R_{so}\lambda_o\left(\frac{\partial P_o}{\partial x}-\gamma_o\frac{\partial z}{\partial x}\right)\right]=\frac{\partial}{\partial t}\left(\frac{\phi S_g}{B_g}+R_{so}\frac{\phi S_o}{B_o}\right)+R_{so}q_o+q_g \text{(Gas)} \tag{A1.2}$$

where

P is the pressure

γ is the gravitational constant.

S_o – saturation in each phase

B_o – formation volume factor in each phase

A1.4 Formulation of the equations to be used for the I.M.P.E.S method

According to the formulation of Settari and Aziz (1979), .The finite difference equation for equations A.1 and A.2 is given by

$$\Delta T_o(\Delta P^{n+1}{}_o)_i=\frac{\Delta_t(V_p\frac{S_o}{B_o})_i}{\Delta t}+Q_{oi} \tag{A1.3}$$

$$\Delta T_g(\Delta P^{n+1}+\Delta P_c)_i+(\Delta R_sT_o\Delta P^{n+1})_i=\frac{\Delta_t V_p(R_{so}\frac{S_o}{B_o}+\frac{S_g}{B_g})_i}{\Delta t}+Q_{gi}+R_{so}Q_o \tag{A1.4}$$

where

$$\Delta_t(\frac{\phi S_l}{B_l}) = (\frac{\phi S_l}{B_l})^{n+1} - (\frac{\phi S_l}{B_l})^n \qquad \text{(A1.5)}$$

$$V_{pi} = \phi_i A_i \Delta x_i = \phi_i V_i \qquad \text{(A1.6)}$$

$$\Delta T \Delta P = T_{i+1/2}[P_{i+1} - P_i] + T_{i-1/2}[P_{i-1} - P_i] \qquad \text{(A1.7)}$$

$$T_{i+1/2} = \lambda_{i+1/2}(\frac{A_{i+1/2}}{\Delta x_{i+1/2}}) \qquad \text{(A1.8)}$$

$$\lambda_{i+1/2} = (\frac{kk_{rl}}{\mu_l B_l})_i \qquad \text{(A1.9)}$$

The I.M.P.E.S formulation for two-phase flow can be written in terms of oil-phase pressure and oil- phase saturation. This is given below.

$$\Delta T_o(\Delta P^{n+1}{}_o)_i = C_{2p}\Delta_t P + C_{2o}\Delta_t S_o + Q_{oi} \qquad \text{(A1.10)}$$

$$\Delta[T_g(\Delta P^{n+1}{}_g + \Delta P^n{}_g)_i + \Delta[R_{so}T_o(\Delta P^{n+1}{}_o)_i = C_{3p}\Delta_t P + C_{3o}\Delta_t S_o + C_{3g}\Delta_t S_g + R_{so}Q_{oi} + Q_g$$

$$\text{(A1.11)}$$

where

$\Delta P^n{}_g$ is the change in capillary pressure.

$$C_{2p} = \frac{V}{\Delta t}[(S_o \phi)b_o{}' + S^n{}_o b_o{}^{n+1} \phi']$$

$$C_{2o} = \frac{V}{\Delta t}[\phi b_o{}']^{n+1}$$

$$C_{3o} = \frac{V}{\Delta t}R_{so}(\phi b_o)^{n+1}$$

$$C_{3p} = \frac{V}{\Delta t}(R_{so}((S_o \phi)^n b_o + S_o{}^n b_o{}^{n+1} \phi) + S_g \phi^{n+1}b'{}_g + S_g \phi' b_g{}^{n+1} + (S_o \phi b_o)^{n+1}R_{so}{}'$$

$$C_{3g} = \frac{V}{\Delta t}(\phi b_g)^{n+1}$$

$$b'_I = (\frac{1}{B_I})' = \frac{d(\frac{1}{B_I})}{dP_I}$$

Equation (A1.10) and (A1.11) are combined by eliminating the saturation terms. First we multiply equation (A1.10) by a variable A_I and add the result to equation (A1.11). All the saturation terms are then equated to zero and the value of A was determine.

Now, $S_g = 1 - S_o$

Adding Equation (A1.10) and (A1.11) we have

$$\Delta T_o(\Delta P^{n+1}) + V_i \Delta T_{gi} \Delta P^{n+1} + V_i \Delta(R_{so} T_o (\Delta P^{n+1})) = (C_{2p} + V_i C_{3p})\Delta_t P + Q_o + V_i(R_{so} Q_o + Q_g)$$

where

$$V_i = \frac{C_{2o}}{C_{3o} - C_{3g}}$$

$$(A1.12)$$

When equation (A1.12) is expanded it becomes.

$$T_{oi+1/2}[P_{i+1}^{n+1} - P_i] + T_{oi-1/2}[P_{i-1}^{n+1} - P_i] + V_i[T_{gi+1/2}^{n+1}(P_{i+1} - P_i) + T_{gi-1/2}(P_{i-1} - P_i)]$$
$$+ V_i[(R_s T_o)_{i+1/2}(P_{i+1} - P_i) + (R_s T_o)_{i-1/2}(P_{i-1} - P_i)] = (C_{2p} + A C_{3p})_i (P^{n+1} - P^n)_i + (1 + V_i R_i)Q_o + V_i Q_{gi}$$
$$- V_i Q_{gi} - V_i[T_{ig+1/2}(P_{i+1} - P_i) + T_{ig-1/2}(P_{i-1} - P_i)]$$

$$(A1.13)$$

A1.5 Assumptions

The assumptions in this model are as follows

- Gravity effect was neglected.

- Flow is isothermal.

- Darcy flow is assumed.

A.1.6 Pressure Matrix

When equation A1.21 is expanded for all the grid points, the following matrix is obtained.

$$T\,P^{(n+1)} = D\,[P^{(n+1)} - P^{(n)}] + G + Q$$

T- is a tri-diagonal matrix similar to the one shown below. It typically contain the transmissibilities functions

$$\begin{bmatrix} T_2 & -(T_2 + T_1) & T_1 & 0 \\ 0 & T_3 & T_3 + T_2 & T_2 \\ 0 & 0 & T_{n-1} & -T_{n-1} + T_{n-2} \\ 0 & 0 & 0 & 0 \end{bmatrix}$$

Matrix D contains compressibilities

Matrix G is a tri-diagonal matrix

$P^{(n)}$ –pressure at previous time

Q- flow-rate vector

The above matrix was solved by Thomas algorithm

A.17 Saturation update

When new pressures are obtained, the saturation is updated explicitly using the equation below

$$T_{oi+1/2}(P_{i+1} - P_i) + T_{oi-1/2}(P_{i-1} - P_i) = C_{2p}\Delta_t(P_i^{n+1} - P_i^{\,n})_i + C_{2o}(S_i^{n+1} - S_i^{\,n}) + Q_{oi} \quad (A1.14)$$

Equation A1.14 also uses upstream weighting scheme,

$$T_{oi+1}(P_{i+1} - P_i) + T_{oi}(P_{i-1} - P_i) = C_{2p}\Delta_t(P_i^{n+1} - P_i^{\,n})_i + C_{2o}(S_i^{n+1} - S_i^{\,n}) + Q_{oi} \quad (A1.15)$$

$$T_{oi+1}P_{i+1} - (T_{oi+1} + T_{oi})P_i + T_{oi}P_{i-1} = C_{2p}\Delta_t(P_i^{n+1} - P_i^{\,n})_i + C_{2o}(S_i^{n+1} - S_i^{\,n}) + Q_{oi}$$

$$T_{oi+1}P_{i+1} - (T_{oi+1} + T_{oi})P_i + T_{oi}P_{i-1} - C_{2p}\Delta_t(P_i^{n+1} - P_i^{\,n})_i - Q_{oi} = C_{2o}(S_i^{n+1} - S_i^{\,n})$$

$$(S_i^{n+1} - S_i^n) = \frac{T_{oi+1}P_{i+1} - (T_{oi+1} + T_{oi})P_i + T_{oi}P_{i-1} - C_{2p}\Delta_t(P_i^{n+1} - P_i^{\ n})_i - Q_{oi}}{C_{2o}}$$

$$S_i^{n+1} = \frac{T_{oi+1}P_{i+1} - (T_{oi+1} + T_{oi})P_i + T_{oi}P_{i-1} - C_{2p}\Delta_t(P_i^{n+1} - P_i^{\ n})_i - Q_{oi}}{C_{2o}} + S_i^{n+1} \qquad (A1.16)$$

This equation is the finite difference equation for one of the phases (in this case oil)

Matrix to be solved is

$$T\ P^{\ (n+1)} = [V] + A\ [S_o^{\ (n+1)}] \qquad (A1.17)$$

T is a tri-diagonal Matrix similar to that shown above. Equation A1.17 is an explicit equation, which is solved using simple matrix algebra.

Once the pressures and saturation for the new time step is obtain at different grid locations, the coefficients (C_{1p}, C_{2p}, C_{2o}, C_{1w}) and transmissibilities, which are themselves functions of saturation and pressure are determined and updated for the next time step.

A.2 Analytical Solution

Above the bubble point pressure, flow is single-phase and there exists an analytical solution. The single-phase solution of flow in the sand-pack can be represented by the one-dimensional diffusivity equation given below. The single-phase solution was used in Chapter 3 to validate the model above the bubble point pressure.

$$\frac{\partial^2 P}{\partial x^2} = \frac{\partial P}{\eta \partial t} \qquad (A.2.1)$$

where

$$\eta = \frac{k}{\phi c_t \mu}$$

with initial condition

$P = P_o$ at $t=0$

And boundary conditions

$$-k_1 \frac{\partial P}{\partial x} = 0 \qquad at \ x = 0$$

$$-k_1 \frac{\partial P}{\partial x} = f(t) \qquad at \ x = L$$

Consider the general non-homogeneous transient equation

$$\nabla^2 P(r,t) + \frac{1}{k_c} g(r,t) = \frac{1}{\eta} \frac{\partial P}{\partial t}(r,t) \quad \text{in region R,} \quad t>0$$

with initial condition,

$P(r,t) = P(r)$ \qquad for $t=0$ in Region R

and boundary condition,

$$k_c \frac{\partial P}{\partial t}(r,t) + h_i P = h_i T_{ai} \equiv f_i(r,t) \qquad \text{on Si} \quad t > 0$$

i is the surface under consideration.

The Green's Theorem solution to this equation in a finite region for rectangular coordinate is given by

$$P(r,t) = \int_R G(r,t/r,\tau)/_{\tau=0} F(r')dv' + \frac{\eta}{k} \int_{\tau=0}^t d\tau \int_R (G(r,t/r'\tau')g(r',\tau)dv' + \frac{\eta}{k} \int_{\tau=0}^t d\tau \sum_{l=1}^N \int_{si} (G(r,t/r'\tau)/r' = r_i \frac{1}{k_i}(f_i(r,\tau)ds_1$$

For the one-dimensional case described above, the solution is given by

$$P(x,t) = \int_R x_p G(x,t/x',\tau)/_{\tau=0} F(x')dx' + \frac{\eta}{k} \int_{\tau=0}^t d\tau \int_R (x'_p G(x,t/r'\tau')g(x',\tau)dx' + \eta \int_{\tau=0}^t d\tau \sum_{l=1}^2 x_p G(x,t/x,t)]_{x'=x_i} \frac{f_i}{k_i}$$

x_p is the Sturm-Liouville weight function. $x_p = 1$ for the heat slab.

Assuming the is similar to a heat slab with heat loss from one surface and no heat accumulation, the solution becomes

$$P(x,t) = \int_L G(x,t/x',\tau)/_{\tau=0} F(x')dx' + \eta \int_{\tau=0}^t d\tau \sum_{l=1}^2 G(x,t/x,t)]_{x'=x_i} \frac{f_i}{k_i} \qquad (A2.2)$$

The problem in Equation A2.2 is similar to the non-homogeneous heat diffusion in a slab and the solution is obtained by determining the Green's functions using separation of variable. Firstly, the solution to the homogeneous problem (Equation A2.3) is obtained.

$$\frac{\partial^2 P}{\partial x^2} = \frac{\partial P}{\eta \partial t} \qquad (A2.3)$$

$$-k_{c1} \frac{\partial P}{\partial x} = 0 \quad \text{at } x = 0$$

$$-k_{c2} \frac{\partial P}{\partial x} = 0 \quad \text{at } x = L$$

at $t = 0$, $P = F(x)$

The solution is given by

$$P(x,t) = \frac{1}{L}\int_0^L F(x')dx' + \frac{2}{L}\sum_{m=1}^{\alpha} e^{-\eta\beta^2_m t}\cos(\beta_{mx})\int_{x'=0}^L F(x')\cos(\beta_m x')dx'$$ (A2.4)

$$P(x,t) = \frac{F}{L}(L-0) + \frac{2}{L}\sum_{m=1}^{\alpha} e^{-\eta\beta^2_m t}\cos(\beta_{mx})\int_{x'=0}^L F\cos(\beta_m x')dx'$$ (A2.5)

if the initial pressure is P then we have

$$P(x,t) = P[1 + \frac{2}{L}\sum_{m=1}^{\alpha} e^{-\eta\beta^2_m t}\frac{\cos(\beta_m x)}{\beta_m}\sin(\beta_m L)]$$ (A2.6)

where

$$\beta_m = \frac{m\pi}{L} \qquad \text{where } m = 1,2,3 \ldots\ldots$$

The Green's function is then given by

$$G(x,t/x',\tau) = [1 + \frac{2}{L}\sum_{m=1}^{\alpha} e^{-\eta\beta^2_m t-\tau}Cos(\beta_m x)\sin(\beta_m L)]$$

As mentioned above, the solution to the non-homogeneous problem is given by

$$P(x,t) = \text{(Solution to the homogeneous part)} + \eta\int_{t=0}^t d\tau\sum_{i=1}^2 G(x,t/x',\tau)/_{x=x_i}\cdot\frac{f_i}{k_i}$$

From Equation A2.6 we have,

$$P(x,t) = P + [1 + \frac{2}{L}\sum_{m=1}^{\alpha} e^{-\eta\beta^2_m t}\frac{\cos(\beta_m x)}{\beta_m}\sin(\beta_m L)] + \eta\int_{\tau=0}^t d\tau[1 + \frac{2}{L}\sum_{m=1}^{\alpha} e^{-\eta\beta^2_m(t-\tau)}\cos(\beta_m x)\sin(\beta_m L)]Q$$

where

$$Q = \frac{f_2}{k_2}$$

$$f_2 = \frac{\mu q}{A}$$

$$k_2 = k$$

Simplifying,

$$P(x,t) = P_i + \frac{\eta Q t}{L} + \frac{2\eta Q}{L}\left\{\sum_{m=1}^{\alpha}\frac{[(1-e^{-\eta\beta_m^2 t})\cdot\cos(\beta_m x)\cdot\sin(\beta_m L)]}{\alpha\beta^2_m}\right\}$$

Re-arranging,

$$P(x,t) = P_i + \frac{\mu q}{Lk} \left\{ \frac{kt}{\phi c_f \mu} + 2 \sum_{m=1}^{\alpha} \frac{[(1 - e^{-\eta \beta_m^2 t}).\cos(\beta_m x).\cos(\beta_m L)]}{\beta_m^2} \right\}$$

$$\beta_m = \frac{m\pi}{L}, m = 1,2,3,\ldots\ldots$$

$$\eta = \frac{k}{\phi c_f \mu}$$

$$P(x,t) = P_i + \frac{\mu q}{Lk} \left\{ \frac{kt}{\phi c_f \mu} + 2 \sum_{m=1}^{\infty} \frac{(-1)^m}{(\frac{m\pi}{L})^2} \cos(m\pi \frac{x}{L}) \times \left[1 - \exp\left(-m^2 \pi^2 \frac{kt}{\phi \mu c_t L^2} \right) \right] \right\}$$

```
                    ┌─────────────────┐
                    │      START      │
                    └────────┬────────┘
                             ▼
        ┌────────────────────────────────────────────┐
        │         Define space and time step         │
        │  Define properties, Conditions and initial values │
        └────────────────────┬───────────────────────┘
                             ▼
        ┌────────────────────────────────────────────┐
        │         Initial guess for Pⁿ⁺¹             │◄──┐
        └────────────────────┬───────────────────────┘   │
                             ▼                            │
        ┌────────────────────────────────────────────┐   │
        │            Calculate matrix terms          │   │
        └────────────────────┬───────────────────────┘   │
                             ▼                            │
    ┌────────────────────────────────────────────────┐   │
    │ Call subroutine for solution of the matrix by Thomas algorithm │
    └────────────────────────┬───────────────────────┘   │
                             ▼                            │
        ┌────────────────────────────────────────────┐   │
        │             Calculate Pⁿ⁺¹                 │   │
        └────────────────────┬───────────────────────┘   │
                             ▼                            │
        ┌────────────────────────────────────────────┐   │
        │        Calculate material balance error    │   │
        └────────────────────┬───────────────────────┘   │
                             ▼                            │
                         ◇ If e<0.001 ◇ ─── No ───────────┘
                             │ Yes
                             ▼
        ┌────────────────────────────────────────────┐
        │    Determine Saturation and Capillary pressure │
        └────────────────────┬───────────────────────┘
                             ▼
        ┌────────────────────────────────────────────┐
        │   Determine Gas relative permeability values │
        │      from saturation and local parameters   │
        └────────────────────┬───────────────────────┘
                             ▼
        ┌────────────────────────────────────────────┐
        │             Calculate outputs              │
        └────────────────────┬───────────────────────┘
                             ▼
        ┌────────────────────────────────────────────┐
        │      Update pressures and Saturations      │
        └────────────────────┬───────────────────────┘
                             ▼
                    ┌─────────────────┐
                    │       END       │
                    └─────────────────┘
```

Flowchart elements:
- START
- Define space and time step / Define properties, Conditions and initial values
- Initial guess for P^{n+1}
- Calculate matrix terms
- Call subroutine for solution of the matrix by Thomas algorithm
- Calculate P^{n+1}
- Calculate material balance error
- If $e<0.001$ — No / Yes
- Determine Saturation and Capillary pressure
- Determine Gas relative permeability values from saturation and local parameters
- Calculate outputs
- Update pressures and Saturations
- END

A2.1 Algorithm for the Solution using the Numerical Model

APPENDIX –II

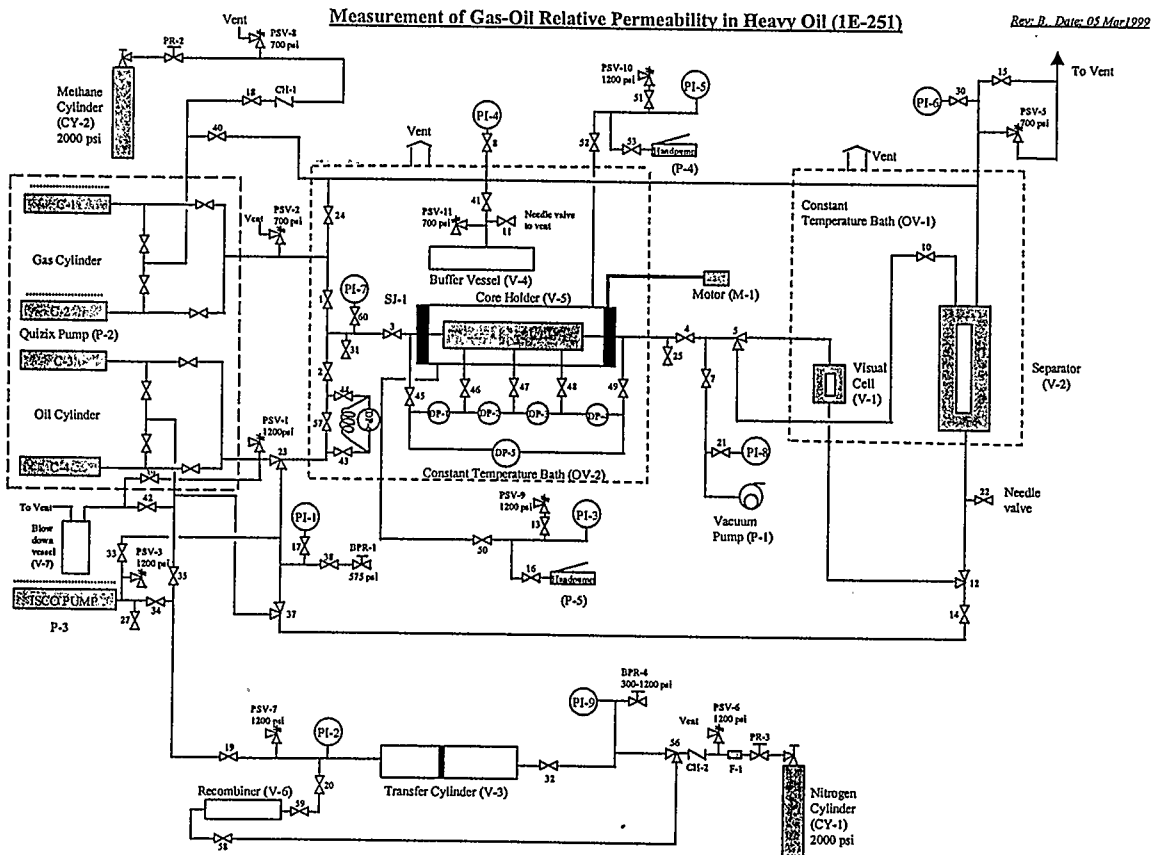**Measurement of Gas-Oil Relative Permeability in Heavy Oil (1E-251)**   *Rev: B. Date: 05 Mar 1999*

Figure A.II Flow diagram for the depletion unit